

# Vasculature and flow in microfluidic systems Kramer, B.

#### Citation

Kramer, B. (2025, October 23). Vasculature and flow in microfluidic systems. Retrieved from https://hdl.handle.net/1887/4279472

Version: Publisher's Version

Licence agreement concerning inclusion of doctoral

License: thesis in the Institutional Repository of the University

of Leiden

Downloaded from: <a href="https://hdl.handle.net/1887/4279472">https://hdl.handle.net/1887/4279472</a>

**Note:** To cite this publication please use the final published version (if applicable).

# Vasculature and Flow in Microfluidic Systems

**Bart Kramer** 

Cover: Vascularized liver spheroid in the OrganoPlate Graft Printing: Ridderprint | www.ridderprint.nl © Copyright, Bart Kramer, 2025 ISBN: 978-94-6522-726-9 All rights reserved. No part of this book may be reproduced in any form or by any means without permission of the author.

### Vasculature and Flow in Microfluidic Systems

#### Proefschrift

ter verkrijging van
de graad van doctor aan de Universiteit Leiden
op gezag van rector magnificus prof.dr.ir. H. Bijl,
volgens besluit van het college voor promoties
te verdedigen op donderdag 23 oktober 2025
klokke 14.30 uur

door

Bart Kramer

geboren te Woerden

in 1991

#### **Promotor:**

Prof. dr. T. Hankemeier

#### **Co-promotores:**

Dr. H.L. Lanz

Dr. L.J. van den Broek

#### **Promotiecommissie:**

Prof. dr. M. van Eck

Prof. dr. E.C.M. de Lange

Prof. dr. B. van de Water

Prof. dr. A.J. van Zonneveld

Prof. dr. R Masereeuw (Utrecht University)

Prof. dr. M. Buchholz (Marburg University)

# Table of contents

Chapter 1	General introduction	7				
Chapter 2	Interstitial Flow Recapitulates Gemcitabine Chemoresistance in A 3D Microfluidic Pancreatic Ductal Adenocarcinoma Model by Induction of Multidrug Resistance Proteins	27				
Chapter 3	3D human microvessel-on-a-Chip model for studying 55 monocyte-to-endothelium adhesion under flow – application in systems toxicology					
Chapter 4	High-throughput 3D microvessel-on-a-Chip model to study defective angiogenesis in systemic sclerosis					
Chapter 5	A robust and high-throughput approach for the quantification of three-dimensional vascular beds					
Chapter 6	Conclusions and perspectives					
Chapter 7	Addendum  Nederlandse samenvatting  Curriculum Vitea  List of publications  Dankwoord	155				

# Chapter 1

**General introduction** 



#### The drug development pipeline

The drug development pipeline (Figure 1) is a complex and lengthy process that requires the use of various preclinical model systems to identify potential drug candidates, usually utilized by pharmaceutical companies. The process starts with thousands of potential drug candidates, which are subsequently narrowed down to a select few through multiple preclinical tests aimed at assessing efficacy and safety.1 Subsequently, the selected drug candidates from the preclinical tests undergo clinical trials, that are divided in 3 phases. In phase 1, the safety of the drug candidate, including its pharmacokinetics (how the body absorbs, distributes metabolizes and excretes the drug) and pharmacodynamics (the drug's biological effects) are evaluated in a small group of healthy volunteers, with the goal of establishing an appropriate dosage range. Moving forward, phase 2 trials focuses on assessing the drug's efficacy in treating the targeted disease, identifying optimal dosing strategies and evaluating further safety. This phase often involves hundreds of patients with the specific condition to determine if the drug candidate has the intended therapeutic effect with manageable side effects. Finally, if the drug is effective and does not show toxicity in phase 2, it will proceed to phase 3 trials, where the drug is tested in an even larger group of patients to confirm its dosage, efficacy and toxicity. Then, the data from the whole process is submitted to the regulatory committees for approval to be released to the public. On average, it takes 10-15 years and costs €1-2 billion for each drug to obtain clinical approval.2

These high costs and lead times are mostly due to the high failure rate of drugs in the (preclinical) pipeline.<sup>3</sup> There are several possible explanations for the high rate of clinical failures in drug development, with the following factors being the most commonly cited: insufficient clinical efficacy (40-50%), excessive toxicity (30%), inadequate drug-like characteristics (10-15%), and insufficient market demand or ineffective strategic planning (10%).<sup>2,3</sup> The inefficiency of the drug development process is evident from the high failure rate of drugs in

the preclinical pipeline, requiring the exploration of more effective approaches to address these challenges, such as better translatable preclinical models. To further address these challenges, traditional preclinical models commonly used in drug development, including 2D cell culture models and animal models, will be discussed. Additionally, the emerging role of complex in vitro systems as translatable alternatives will be explored, highlighting their potential to improve predictive accuracy in the drug development pipeline.

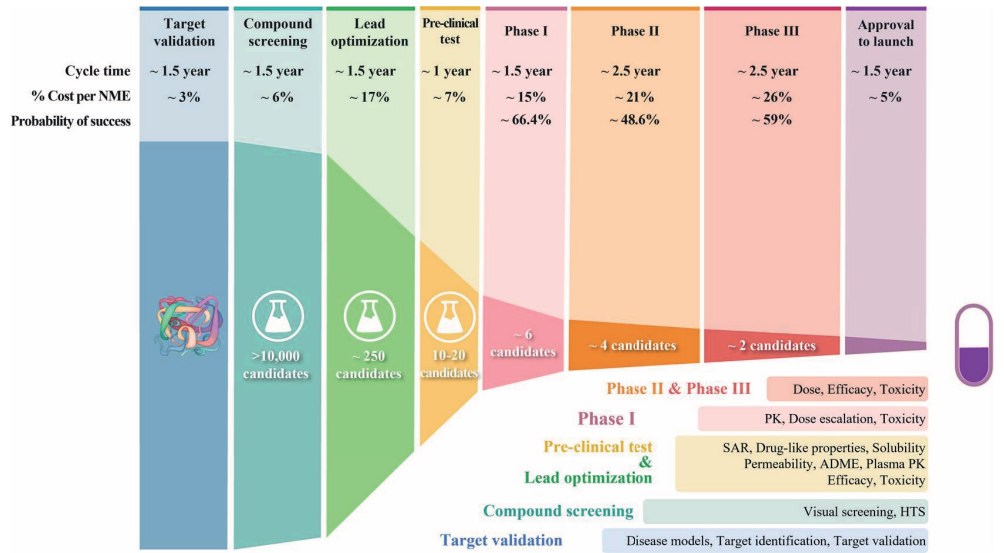


**Figure 1 The process of drug discovery, with the failure rates on each step.** Abbreviations: NME: New Molecular Entity, PK: Pharmacokinetics, SAR: Structure-Activity Relationships, ADME: absorption, distribution, metabolism and excretion, HTS: High-throughput screening.<sup>2</sup>

#### 2D cell culture models

2D cell culture models have been used for decades in preclinical drug development,<sup>4</sup> and are still widely used in preclinical research to study disease mechanisms and drug development.<sup>5</sup> Due to the relative simplicity of the culture method and the widespread availability of primary cells and cell lines, they are an effective tool to assess thousands of compounds for their potential effectivity and safety as a drug.<sup>6</sup> However, these systems have many limitations. A few examples are the lack of 3D tissue architecture,<sup>7</sup> sufficient cell differentiation<sup>7</sup> and an unnaturally high proliferation rate.<sup>4</sup> This all impacts the accuracy of predicting which compounds should be selected for further evaluation during a compound screen.

Despite these limitations, 2D cell culture models remain a valuable tool in preclinical drug development and basic research, particularly for initial screening of large numbers of compounds or for studying cell behaviour under controlled conditions.<sup>1</sup> However, it is important to recognize that the aforementioned limitations of 2D culture could lead to an incorrect prediction of the efficacy of a potential new drug. Supplementing these models with more physiologically relevant models, such as animal models or 3D cell culture, to validate findings and ensure that they are translatable to human disease is needed, especially in the context of developing new drugs but also for ensuring the successful repurposing of existing drugs for new therapeutic applications.<sup>5</sup>

#### Animal models in preclinical studies

Animal models are currently an essential tool in preclinical studies, serving as a bridge between basic research of 2D cell cultures and clinical trials. By using animal models, researchers gain insight into the drug pharmacodynamics, pharmacokinetics and toxicity. Animal research can not only provide information about the potential drug's efficacy, but also its off-target effect on other organs after metabolism, as well as potential interactions with other drugs.<sup>8</sup>

However, there are also some limitations for the use of animal models in preclinical development. Firstly, there are ethical concerns for the use of animal models that are widely recognized by the public. Secondly, animal experiments are costly and time consuming. Lastly, the translation of the results of a drug study from animal models to humans is an issue. The physiology and genetics are vastly different between humans and animals, and drugs proven safe in animals may still cause unexpected adverse effects in humans. These complexities can substantially impact the drug discovery pipeline, requiring a cautious and thorough approach to ensure both efficacy and safety in human applications.

An example is the clinical trial for the CD28 superagonist antibody TGN1412, which was hypothesized to treat multiple autoimmune diseases. After preclinical studies performed on multiple animal models, including rhesus monkeys, TGN1412 was tested in a phase I clinical study on 6 human volunteers. After administering a dose 500 times smaller than was found safe from animal studies, all humans suffered from severe allergic reactions within minutes, and faced life-threatening conditions when they were moved to the intensive care unit. It was hypothesized that the difference in observed effect was caused by a 4% difference in the amino acid sequence of the C"D loop of the CD28 receptor in humans and monkeys.

#### Bridging the gap between basic cell culture models and animal studies

Bridging the gap between basic cell culture models and animal studies requires the use of more complex in vitro models that incorporate physiological cues that better mimic in vivo conditions. These models include organoids, Organon-a-Chip systems, and Transwells.<sup>5,6</sup> Recent advances in stem cell biology, tissue engineering, and microfabrication techniques have enabled the development of these more sophisticated models, which have the potential to accelerate drug discovery and provide more reliable predictions of drug efficacy and toxicity. These advancements are particularly significant in the context of replacing or reducing the reliance on animal studies. Organ-on-a-Chip technology, for example, can replicate organ-level functions, offering a promising alternative to animal models.

The evolving landscape of advanced methodologies offers several advantages over conventional approaches, such as improved physiological relevance, reproducibility, and high-throughput capabilities. Moreover, they can provide a better understanding of the mechanisms of drug action, toxicity, and efficacy, thereby facilitating the identification of promising drug candidates early in the drug development process.

Advancements in in vitro modeling have increasingly focused on developing systems that better replicate the complexity of human physiology. The complexity of complex in vitro systems extends beyond their structural complexity and arises from their ability to incorporate additional features that mimic physiological conditions. For instance, these systems allow for the inclusion of multiple cell types to establish co-cultures, enabling the study of cell-cell interactions. Furthermore, external factors such as fluid flow, compartmentalization of cells and media and integrated measurement tools, such as electrodes for real time monitoring, can be integrated in some systems to enhance functionality.

#### **Legislation for complex in vitro systems**

The innovative momentum of complex in vitro systems was recognized with the recent progression in legislation. On 29 December 2022, the US government passed the FDA Modernization Act 2.0.12 This bill follows up on the original 'Federal Food, Drug and Cosmetics Act' of 1938, which included mandatory animal testing for every new drug development study. Where this originally was included to improve the safety of new drug developments, the recent scientific advancements in alternatives for animal testing, such as Organ-on-a-Chip technology now offers a realistic alternative to animal testing.<sup>13</sup> The new act opens the door to allow clinical testing of drugs without performing preclinical animal test studies. Nevertheless, these models need to be validated if companies want to replace animal testing in preclinical research with alternatives such as Organ-on-a-Chip systems.

The current state of complex in vitro systems would not be able to immediately replace all animal studies. In the aforementioned example of systemic immune-mediated failures – the TGN1412 cytokine storm (which depended on human-specific CD28 receptor biology and tissue-resident T-cell populations) – these types of immune failures would likely remain undetected in current complex in vitro systems lacking functional adaptive immunity. However, the possibility of using human-derived cells in these systems could overcome species-specific genetic differences in protein structures between humans and animals, potentially preventing similar failures from occurring. In the following section, examples of complex in vitro systems are described.

#### **Transwell system**

One of the most widely adopted complex system in biomedical research is the Transwell system. Comprising a permeable membrane insert placed within a well, the Transwell system facilitates the creation of a bi-phasic environment, allowing researchers to investigate the interactions between different cell types, cellular layers, and their respective media (Figure 2).14 One of the key applications of this system is the use for barrier function studies of epithelial and endothelial cells, as the easy access to the apical and basal side of these cells allow for the measurement of Transepithelial (or endothelial) Electrical Resistance (TEER).<sup>15</sup> This system is also widely used for cell migration assays and drug transport studies. Although the system is relatively simple (for a 'complex' system), reproducible and adaptable to various studies, it also has some limitations. The throughput is relatively low and to initiate and maintain the cultures a high amount of medium and cells are needed. The static nature of the system does not recapitulate the dynamic flow conditions that are present in vivo. Moreover, the system lacks the architectural complexity of three-dimensional tissues, which can impact cellular behavior and response to stimuli.16

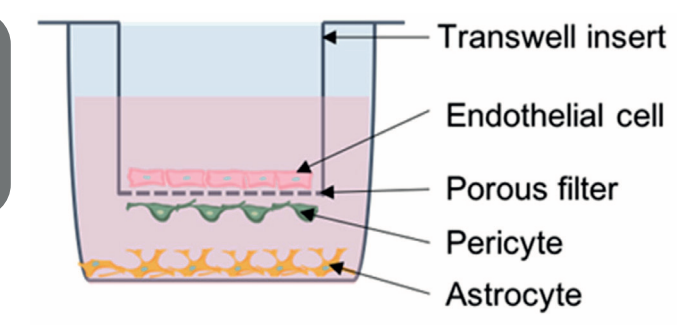


**Figure 2 Schematic image of the Transwell system.** A Transwell insert with a porous membrane is inserted in a well filled with medium. Cells (in this case endothelial cells, pericytes and astrocytes) are loaded on either side of the membrane, allowing for crosstalk between the cell types while keeping them separated. (adapted from<sup>17</sup>)

#### **Bioprinting**

Another example of such complex systems are bioprinting based systems. These systems offer a technological platform to create more physiologically relevant 3D tissue models. Bioprinting involves the use of 3D printing technology to deposit cells, biomaterials, and supporting components in a layer-by-layer fashion to construct tissue-like structures (Figure 3). 18,19 This technology is used by researchers to fabricate 3D cellular constructs that mimic the architecture and functionality of native tissues, thereby providing a more accurate platform for studying tissue biology, disease modeling, and drug testing. The main advantage of bioprinting is their highly customizable nature, allowing researchers to tailor the model to their specific research questions. The created microenvironments can closely represent the architecture of the in vivo structures, and therefore adequately mimic the cellular complexity of tissues, enabling the study of cellcell interactions.<sup>20</sup> However, although the complexity of this system is high, it is difficult to scale this technique to replace the current preclinical in vitro systems. The specialized equipment needed is another barrier that limits accessibility and widespread adaption.<sup>21</sup>

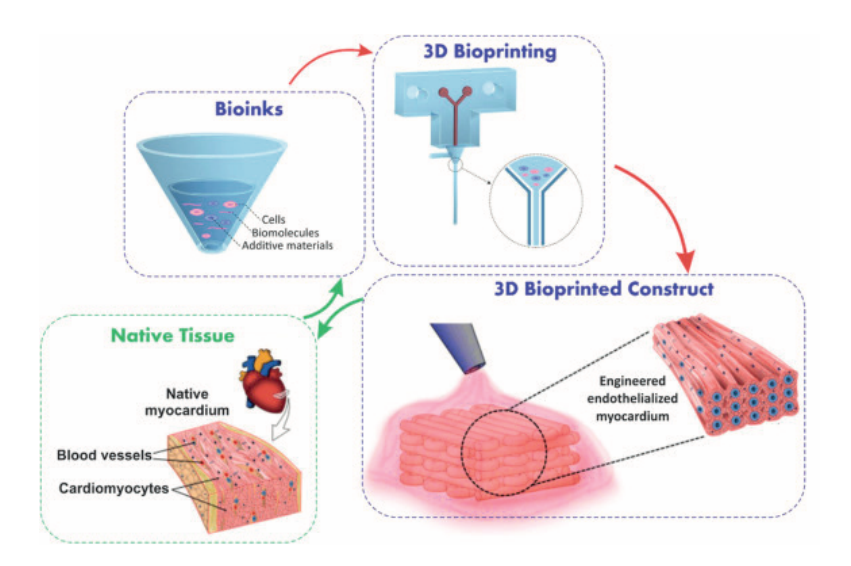


**Figure 3 Schematic overview of the bioprinting process.** Cells, biomolecules and additive materials are mixed into a bioink, which is 3D printed into a layered construct.<sup>22</sup>

#### **Organoids**

Organoids, often referred to as "mini-organs," have emerged as a revolutionary tool in the field of biomedical research, providing a 3D complex in vitro platform that mimics the structural and functional aspects of real organs. Derived from stem cells, organoids have the capability to self-organize and differentiate into various cell types, thereby recapitulating the architecture and functionality of their in vivo counterparts.<sup>23</sup>

A major advantage of organoids is their ability to model human disease, with cells directly derived from the patient, which makes it an interesting platform for investigating pathogenesis and developing new therapeutic interventions, known as personalized medicine. This can be used to predict the most favorable treatment option for the patient.<sup>24</sup> A key example of personalized medicine approaches for organoids is in the case of cystic fibrosis (CF), where organoids have demonstrated profound efficacy in tailoring personalized treatment approaches. Organoids can be used to functionally test the CF transmembrane conductance regulator (CFTR) gene, and predict treatments aimed at restoring

its function.<sup>25</sup> A limitation of the use of organoids is the lack of vascularization which limits the ability to mimic the in vivo environment fully.<sup>24</sup> Additionally, (iPSC-derived) organoids often remain in a fetal-like developmental state, lacking the full functional maturation and functionality of adult tissues. This immaturity can affect their ability to accurately model diseases and limits their applicability in certain therapeutic contexts.<sup>26</sup>

#### **Organ-on-a-Chip systems**

Advancing at the forefront of these technologies is Organ-on-a-Chip (OOC) technology. This approach enables the development of robust and reliable model systems that accurately recapitulate the complex physiological and biochemical features of the target organ. By incorporating relevant cell types, extracellular matrix components, and microfluidic channels that enable controlled flow of nutrients and metabolites, Organ-on-a-Chip technology facilitates the development of robust and reliable model systems and accurately recapitulates the physiological and biochemical features of the target organ.

OOC systems can roughly be divided into 2 classifications: a lower throughput system that offers high complexity in the use of cell types and configuration and a class of higher throughput devices, that standardized the configuration of the microfluidic channels, but offer higher throughput, which could be used to perform drug screening. In the following section, examples of both classifications will be discussed.

#### Low throughput with high complexity OOC systems

The first class of OOC systems, the lower throughput systems that offer high complexity, are often Polydimethylsiloxane (PDMS) based. PDMS is a material that is often used in OOC systems because of its ease of use, which makes it a favorable material to make quick adaptations to the chip design due to iterative prototyping, allowing researchers to easily create complex chip layouts.<sup>27</sup> PDMS is inexpensive, elastic and is optically clear, which makes it compatible with

(fluorescent) microscopy imaging.<sup>28,29</sup> A limitation of PDMS based systems is that the material absorbs small hydrophobic molecules, which makes it a less favorable material to use for drug testing.<sup>28</sup>

A major player in the field of PDMS based OOC devices is Emulate, a company that manufactures Organ-on-a-Chip devices that are suitable for a wide range of applications. They offer a wide range of organ models on the chip, ranging from Brain and Colon to Kidney and Liver (Figure 4).<sup>30</sup> The chips are connected to an ecosystem of hardware that provide medium to the chips, regulate flow, provide strain and control the humidity and temperature.<sup>31</sup> In addition to the commercialized platforms, there are many academic groups developing chips for their research needs.<sup>32,33</sup>

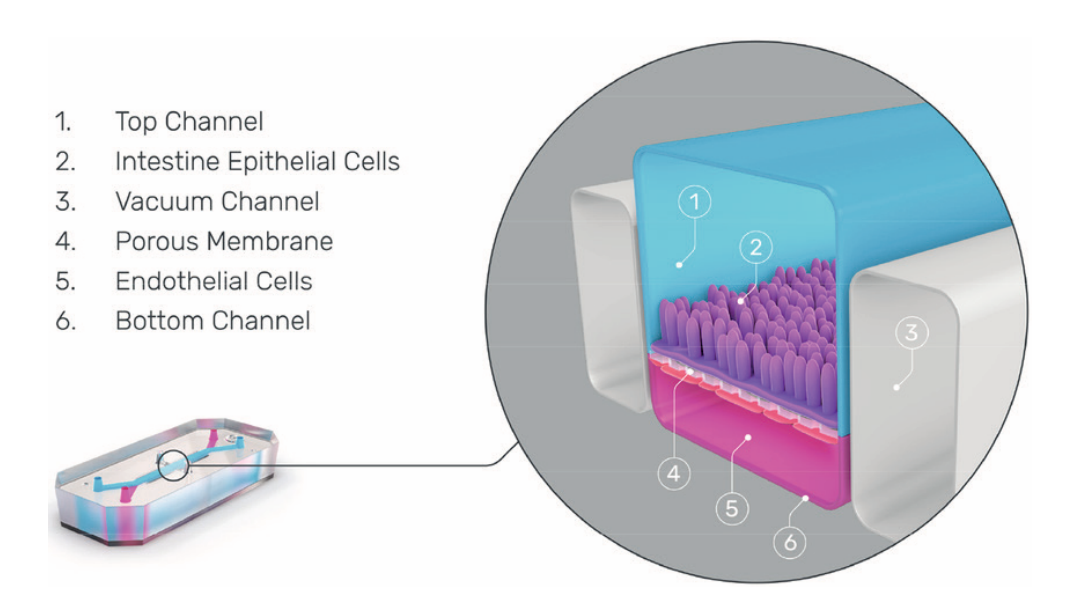


**Figure 4 The Emulate OOC platform.** Two parallel microfluidic channels are separated with a porous membrane. Different cell types can be loaded into the channels, allowing for cross talk between the cell types. Flow is applied through the channels.<sup>35</sup>

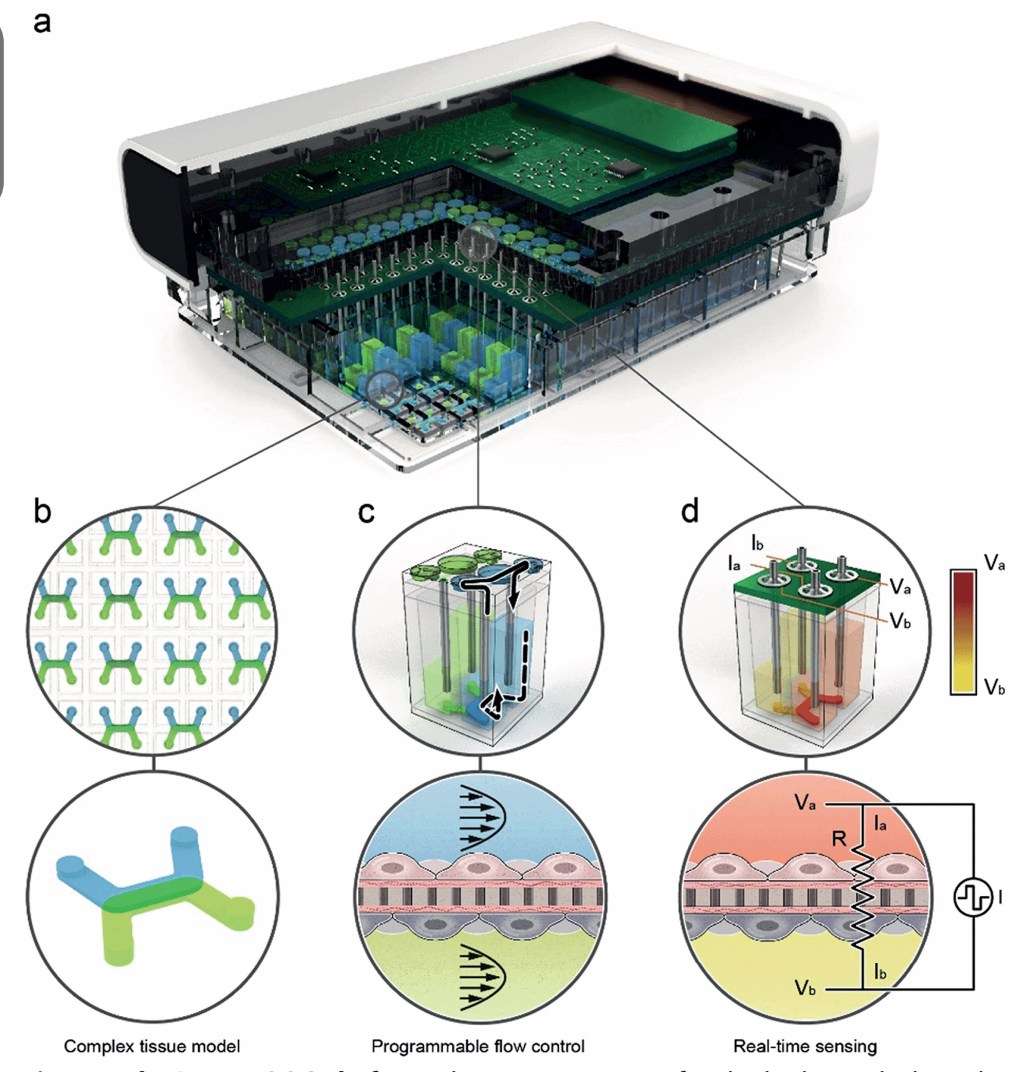


**Figure 5 The Draper OOC platform.** The system consists of multiple chips, which can be loaded with multiple cell types. The system is integrated with a pumping system for flow and sensing of electrical resistance (TEER).<sup>37</sup>

#### **High throughput OOC systems**

The second class of OOC devices focuses on high-throughput applications. This class is usually characterized by the accumulation of multiple similar chips in one larger entity, so that handling of large amounts of cultures is made possible by hand or can be automated by robotics. This opens the door for screening of large

amounts of compounds to evaluate the efficacy of new potential drugs, or screen for toxic effects of compounds.<sup>35</sup> The disadvantage to the first class of systems is that this limits the complexity of the design of chips more compared to first class. The high-throughput nature prioritizes volume and speed over detailed, individualized analysis. As a result, while these systems are excellent for broad screenings and preliminary evaluations, they might not capture the full depth of organ-specific responses or nuanced cellular behaviors that more complex, specialized chips can.

One example of a high-throughput Organ-on-a-Chip system is developed by Draper. Their platform, Predict96, is an advanced microfluidic platform designed to mimic the human physiological environment on a scalable platform (Figure 5). It is possible to establish 96 individual cultures on a titer plate, which is compatible with standard laboratory equipment and microscopy. Flow in the cultures is established with a pneumatic pump, that is added as a lid on top of the plate. The lid is connected with tubing for air and vacuum connections with a main control unit. 36,37

Another illustration of a microfluidic platform is the OrganoPlate, developed by MIMETAS (Figure 6). This system also has the footprint of a titer plate, which houses 40 to 96 chips, depending on the plate design. The microfluidic channels are separated by small ridges, PhaseGuides, that act as a pressure barrier, allowing the channels to be patterned individually, without the use of artificial membranes.<sup>38</sup> This offers a versatile and scalable solution for applications in biology and drug discovery. MIMETAS has developed models for a wide range of organs, ranging from neuronal<sup>39</sup> and kidney<sup>40</sup>, to vasculature<sup>41</sup> and liver.<sup>42</sup> Flow is added to the system in a gravity driven manner, by placing the plate on a rocking platform in the incubator. The incorporation of flow is important for mimicking the in vivo conditions, which is underscored by recent research highlighting the significance of flow dynamics in microfluidic devices.<sup>43,44</sup>The standard titerplate based platform and the pumpless system to generate flow demonstrate the system's scalability,

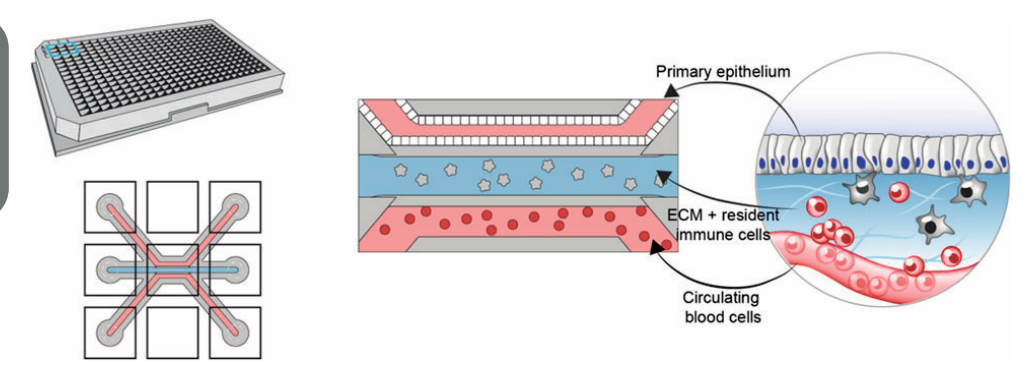


**Figure 6. The microfluidic platform the OrganoPlate 3-lane 40 (MIMETAS).** The platform consists of microfluidic channels separated by PhaseGuides, which allow direct interaction between the different channels without the use of membranes. 46

as exemplified by its successful execution of a comprehensive screening of 1537 kinase inhibitors to assess their impact on angiogenesis.<sup>45</sup>

In order to gain insights into the potential of Organ-on-a-Chip technology for the future of drug development, it is crucial to understand the key requirements for developing physiologically relevant models and the advantages and limitations they have over the currently established models. To this end, extensive research and model optimization are needed to develop physiologically relevant in vitro models in Organ-on-a-Chip technology.<sup>47</sup> Another challenge lies in ensuring the translatability of these models to real-world human situations. The incorporation of flow in Organ-on-a-Chip technology could significantly boost its physiological relevance, addressing one of the limitations of static 2D cell culture models.<sup>48</sup> However, for Organ-on-a-Chip technology to effectively replace or supplement animal models in the drug development pipeline, the model must not only possess complexity but also demonstrate scalability. The ability to rapidly generate large scale data through high-throughput Organ-on-a-Chip platforms will be essential for integrating these models into drug screening processes, enabling more efficient and predictive testing of both new and repurposed drugs.

## Scope of this thesis

The aim of the research described in this thesis is to develop physiological relevant models that utilize the capabilities of Organ-on-a-Chip technology, such as the incorporation of vasculature and fluid flow. Fluid flow is pivotal in various physiological processes, including the transport of molecules and cells, cell signaling, and tissue development. The hypothesis of this thesis is that incorporating flow in Organ-on-a-Chip systems is crucial for accurately mimicking the physiological conditions of in vivo organs. The dynamic environment created by fluid flow will contribute to model tissue specific functions by enabling the formation of gradients, to promote cellular (re)organization and to enhance the development physiologically relevant tissue structures. This incorporation enhances the predictive power of drug responses, thereby ultimately improving the efficiency and reliability of the drug development pipeline.

Almost all tissues in the human body are supplied with oxygen and nutrients by a network of blood vessels, known as the vascular network. Cells outside the diffusion range of this network will be subjected to hypoxia and apoptosis. To this end, the OrganoPlate (Figure 6) is used to create different microphysiological models that utilize vasculature and flow, aiming to more accurately replicate these in vivo conditions and validate our hypothesis.

In Chapter 2, the aim is to develop a three-dimensional Pancreatic Ductal Adenocarcinoma (PDAC) model that is suitable to assess drug resistance of existing and new therapies. Special focus is placed on the incorporation of interstitial flow, which is an important characteristic of PDAC. A difference in chemoresistance in two-dimensional versus three-dimensional cell culture is observed, and in addition the relevance of interstitial flow on drug resistance in the three-dimensional culture is demonstrated.

In Chapter 3, the focus shifts from fluid flow to vasculature. A vasculature-on-achip model for the toxicological assessment of substances on the early stage of atherosclerosis is described. A vascular model with coronary artery endothelial cells is developed and a method for assessing the presence of adhesion molecules and oxidative stress is evaluated. In addition, a functional assay for the live assessment of adhesion of monocytes to the endothelium is established. Finally, the adverse effect of cigarette smoke conditioned medium on the developed readouts is studied as a proof-of-concept.

Another application of the use of vasculature in Organ-on-a-Chip systems is developed in Chapter 4. The aim of this chapter is the development of a microvessel-on-a-chip to study defective angiogenesis in Systemic Sclerosis (SSc). Angiogenesis is often dysregulated in Systemic Sclerosis, and most of the research regarding angiogenesis in SSc is performed in animal models. A microfluidic angiogenesis model with dermal endothelial cells is developed and the use of human serum is optimized. The effect of compounds and inhibitors is studied on the stability of the angiogenic sprouts. Finally, the effect of serum from SSc patients is assessed on the model as a proof of concept.

Incorporating Organ-on-a-Chip technology into the drug development pipeline requires not only thorough model development but also the acquisition of precise quantitative data. In chapter 5, a robust and high-throughput approach for the quantification of three-dimensional vascular beds is developed. Vascular beds comprising of Human Umbilical Cord Endothelial Cells (HUVECs) and pericytes are generated on the OrganoPlate Graft. The vascular beds are imaged with high-throughput confocal imaging in 3D, and the images are processed to assess the characteristics of the vascular bed. The effect of withdrawing (part of) the angiogenic sprouting cocktail and addition of the pericytes on the characteristics of the vascular bed is studied.

In chapter 6, a summary is provided of the findings of the previous chapters. The limitations of the thesis are discussed, as well as directions for future research are proposed.

## References

- 1. Mayr, L. M. & Fuerst, P. The future of high-throughput screening. Journal of Biomolecular Screening vol. 13 443–448 Preprint at https://doi.org/10.1177/1087057108319644 (2008).
- 2. Sun, D., Gao, W., Hu, H. & Zhou, S. Why 90% of clinical drug development fails and how to improve it? Acta Pharmaceutica Sinica B vol. 12 3049–3062 Preprint at https://doi.org/10.1016/j.apsb.2022.02.002 (2022).
- 3. Dowden, H. & Munro, J. Trends in clinical success rates and therapeutic focus. Nature reviews. Drug discovery vol. 18 495–496 Preprint at https://doi.org/10.1038/d41573-019-00074-z (2019).
- 4. Langhans, S. A. Three-dimensional in vitro cell culture models in drug discovery and drug repositioning. Frontiers in Pharmacology vol. 9 Preprint at https://doi.org/10.3389/fphar.2018.00006 (2018).
- 5. Jensen, C. & Teng, Y. Is It Time to Start Transitioning From 2D to 3D Cell Culture? Frontiers in Molecular Biosciences vol. 7 Preprint at https://doi.org/10.3389/fmolb.2020.00033 (2020).
- 6. Costa, E. C. et al. 3D tumor spheroids: an overview on the tools and techniques used for their analysis. Biotechnology Advances vol. 34 1427–1441 Preprint at https://doi.org/10.1016/j.biotechadv.2016.11.002 (2016).
- 7. Imamura, Y. et al. Comparison of 2D- and 3D-culture models as drug-testing platforms in breast cancer. Oncol Rep 33, 1837–1843 (2015).
- 8. Denayer, T., Stöhrn, T. & Van Roy, M. Animal models in translational medicine: Validation and prediction. New Horiz Transl Med 2, 5–11 (2014).
- 9. Ormandy, E. H. & Schuppli, C. A. Public attitudes toward animal research: A review. Animals vol. 4 391–408 Preprint at https://doi.org/10.3390/ani4030391 (2014).
- 10. Attarwala, H. TGN1412: From discovery to disaster. Journal of Young Pharmacists vol. 2 332–336 Preprint at https://doi.org/10.4103/0975-1483.66810 (2010).
- 11. Hansen, S. & Leslie, R. G. Q. TGN1412: scrutinizing preclinical trials of antibody-based medicines. Nature 441, 282 (2006).
- 12. https://www.congress.gov/bill/117th-congress/senate-bill/5002. (2022).
- 13. Han, J. J. FDA Modernization Act 2.0 allows for alternatives to animal testing. Artif Organs 47, 449–450 (2023).
- 14. Rohrschneider, M. et al. Evaluation of the Transwell System for Characterization of Dissolution Behavior of Inhalation Drugs: Effects of Membrane and Surfactant. Mol Pharm 12, 2618–2624 (2015).
- 15. Linz, G. et al. Cell barrier characterization in transwell inserts by electrical impedance spectroscopy. Biosens Bioelectron 165, (2022).
- 16. Youhanna, S. & Lauschke, V. M. The Past, Present and Future of Intestinal In Vitro Cell Systems for Drug Absorption Studies. J Pharm Sci 110, 50–65 (2021).
- 17. Ippolitov, D., Arreza, L., Munir, M. N. & Hombach-Klonisch, S. Brain Microvascular Pericytes—More Than Bystanders in Breast Cancer Brain Metastasis. Cells vol. 11 Preprint at https://doi.org/10.3390/cells11081263 (2022).
- 18. Daly, A. C., Prendergast, M. E., Hughes, A. J. & Burdick, J. A. Bioprinting for the Biologist. Cell 184, 18–32 (2021).
- 19. Gungor-Ozkerim, P. S., Inci, I., Zhang, Y. S., Khademhosseini, A. & Dokmeci, M. R. Bioinks for 3D bioprinting: an overview. Biomater Sci 6, 915–946 (2018).
- 20. Seol, Y. J., Kang, H. W., Lee, S. J., Atala, A. & Yoo, J. J. Bioprinting technology and its applications. European Journal of Cardio-Thoracic Surgery 46, 342–348 (2014).
- 21. Sun, W. et al. The bioprinting roadmap. Biofabrication 12, 022002 (2020).
- 22. Ashammakhi, N. et al. Bioinks and bioprinting technologies to make heterogeneous and biomimetic tissue constructs. Materials Today Bio vol. 1 Preprint at https://doi.org/10.1016/j.mtbio.2019.100008 (2019).

- 23. Clevers, H. Review Modeling Development and Disease with Organoids. Cell 165, 1586–1597 (2016).
- 24. Li, Y., Tang, P., Cai, S., Peng, J. & Hua, G. Organoid based personalized medicine: from bench to bedside. Cell Regeneration 2020 9:1 9, 1–33 (2020).
- 25. Dekkers, J. F. et al. A functional CFTR assay using primary cystic fibrosis intestinal organoids. Nature Medicine 2013 19:7 19, 939–945 (2013).
- 26. Xu, Z. et al. Merits and challenges of iPSC-derived organoids for clinical applications. Front Cell Dev Biol 11, 1188905 (2023).
- 27. Cameron, T. C. et al. PDMS Organ-On-Chip Design and Fabrication: Strategies for Improving Fluidic Integration and Chip Robustness of Rapidly Prototyped Microfluidic In Vitro Models. Micromachines (Basel) 13, (2022).
- 28. Campbell, S. B. et al. Beyond Polydimethylsiloxane: Alternative Materials for Fabrication of Organ-on-a-Chip Devices and Microphysiological Systems. ACS Biomater Sci Eng 7, 2880–2899 (2021).
- 29. Cameron, T. C. et al. PDMS Organ-On-Chip Design and Fabrication: Strategies for Improving Fluidic Integration and Chip Robustness of Rapidly Prototyped Microfluidic In Vitro Models. Micromachines (Basel) 13, (2022).
- 30. Emulate. Emulate Product Page. https://emulatebio.com/products-services/(2023).
- 31. Workman, M. J. et al. Enhanced Utilization of Induced Pluripotent Stem Cell-Derived Human Intestinal Organoids Using Microengineered Chips. Cell Mol Gastroenterol Hepatol 5, 669-677.e2 (2017).
- 32. Leung, C. M. et al. A guide to the Organ-on-a-Chip. Nature Reviews Methods Primers 2022 2:1 2, 1–29 (2022).
- 33. Driver, R. & Mishra, S. Organ-on-a-Chip Technology: An In-depth Review of Recent Advancements and Future of Whole Body-on-chip. BioChip Journal 2022 17:1 17, 1–23 (2022).
- 34. Wang, H. et al. 3D cell culture models: Drug pharmacokinetics, safety assessment, and regulatory consideration. Clinical and Translational Science vol. 14 1659–1680 Preprint at https://doi.org/10.1111/cts.13066 (2021).
- 35. Du, G., Fang, Q. & den Toonder, J. M. J. Microfluidics for cell-based high throughput screening platforms—A review. Anal Chim Acta 903, 36–50 (2016).
- 36. Tan, K. et al. A high-throughput microfluidic microphysiological system (PREDICT-96) to recapitulate hepatocyte function in dynamic, re-circulating flow conditions. Lab Chip 19, 1556–1566 (2019).
- 37. Azizgolshani, H. et al. High-throughput organ-on-chip platform with integrated programmable fluid flow and real-time sensing for complex tissue models in drug development workflows. Lab Chip 21, 1454–1474 (2021).
- 38. Trietsch, S. J., Israëls, G. D., Joore, J., Hankemeier, T. & Vulto, P. Microfluidic titer plate for stratified 3D cell culture. Lab Chip 13, 3548 (2013).
- 39. Wevers, N. et al. 3D networks of iPSC-derived neurons and glia for high-throughput neurotoxicity screening. Toxicol Lett 258, S157 (2016).
- 40. Vormann, M. K., Gijzen, L., Hutter, S. & others. Nephrotoxicity and kidney transport assessment on 3d perfused proximal tubules. AAPS J 20, 90 (2018).
- 41. van Duinen, V. et al. Perfused 3D angiogenic sprouting in a high-throughput in vitro platform. Angiogenesis 22, 157–165 (2019).
- 42. Bonanini, F. et al. In vitro grafting of hepatic spheroids and organoids on a microfluidic vascular bed. Angiogenesis 25, 455–470 (2022).
- 43. Wilkinson, J. M. A review of complex in vitro cell culture stressing the importance of fluid flow and illustrated by organ on a chip liver models. Frontiers in toxicology 5, (2023).
- 44. Regmi, S., Poudel, C., Adhikari, R. & Luo, K. Q. Applications of Microfluidics and Organ-on-a-Chip in Cancer Research. Biosensors (Basel) 12, (2022).
- 45. Soragni, C. et al. Phenotypic screening in Organ-on-a-Chip systems: a 1537 kinase

inhibitor library screen on a 3D angiogenesis assay. Angiogenesis 1, 1–13 (2023).

46. Lewin, T. D. et al. An in silico Model of T Cell Infiltration Dynamics Based on an Advanced in vitro System to Enhance Preclinical Decision Making in Cancer Immunotherapy. Front Pharmacol 13, (2022).

47. Vulto, P. & Joore, J. Adoption of organ-on-chip platforms by the pharmaceutical

industry. Nat Rev Drug Discov 0123456789, (2021).

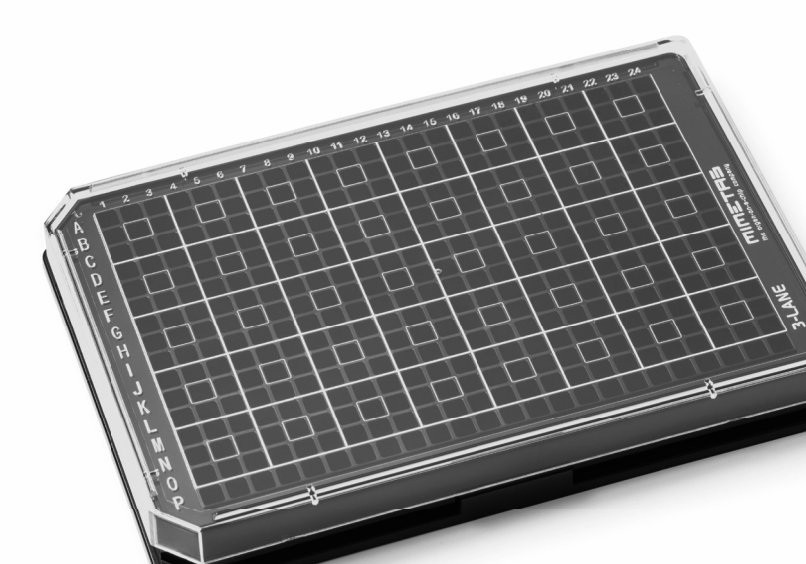
48. Dellaquila, A., Le Bao, C., Letourneur, D. & Simon-Yarza, T. In Vitro Strategies to Vascularize 3D Physiologically Relevant Models. Advanced Science vol. 8 Preprint at https://doi.org/10.1002/advs.202100798 (2021).

## Chapter 2

Interstitial Flow Recapitulates Gemcitabine Chemoresistance in A 3D Microfluidic Pancreatic Ductal Adenocarcinoma Model by Induction of Multidrug Resistance Proteins

Bart Kramer, Luuk de Haan, Marjolein Vermeer, Thomas Olivier, Thomas Hankemeier, Paul Vulto, Jos Joore, Henriëtte L. Lanz

Published in: International Journal of Molecular Sciences (2019), 20(18), 4647



## **Abstract**

Pancreatic Ductal Adenocarcinoma (PDAC) is one of the most lethal cancers due to high chemoresistance and poor vascularization which results in ineffective systemic therapy. PDAC is characterized by high intratumoural pressure, which is not captured by current 2D and 3D in vitro models. Here, we demonstrate a 3D microfluidic interstitial flow model to mimic the intratumoural pressure in PDAC. We found that subjecting the S2-028 PDAC cell line to interstitial flow inhibits the proliferation, while maintaining a high viability. We observed increased gemcitabine chemoresistance, with an almost nine-fold higher EC50 compared to monolayer culture (31 nM vs 277 nM) and an elevated expression and function of the multidrug resistance protein (MRP) family. In conclusion, we developed a 3D cell culture modality for studying intratissue pressure and flow that exhibits more predictive capabilities than conventional 2D cell culture and is less time consuming, more scalable and accessible than animal models. This increase in microphysiological relevance may support improved efficiency in the drug development pipeline.

## Introduction

The 5-year-survival rate for Pancreatic Ductal Adenocarcinoma (PDAC) is as low as 8%, which is the lowest of all solid tumours, and has little to no change in the past years despite advances in anti-cancer therapy.<sup>1</sup> Due to a lack of early detection methods and few early symptoms, most patients suffering from PDAC are diagnosed at a later stage when the disease is already advanced. While surgery would be the only curative treatment at this point, only a small number of patients are eligible for surgery, leaving the use of chemotherapeutic compounds as the only option of treatment. The chemotherapeutic compound gemcitabine is widely used to treat various solid cancers, among which PDAC. Gemcitabine inhibits DNA synthesis by acting as an analogue of cytidine, preventing chain elongation after its incorporation through blocking of DNA polymerases.<sup>2</sup> Furthermore, gemcitabine is known to induce apoptosis in pancreatic cancer cells via caspase signalling.<sup>3,4</sup> Despite its various cytotoxic effects on pancreatic cancer cells, the effect of gemcitabine on the survival of patients is modest, 5 while the side-effects are guite severe. In addition, gemcitabine remains ineffective in treating PDAC due to the characteristics of the disease. In contrast to most solid tumours, PDAC is characterized by a paucity of blood vessels resulting in systemic therapy being rendered ineffective due to a lack of delivery of the therapy.<sup>6</sup> Furthermore, the presence of a high intratumoural pressure and a corresponding inordinate interstitial flow from the tumour centre towards the tumour periphery further limits therapeutic efficacy by hampering delivery and is hypothesized to induce a higher resistance to chemotherapy in pancreatic cancer cells. In addition, the patient initially responds well to the treatment, but there is a high occurrence of acquired chemoresistance. Themoresistance in cancer is linked to the expression of Multidrug Resistance Proteins (MRPs), which are a subfamily of the ATP-binding cassette (ABC) transporters. Indeed, overexpression of MRPs has been observed in gemcitabine-resistant PDAC cell lines, which may explain the acquired chemoresistance in PDAC.8

The alarming lack of progress in the treatment of PDAC, and concomitantly, the urgent need for a better understanding of the disease, calls for the development and characterization of novel disease models. Up until now, conventional two-dimensional cell culture techniques and animal models have been used to study PDAC. However, two-dimensional cell culture is known to fail to fully recapitulate tumour biology due to a lack of physiological relevance.<sup>9</sup> Animal models are expensive, labour-intensive, and suffer from ethical as well as biological limitations.<sup>10</sup>

In order to overcome the limitations of traditional disease model systems, Organon-a-Chip systems are gaining widespread interest. <sup>11</sup> Organ-on-a-Chip microfluidic systems aim to faithfully recapitulate the physiology and microenvironment of tissues through spatial control of the tissue architecture and the addition of fluid control. These systems typically feature micrometre-sized channels that allow controlled patterning of extracellular matrices (ECMs) and cells. <sup>12</sup> Organ-on-a-Chip systems have been proven to be applicable to a wide variety of tissues, such as vasculature, <sup>13,14</sup> brain, <sup>15</sup> kidney, <sup>16</sup> and liver. <sup>17</sup>

Recently, we described the use of a high-throughput Organ-on-a-Chip platform, the OrganoPlate, for therapy response testing of breast cancer, showing the potential of the platform for three-dimensional tumour models and its application to assess the resistance of cells to chemotherapeutic agents for personalised medicine.<sup>18</sup>

Here, we set out to develop and characterize a PDAC three-dimensional cell culture model using the previously mentioned microfluidic platform to assess differences in resistance to chemotherapeutic agents under interstitial flow. First, we characterize flow profiles in the platform with the aim to recapitulate the effects of high interstitial fluid pressure in PDAC. Second, we investigate how the different flows affect a non-metastatic pancreatic cancer cell line (S2-028), <sup>19</sup> by assessing morphology, proliferation, viability, and chemoresistance. Finally, we further characterize the model using gene expression analysis and a functional

assay for the MRP family. In our discussion, we present our view on how Organon-a-Chip tissue models can potentially be used to further our understanding of PDAC progression and treatment.

## Materials and Methods

#### **Cell culture**

The S2-028 Pancreatic Ductal AdenoCarcinoma cell line (kind gift from Dr. Buchholz, Marburg University) was cultured in T-75 flasks (Corning 431464U) in DMEM (Sigma D6546) culture medium supplemented with 10% heat inactivated Fetal Bovine Serum (FBS, Gibco 16140-071) and 1% Penicillin-Streptomycin (Sigma P4333). S2-028 were used between passage number +7 till +11.

#### **OrganoPlate culture**

The three-lane OrganoPlate with 400  $\mu$ m  $\times$  220  $\mu$ m (w  $\times$  h) channels (MIMETAS 4003-400B, Leiden, The Netherlands) was used to set up the three-dimensional PDAC model. OrganoPlate ECM loading and cell seeding protocol and PhaseGuide functioning was previously described, the gel and perfusion channel lengths are 9 mm and 12.2 mm, respectively. In short, the protocol is as follows: before seeding, 50  $\mu$ L of Hank's balanced salt solution (HBSS) was dispensed into the observation window to prevent evaporation and enhance optical clarity (Figure 1A). S2-028 were trypsinized using 0.25% trypsin in phosphate-buffered saline/ethylenediaminetetraacetic acid (Gibco 15090-046) and resuspended in the appropriate volume (2.5x106 cells/mL) of ECM gel composed of 7.2 mg/mL collagen I (Corning 354249 rat tail collagen 1, 9 mg/mL), 100 mM HEPES (Gibco 15630-056), and 3.7 mg/mL Na2HCO3 (Sigma-Aldrich S5761). Two microliters of the ECM-cell suspension was dispensed in the gel inlet and incubated for 30 minutes at 37 °C allowing gelation of the ECM (Figure 1B). After gelation of the ECM, 50  $\mu$ L of DMEM 10% FCS medium was dispensed in the perfusion inlets and outlets.

Subsequently, the plate was placed in the incubator (37 °C, 5%  $\rm CO_2$ ) on a rocking platform (8-minute interval at an angle of 7°, Figure 1C). For the interstitial flow condition, the plate was placed perpendicular to the perfusion flow condition to introduce a flow through the gel channel (Figure 1D). The medium was changed three times per week.

#### Interstitial flow simulation

To study the flow profile of the interstitial flow condition, a 7.2 mg/mL collagen I gel (without cells) was loaded in the 3-lane OrganoPlate as described above. The perfusion in- and outlets were filled with 50 µL of HBSS to prevent the channels from drying out. After 24 hour incubation in the incubator (37 °C, 5% CO<sub>2</sub>), ECM filled chips were subjected to interstitial flow by pipetting a 40 µL volume difference (60 µL in the top in- and outlet of 0.5 mg/mL TRITC-Dextran 4.4 kDa (Sigma-Aldrich T1037) in HBSS, 40 µL HBSS in the bottom in- and outlet). This recreates the fluid pressure in the microfluidic chip comparable to placing an OrganoPlate® on a 7° rocking platform in the interstitial flow orientation (Figure 1C). Chips with equal volume (50 µL in the perfusion in- and outlets) were used to mimic the perfusion flow condition. Directly after applying the volume difference, a time lapse series of images were captured (interval 10 seconds for 3 minutes) on an ImageXPress XLS fluorescent microscope (Molecular Devices). Images acquired were analysed using Fiji (version 2, build 1.52e).<sup>21</sup> For the visualization of images, a lookup table was applied to map the colour scale. For quantification, regions of interest (ROIs) of the perfusion channel and the gel channel were manually drawn and the average fluorescent intensity was measured. By dividing the intensity of the gel channel by the intensity of the perfusion channel the fluorescent ratio was calculated.

Interstitial flow was further characterised using the fluorescent recovery after photobleaching (FRAP) method. After 24 hour incubation in the incubator (37 °C, 5%  $CO_2$ ), the HBSS was aspirated from the 7.2 mg/mL collagen I gel and a volume difference was created (60  $\mu$ L in the top in- and outlet, 40  $\mu$ L in the bottom in- and

outlet) using 2.5 ng/mL fluorescein (Sigma 46960) in HBSS to mimic the interstitial flow condition. After 2, 5 and 8 minutes, a spot in the middle of the gel channel was bleached with the ImageXPress Micro Confocal High-Content Imaging System (Molecular Devices) for 5 seconds with 60x magnification. Subsequently a time-series of images was captured (2 second interval for 20 seconds). Images were processed using Fiji (version 2, build 1.52) by creating a threshold image of the bleached area. The center of mass was calculated with the 'analyze particles' option (size: 1000-infinity). For each image, the shift in the center of mass per second was calculated from the original bleached image.

#### Live/dead assay

Viability of the cells was assessed at day 7 of culture in the OrganoPlate. Medium was aspirated from the cultures and replaced with a mixture of NucBlue (2 drops/mL, Life Technologies R37610), Propidium Iodide (PI, 2 drops/mL, Life Technologies R37610) and 0.5 µg/mL Calcein-AM (ThermoFisher Scientific C3099, 25 µL in each perfusion inlet and outlet). The cultures were incubated on a rocking platform (8-minute interval at an angle of 7°) for 1 hour in the incubator (37 °C, 5% CO<sub>3</sub>). Subsequently, the culture was imaged on an ImageXPress XLS fluorescent microscope (Molecular Devices). Images acquired were analysed using Fiji (version 2, build 1.52e). The number of nuclei was extracted using an approach based on morphological shape filtering using built-in tools available in Fiji. Nuclei were extracted by removing the background signal via a Rolling Ball method.<sup>22</sup> Afterwards, a threshold was applied to the remaining signal to highlight the nuclei, and a particle detection was subsequently performed to count the number of nuclei. A similar approach was used to quantify the number of PI positive cells, after which the viability was calculated by calculating the ratio of live cells (total nuclei minus PI positive cells) and total cell count.

#### **EdU** proliferation assay

The proliferation rate of day 3 cultures was assessed with the EdU Click-iT Plus assay (Thermo Fisher, C10640) according to manufacturer's protocol. Culture medium was replaced with a 50  $\mu$ M dilution of EdU in culture medium for 24 hour after which the cultures were fixed with 3.7% formaldehyde (Sigma-Aldrich 252549) in HBSS for 10 minutes, washed twice with HBSS for 5 minutes, and permeabilized with 0.3% Triton X-100 (Sigma-Aldrich T8787) in HBSS for 10 minutes, after which the HBSS was aspirated. The proliferating cells were visualized by adding 20  $\mu$ L of Click-iT Plus reaction cocktail for 30 minutes. Subsequently all DNA was visualized by adding 5  $\mu$ g/mL Hoechst 33342 (ThermoFisher H3570) for 2 hours. Z-series images were captured on the ImageXPress Micro Confocal High-Content Imaging System (Molecular Devices) and the summarized intensity-projections were saved for quantification. Images were analyzed using Fiji (version 2, build 1.52e) by measuring the average fluorescent intensity of the gel channel after background correction.

#### **Immunohistochemistry**

Cultures were fixed using 3.7% formaldehyde (Sigma-Aldrich 252549) in HBSS (Sigma-Aldrich H6648) for 20 minutes, washed twice with HBSS for 5 minutes, and permeabilized with 0.3% Triton X-100 (Sigma-Aldrich T8787) in HBSS for 10 minutes. After washing with 4% FBS in HBSS for 5 minutes, the cultures were incubated for 60 minutes with a mixture of ActinRed 555 Readyprobes (2 drops/mL, ThermoFisher R37112) and 5  $\mu$ g/mL Hoechst 33342 (ThermoFisher H3570). Z-series images were captured on the ImageXpress Micro Confocal High-Content Imaging System (Molecular Devices) and the maximum intensity-projections were used for further representation.

#### Drug exposure and viability assessment

On the third day, three-dimensional cultures were exposed to the chemother apeutic compound gemcitabine (Sigma G6423) in a concentration range (4 – 64.000 nM)

for 72 hours in the incubator (37 °C, 5%  $CO_2$ ) on a rocking platform (8-minute interval at an angle of 7°) in both perfusion settings (Figure 1D). For the two-dimensional culture exposure, the cells were grown in a 96-well plate (Corning) for 1 day until 50% confluency and exposed to the same concentration range of gemcitabine for 72 hours in the incubator (37 °C, 5%  $CO_2$ ).

#### **Enzymatic activity assessment**

The enzymatic activity of the cultures after treatment was determined using the WST-8 viability assay. The culture medium in the OrganoPlate was replaced with 25  $\mu$ L of WST-8 reagent (Sigma 96992) diluted 1:11 in HBSS in each perfusion inlet and outlet. The cultures were incubated for 2 hours in the incubator (37 °C, 5% CO<sub>2</sub>) on a rocking platform (8-minute interval at an angle of 7°) and the absorbance was measured at 450 nm using the Fluoroskan Ascent plate reader (Thermo Scientific). The measurements of the gel inlet, perfusion inlet and outlet, and observation window were adjusted for volume differences and combined. Data was normalized against the vehicle control and plotted in Prism (GraphPad Software). The nonlinear regression analysis 'log(inhibitor) vs. response – Variable slope (four parameters)' was performed to obtain the half maximal effective concentration (EC50) values.

#### qPCR

To assess the mRNA levels S2-028 OrganoPlate cultures were exposed to gemcitabine (Sigma G6423) at day 3 for 72 hours. Cells were lysed and RNA was purified using the TRIzol reagent (Thermo Fisher 15596026) with 7  $\mu$ g Rnase-free glycogen (Thermo Fisher R0551) per sample added as a carrier according to manufacturer's protocol. Four to twenty chips were pooled into 1 sample, depending on the condition to compensate for the difference in cell density between the conditions. RNA concentration was measured using a NanoDrop (Thermo Fisher) and the samples were diluted to 30 ng/ $\mu$ L with RNase-free water. cDNA synthesis was performed using M-MLV reverse transcriptase (Thermo Fisher

28025013) according to manufacturer's protocol. qPCR was performed using FastStart Essential DNA Green (Roche 06402682001) using specific primers for the different MRP genes and using TBP as housekeeping gene, see Supplementary table 1. The data was analyzed using the LightCycler software (Roche) and the  $2^{-\Delta\Delta Ct}$  method, normalizing all values to perfusion flow vehicle control per experiment.

#### MRP efflux assay

MRP transport in the microfluidic platform was measured as previously described.<sup>23</sup> Day 3 OrganoPlate cultures were exposed to 0 or 50 nM gemcitabine. After 72 hours of drug exposure, the medium was replaced with 25 µL 1.25 µM Cell tracker reagent 5-chloromethylfluorescein diacetate (CMFDA, Molecular Probes) in Opti-HBSS (1:2 Opti-MEM (Gibco) and HBSS) in all perfusion in and outlets with and without inhibitor (50 µM MK571 (Sigma-Aldrich)). The culture was incubated for 30 minutes in the incubator (37 °C, 5% CO<sub>3</sub>) on a rocking platform (8-minute interval at an angle of 7° in the perfusion flow orientation), after which the observation window reservoir was used to cool down the culture with 50 µl 4°C HBSS. The inchip assay solutions were replaced by 50µl of 4°C inhibition cocktail (10 µM MK571, 10 μM Ko143 (Sigma-Aldrich) and 5 μg/mL Hoechst 33342). The inhibition cocktail was incubated for 30 minutes at RT. Z-slices were imaged using the ImageXPress Micro Confocal High-Content Imaging System (Molecular Devices). The data was analyzed using Fiji to calculate the intensity of the sum-projection of the z-slices of the FITC channel for the amount of CMFDA. The number of nuclei was obtained in the same manner as described in the live/dead assay section. Relative intensity was calculated by first subtracting the background intensity from the measured intensity and subsequently dividing by the number of cells. Statistics were done with the 'multiple 2-sided t-tests' function in GraphPad Prism.

## Results

#### Interstitial flow modelling in a microfluidic platform

Regular two-dimensional tissue cultures do not allow the incorporation of interstitial flow. In order to be able to assess the response of S2-028 PDAC cells to different flow orientations, a three-dimensional tissue model was developed in a microfluidic culture platform. The microfluidic culture platform, the OrganoPlate, is based on a 384-well microtiter plate format. The glass bottom contains 40 microfluidic chips (Figure 1A), with each microfluidic chip positioned under 9 wells in a 3x3 grid. A single chip consists of 3 channels: a centre channel ('gel channel') which is used to load an extracellular matrix (ECM) and 2 adjacent 'perfusion channels', which are loaded with medium. Each channel is connected to 2 wells of the microtiter plate, which act as medium reservoirs. The channels merge together in the centre of the chip and three lanes are marked by 2 phaseguides,<sup>24</sup> small ridges that form a capillary pressure barrier which confine the ECM precursor mixed with cells to the centre lane. Upon gelation, culture media is added to the exterior channels, resulting in a stratified setup without physical barriers between the channels, such as artificial membranes (Figure 1B). In order to generate flow parallel to the ECM lane with PDAC cells, the plate is placed on a tilted rocking platform, creating a height, and thus pressure, difference between the plate wells connected to a single channel ('Perfusion flow', Figure 1C). In order to generate flow through the ECM lane with PDAC cells, the plate is placed on the rocking platform perpendicular to the position in the perfusion flow condition, thus mimicking interstitial flow ('Interstitial flow', Figure 1D). The rocking platform switches between inverted 7° angles of inclination every 8 minutes to sustain medium flow over longer periods of time.

To visualize and quantify interstitial flow through the ECM gel, a fluorescent dye, coupled to 4.4kDa TRITC-dextran, was introduced into the top perfusion channel of a device containing a gelated ECM in the gel channel. The pressure difference,

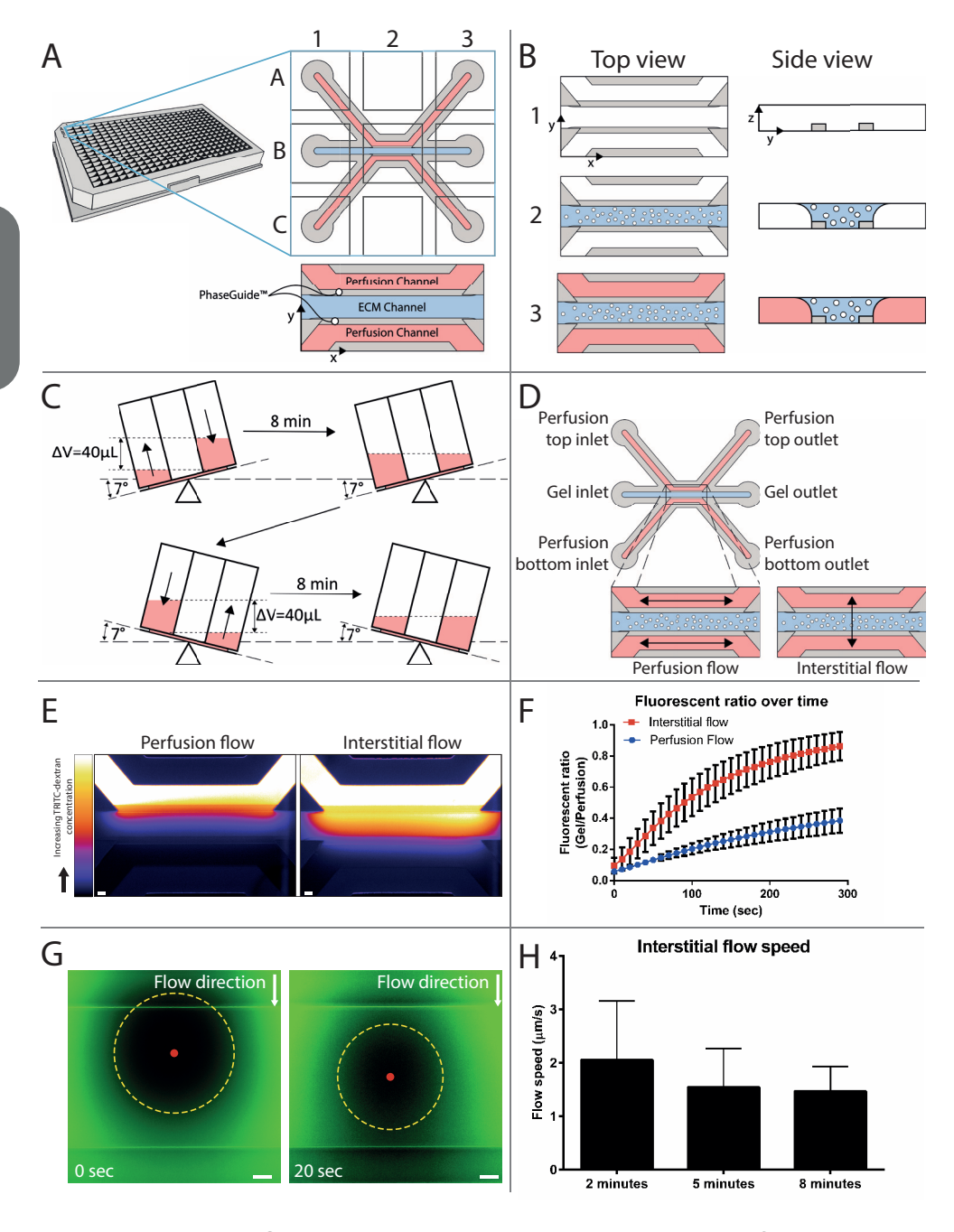


**Figure 1. Interstitial flow-on-a-chip characterization. (A)** The microfluidic microtiter plate 'OrganoPlate' used for 3D cell culture, based on a 384 well plate interface with 40 microfluidic chips integrated in the bottom. A gel channel (blue) holds the extracellular

### Interstitial flow recapitulates chemoresistance in PDAC | 39

matrix (ECM) in place through the PhaseGuide's pressure barrier function. (B) Cells can be introduced in the middle lane (gel channel) to create a 3D cell culture with interstitial flow in a collagen ECM. Following addition of medium in the adjacent channels (B2), the plate is placed on a tilted rocking platform with a rocking interval of 8 minutes (C) that creates a height difference (which is equivalent to a 40 µL volume difference), resulting in gravity driven, continuous and bi-directional perfusion of the cultures (D, Perfusion flow). By placing the plate perpendicular to the perfusion flow condition, the flow is directed through the ECM gel in an interstitial flow (D, Interstitial flow). The interstitial flow was visualized by introducing a medium volume containing a fluorescent dye coupled to a dextran molecule in the top perfusion channel, thus, creating a pressure difference between the perfusion channels, image is acquired 2 min after introduction of the dye, scale bar = 100  $\mu$ m). (E) Quantification was performed by calculation of the fluorescence ratio in the top perfusion and gel channels (F, plot represents average  $\pm$ SD, n = 12-15 technical replicates). More detailed interstitial flow measurements within the ECM gel were performed using FRAP. (G) Images of the photobleached spot at two consecutive timepoints. The movement of the bleached spot (yellow circle) was tracked by the displacement of its center of mass (red dot). (H) The movement of the spot was calculated as an indication of the flow speed over time (n = 17 technical replicates, bar plots represent average + SD, scale bar =  $50 \mu m$ ).

which is normally generated by placing the plate on a tilted rocker, was simulated by applying a 40 µL volume difference between the top and bottom in- and outlet. The distribution of the fluorescent signal is shown in Figure 1E. By calculating the ratio over time between the average fluorescent intensity in the ECM gel and in the perfusion channel, a measure for flow in the ECM gel is obtained (Figure 1F). A 3.3-fold faster increase of this ratio was observed for the interstitial flow condition as compared to the parallel flow condition, indicating a higher flow speed through the ECM gel. To quantify the interstitial flow speed, we utilized the Fluorescence Recovery After Photobleaching (FRAP) method. In short, a localized spot within the gel channel was bleached using a fluorescent light beam and its movement was measured by following the centre of mass using imaging and image-processing techniques (Figure 1G). Similar volumes of fluorescent dye-containing solution were applied as in Figure 1E and the flow speed was measured after 2, 5 and 8 minutes, the latter time interval being the interval of the rocking platform. The average flow speed varied between 1.5 and 2 µm/s (Figure 1H), which is in the range of interstitial flow speeds found in vivo.<sup>25</sup>

### Interstitial flow inhibits proliferation of PDAC cells

In order to study the influence of interstitial flow on pancreatic cancer cells, the non-metastatic pancreatic ductal adenocarcinoma (PDAC) cell-line S2-028 was loaded in collagen ECM and subjected to either the Perfusion or Interstitial flow profile (Figure 1D). Rapid proliferation and spheroid formation were observed when the cells were subjected to perfusion flow (Figure 2A, top row). When the cells in ECM were subjected to interstitial flow, smaller spheroids were observed from day 3 onwards (Figure 2A, bottom row). Immunofluorescent staining of the PDAC cells in the ECM channel at day 7 confirms this observation (Figure 2A, right). Figure 2A also shows that cells cultured with perfusion flow seemed to contract the ECM, in contrast to cells cultured with interstitial flow. Immunofluorescent viability staining for live (Calcein-AM) and dead (Propidium Iodide) cells (Figure 2B) showed a decreased cell count in the interstitial flow condition (Figure 2C), whereas no difference was observed in the overall viability of cells (Figure 2D), suggesting a decreased proliferation rate as a result of interstitial flow. Similarly, the PDAC cells showed a lower EdU incorporation under interstitial flow as compared to the perfusion flow condition, also suggesting a decreased proliferation rate (Figure 2E-F).

# PDAC cells are more resistant to gemcitabine in the presence of interstitial flow

The chemotherapeutic compound gemcitabine remains a cornerstone of PDAC treatment in all stages of the disease, although its contribution of survival is negligible due to resistance of the tumour.<sup>26</sup> Particularly in PDAC, the tumour microenvironment plays a crucial role in therapy resistance with a suggested role of matrix deposition blocking delivery of the chemotherapeutic agent to the tumour cells by increasing interstitial fluid pressure.<sup>27</sup> Gemcitabine acts as an analogue of cytidine and its incorporation results in chain termination.

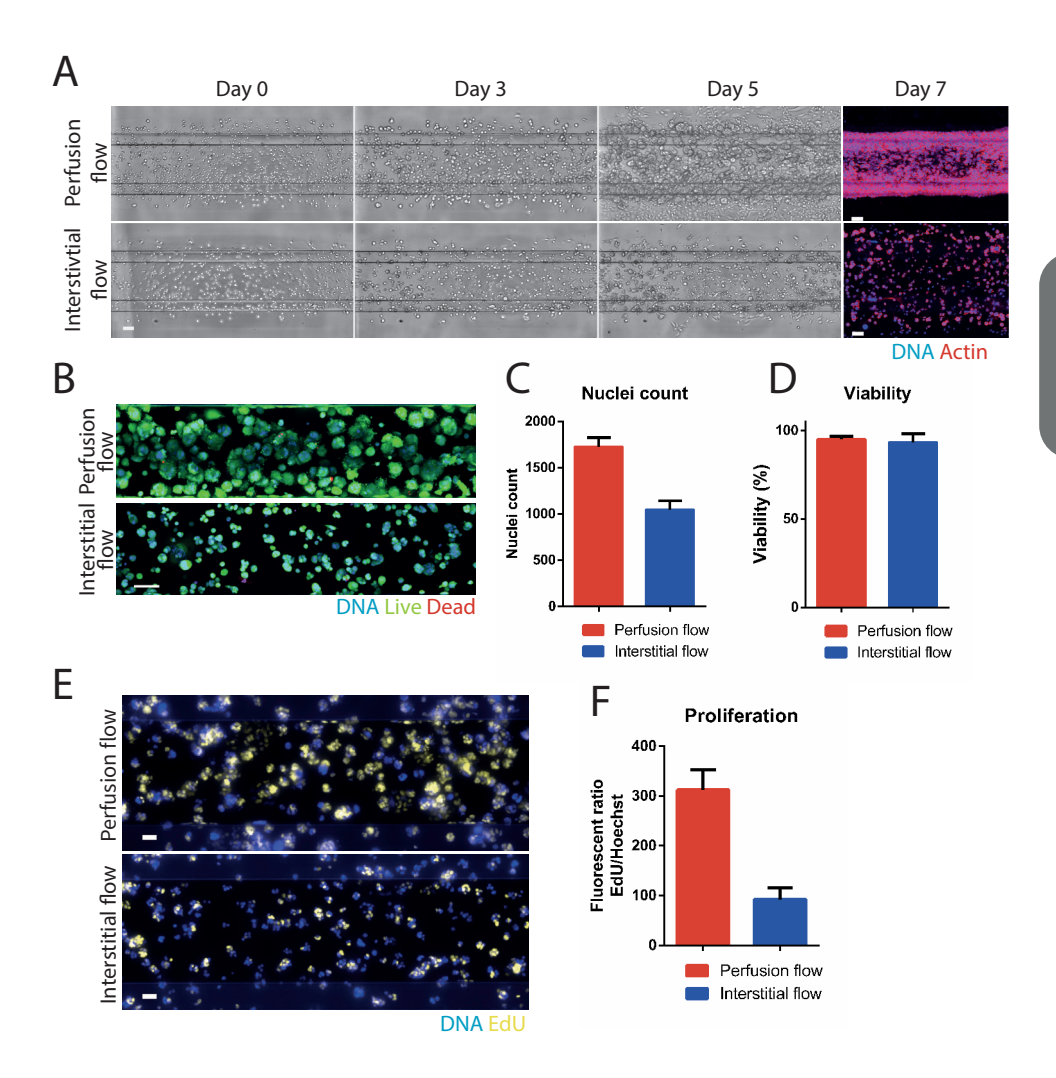


**Figure 2. Interstitial flow has pronounced effects on S2-028 cells. (A)** 2.5 million S2-028 cells/mL were loaded in the 3-lane OrganoPlate and cultured under different flow conditions. Right: Immunofluorescent visualization for actin and DNA (Hoechst) of the ECM compartment at day 7. A maximum projection of z-stacks is shown. **(B)** Live (Calcein-AM / dead (propidium lodide) staining at day 5. Representative images are shown for both flow types. **(C-D)**, Quantification of the number of nuclei and viability (n = 10-18 technical replicates). Bar plot represents average + SD. **(E-F)**, The proliferation rate of the S2-028 cell line was assessed with an EdU incorporation assay, determining average EdU fluorescence, normalized for the amount of DNA using the Hoechst signal (n = 14 technical replicates, bar plot represents average + SD). Scale bar in fig. A-C is 100 μm, E is 50 μm.

Furthermore, gemcitabine enhances its own activity by depleting the intracellular pool of cytosine triphosphates and induces apoptosis through caspase signalling. To assess the effect of different flow directions on the cytotoxic effect of gemcitabine, 72-hour dose response curves of gemcitabine were obtained. The results showed an EC50 of 85 nM and 277 nM for the perfusion and interstitial flow models, respectively, representing a 3-fold lower sensitivity with interstitial flow (Figure 3). When compared to the 31 nM EC50 in 2D monolayers, EC50 values are almost 3- and 9-fold higher for perfusion and interstitial flow in 3D cultures, respectively. Representative phase contrast images of S2-028 cultures after 72-hour exposure to a concentration range of gemcitabine can be found in Supplementary Figure 1.

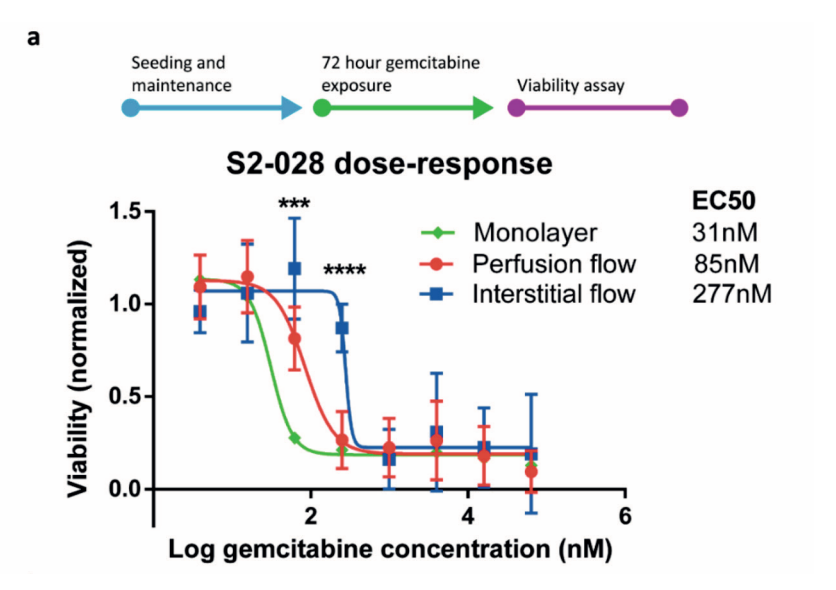
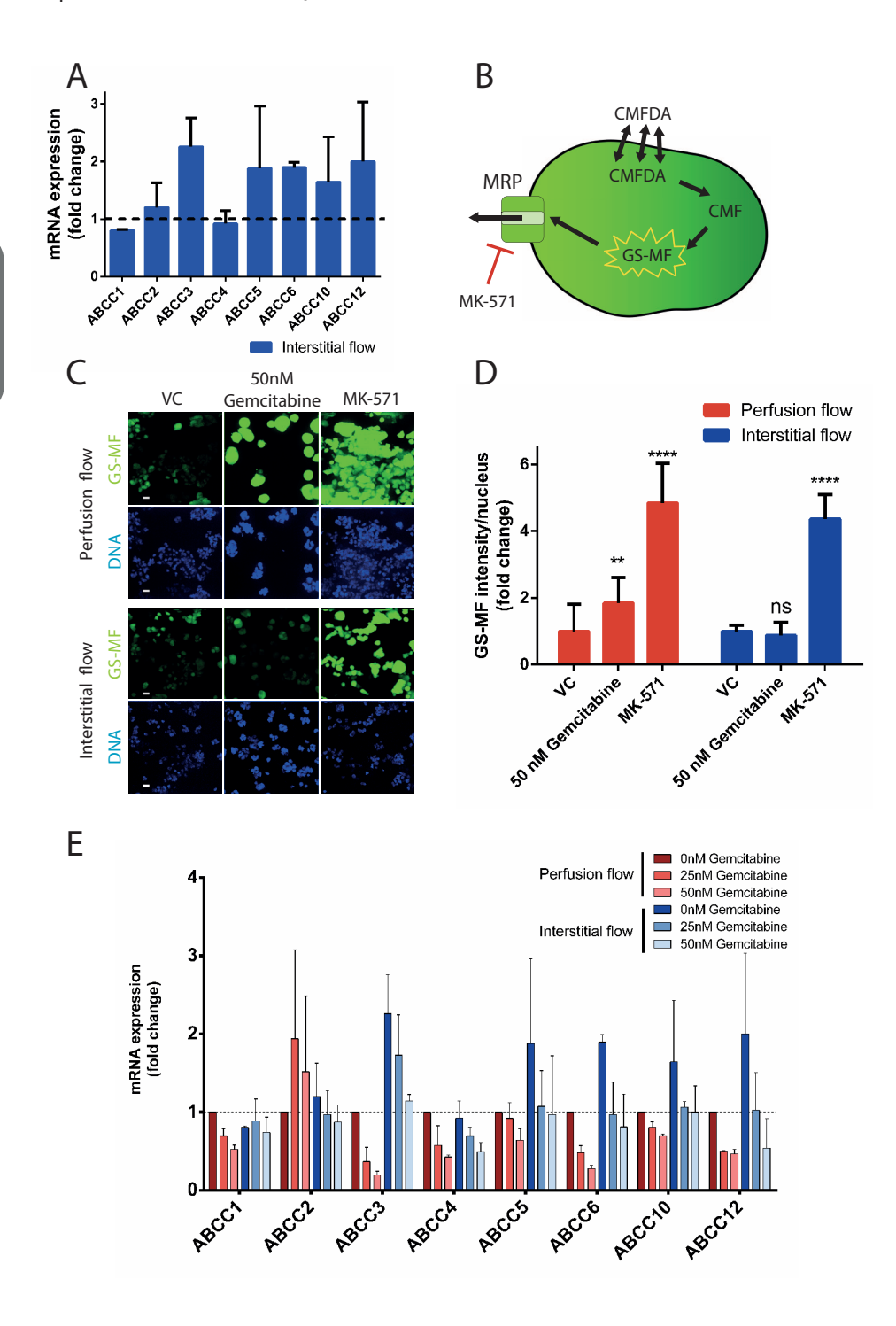


Figure 3. PDAC cells cultured with interstitial flow are less responsive to gemcitabine. S2-028 cultures were exposed to a dose-range of gemcitabine for 72 hours. Shown are dose-response curves for the two-dimensional monolayer and both flow models with the EC50 values extracted from these curves. N=3 independent experiments for both 3D models and N=2 for the monolayer with n=4-11 technical replicates for each iteration. Shown is the average value normalized to the vehicle control  $\pm$  SD. Statistical test: multiple 2-sided T-test, shown is significance for perfusion flow vs interstitial flow \*\*\* p<0.001, \*\*\*\* p<0.0001.

#### MRP protein function is altered under interstitial flow

Development of tumour resistance to gemcitabine critically limits the efficacy of this cornerstone treatment of pancreatic cancer.<sup>5</sup> One class of transporters associated with cancer resistance is the multidrug resistance protein (MRP) family.<sup>28</sup> To investigate whether our 3D culture flow models can be used to assess mechanisms of acquired chemoresistance, the models were subjected to a gene expression analysis of MRP transporters and a functional MRP assay. Gene expression analysis revealed that 5 out of 8 MRP genes showed elevated mRNA expression levels in interstitial flow compared to perfusion flow (Figure 4A). A functional CMFDA efflux assay was performed to evaluate the effects of perfusion and interstitial flow models on the activity of MRP transporters in the presence of gemcitabine. The principle of the assay is depicted in Figure 4B. In short, CMFDA, a compound that can freely pass through cell membranes, is metabolized to 5-chloromethylfluorescein (CMF) and then further metabolized to carboxylfluorescein-glutathione (GS-MF, a fluorescent cell membrane impermeant compound). GS-MF is a substrate for MRPs that transport the compound out of the cell, therefore its fluorescent signal is inversely related to MRP activity.<sup>29</sup> In cultures subjected to interstitial flow, exposure to 50 µM gemcitabine yielded no significant change in MRP activity, whereas perfusion flow resulted in a significant (1.8-fold) increase in GS-MF signal, suggesting a decrease in MRP activity (Figure 4C-D). No significant difference was observed between perfusion flow and interstitial flow 3D models when MRP transporters were blocked with the pharmacological inhibitor MK-571 (4.8 and 4.3-fold, respectively). Our results strongly suggest that in these models, interstitial flow contributes to gemcitabine resistance by increasing its inherent activation of efflux pumps.



**Figure 4. MRP function is increased by interstitial flow. (A)** mRNA expression levels in S2-028 cells for 8 ABCC genes. Gene expression levels were normalized to the reference gene, TBP, and a fold change difference compared to S2-028 cultures under perfusion flow was calculated (N = 2 independent experiments, n = 2 technical replicates, bar plot represents average + SD). **(B)** Principle of the MRP efflux assay. **(C)** Representative images of intracellular accumulation of GS-MF in S2-028 cells (scalebar =  $50 \mu m$ ). **(D)** quantification of the fold change of the average fluorescent intensity per nucleus of the fluorescent GS-MF signal. Values were normalized to vehicle control (VC) per experiment (N = 2 independent experiments, n = 7-8 technical replicates). Significance was calculated with a two-sided t-test (ns = not significant, \*\* p<0.01, \*\*\*\*\*\* p<0.0001).

## Discussion

A substantial amount of cancer research aimed at finding new targets and preclinical drug testing is performed in conventional 2D cell culture and animal models. Typically, 2D cell culture models offer higher throughput and lower cost, but are less physiologically relevant and known to be unpredictive.<sup>30</sup> Animal models, on the other hand, offer tissue environments more representative of the human body, but have various biological and ethical limitations, are expensive and labour intensive and often lack predictivity.<sup>9</sup>

To alleviate the need for better models for cancer research, scientists increasingly embrace 3D tissue culture in extracellular matrices (ECMs). The culturing of cells in 3D is known to be biologically more relevant as compared to conventional 2D cell culture. For example, it has previously been found that cultures of breast cancer cells respond differently to chemotherapeutic compounds when cultured in 3D compared to 2D, most likely better reflecting in vivo efficacies in patients. In this study, we observed that the EC50 value for gemcitabine increases threefold when tested on cells cultured in 3D compared to cells cultured as a monolayer, which is closer to the plasma concentration of gemcitabine found in PDAC patients. Thus, the development of novel 3D models that capture specific characteristics of PDAC are likely to spur the development of novel therapies against this disease.

Interestingly, PDAC is characterized by a high intratumoural fluid pressure, a characteristic which is not captured by existing in vitro PDAC models. In this

report, we describe a novel microfluidic 3D cell culture approach to develop and characterize interstitial flow models for PDAC to mimic intratumoural fluid pressure, using the pancreatic cancer cell line S2-028 embedded in ECM gel. We observed increased chemoresistance of S2-028 cells cultured in 3D compared monolayer cultures. Interestingly, subjecting 3D cultures of S2-028 cells to a flow profile mimicking interstitial flow in PDAC had pronounced effects on cell morphology and proliferation, without affecting viability. Furthermore, the 3D PDAC cultures were less responsive to gemcitabine treatment when subjected to interstitial flow.

Since gemcitabine acts as an analogue of cytidine and exerts its cytotoxic effect by being incorporated into the DNA of a replicating cell, it stands to reason that slower proliferating cells are affected less by this chemotherapeutic compound. However, it seems unlikely that slower proliferation singularly accounts for the significant increase in chemoresistance observed, as gemcitabine is known to have multiple cytotoxic effects on target cells, e.g. induction of apoptosis via caspase signalling.33 In addition, Hagmann et al. observed an increased expression of multidrug resistance protein 5 (MRP5) in gemcitabine resistant pancreatic cancer cell line.<sup>34</sup> To investigate this potential, additional mechanism for the increased resistance to gemcitabine with the interstitial flow model, we focussed on the expression and function of the family of MRP transporters. In these experiments, we observed a marked increase in the mRNA expression of 5 MRPs when PDAC cells were subjected to interstitial flow. These results strongly suggest that flowinduced MRP expression contributes to our observed increase in chemoresistance by elevating efflux transport of the drug.<sup>35–37</sup> This notion is further substantiated by our observation that interstitial flow appears to neutralize an inherent deactivation of MRP activity by gemcitabine, which we observed under perfusion flow. We hypothesize that the apparent increase in MRP activity is caused by an even further increase of MRP expression after exposure to gemcitabine under interstitial flow (Supplementary Figure 2). Although these preliminary results need further investigation, they hint towards an interesting additional role of interstitial

## Interstitial flow recapitulates chemoresistance in PDAC | 47

flow in establishing gemcitabine resistance. Although the family of MRPs are known to be involved in the acquisition of chemoresistance by cancer cells, the mechanism underlying this process remains enigmatic. Promoter methylation of the ABCC genes is possibly involved, however these studies have been performed using monolayers of pancreatic cancer cells and should be verified using more relevant three dimensional models.<sup>38</sup>

Interstitial pressure and associated interstitial flow, being hallmarks of PDAC, are bound to have other profound effects on the cancer cells that contribute to PDAC pathogenesis, in addition to their effects on MRP function and expression. For example, interstitial flow has been linked to the migratory behaviour of cancer cells in biological as well as mathematical models.<sup>39</sup> These results suggest there are competing tumour cell migration mechanisms occurring due to interstitial flow, a CCR7-dependent mechanism that induces downstream migration and a CCR7-independent mechanism that promotes cells to migrate upstream. Although flow in our model is bidirectional due to the utilization of a pump-free rocker system, it would of interest to test whether expression of genes previously implicated to affect migration in cancer, like EPCAM and integrin- $\beta 4$ ,<sup>40</sup> is affected in our interstitial flow model.

In conclusion, we developed the basis for a 3D cell culture model for PDAC using a microfluidic platform. We have demonstrated the effects of interstitial flow on the drug response of perfused 3D cell cultures of S2-028 cells, a non-metastatic pancreatic cancer cell line. While our current model does not yet fully capture the in vivo complexity of PDAC, it likely exhibits higher predictive capabilities than conventional 2D cell culture and is less time consuming, more scalable and more accessible in comparison to animal models. Drug screening on monolayers is very likely to result in an overestimation of the effects of chemotherapeutics, as is evident from our study. Furthermore, we showed that our model is amenable to interrogation by imaging, functional assays and gene expression analysis. Finally, containing as much as 40 chips on a microplate footprint, the OrganoPlate offers

a high-throughput platform for predictive drug testing and could potentially even be used for personalized therapy selection. Thus, we strongly believe that models presented here point the way towards valuable tools for the search for novel therapies against PDAC.

#### **Acknowledgements**

We thank Dr. Buchholz (Marburg University) for supplying the S2-028 cell line, Mr. Frederik Schavemaker for the artwork and Ms. Haley Ehlers for proofreading.

### **Funding**

This project has received funding from the European Union's Seventh Framework Programme for research, technological development and demonstration under grant agreement no 602783.

#### **Competing interests**

Jos Joore, Paul Vulto and Thomas Hankemeier have ownership interest in Mimetas B.V, which has developed the OrganoPlate technology reported in this publication. Bart Kramer, Luuk de Haan, Marjolein Vermeer, Thomas Olivier and Henriette Lanz are employees of Mimetas B.V. The OrganoPlate is a registered trademark of Mimetas B.V.

# References

- 1. Ghaneh, P., Costello, E. & Neoptolemos, J. P. Biology and management of pancreatic cancer. Postgraduate Medical Journal 84, 478–497 (2008).
- 2. Plunkett, W. et al. Gemcitabine: metabolism, mechanisms of action, and self-potentiation. Seminars in oncology 22, 3–10 (1995).
- 3. Chandler, N. M., Canete, J. J. & Callery, M. P. Caspase-3 drives apoptosis in pancreatic cancer cells after treatment with gemcitabine. Journal of Gastrointestinal Surgery 8, 1072–1078 (2004).
- 4. Habiro, A. et al. Involvement of p38 mitogen-activated protein kinase in gemcitabine-induced apoptosis in human pancreatic cancer cells. Biochemical and Biophysical Research Communications 316, 71–77 (2004).
- 5. Amrutkar, M. & Gladhaug, I. P. Pancreatic cancer chemoresistance to gemcitabine. Cancers 9, 1–23 (2017).
- 6. Olive, K. P. et al. Inhibition of Hedgehog signaling enhances delivery of chemotherapy in a mouse model of pancreatic cancer. Science (New York, N.Y.) 324, 1457–1461 (2009).
- 7. Munson, J. M. & Shieh, A. C. Interstitial fluid flow in cancer: implications for disease progression and treatment. 317–328 (2014).
- 8. Dhayat, S. A. et al. MicroRNA profiling implies new markers of gemcitabine chemoresistance in mutant p53 pancreatic ductal adenocarcinoma. PLoS ONE 10, (2015).
- 9. Hoarau-Véchot, J., Rafii, A., Touboul, C. & Pasquier, J. Halfway between 2D and animal models: Are 3D cultures the ideal tool to study cancer-microenvironment interactions? International Journal of Molecular Sciences 19, (2018).
- 10. Cekanova, M. & Rathore, K. DDDT-49584-animal-models-of-cancer---utility-and-limitations. Development and Therapy 8, 1911–1922 (2014).
- 11. Zhang, B., Korolj, A., Lai, B. F. L. & Radisic, M. Advances in Organ-on-a-Chip engineering. Nature Reviews Materials 3, 257–278 (2018).
- 12. Bhatia, S. N. & Ingber, D. E. Microfluidic organs-on-chips. Nature Biotechnology 32, 760–772 (2014).
- 13. van Duinen, V. et al. High-throughput permeability assay in vitro on perfused 3D microvessels. Circulation Research submitted, (2017).
- 14. Buchanan, C. F., Verbridge, S. S., Vlachos, P. P. & Rylander, M. N. Flow shear stress regulates endothelial barrier function and expression of angiogenic factors in a 3D microfluidic tumor vascular model. Cell Adhesion and Migration 8, 517–524 (2014).
- 15. Wevers, N. R. et al. High-throughput compound evaluation on 3D networks of neurons and glia in a microfluidic platform. Scientific Reports 6, 38856 (2016).
- 16. Wilmer, M. J. et al. Kidney-on-a-Chip Technology for Drug-Induced Nephrotoxicity Screening. Trends in Biotechnology xx, 1–15 (2015).
- 17. Åu, S. H., Chamberlain, M. D., Mahesh, S., Sefton, M. V. & Wheeler, A. R. Hepatic organoids for microfluidic drug screening. Lab on a chip 14, 3290–9 (2014).
- 18. Lanz, H. L. et al. Therapy response testing of breast cancer in a 3D high-throughput perfused microfluidic platform. BMC Cancer 17, 709 (2017).
- 19. Iwamura, T., Katsuki, T. & Ide, K. Establishment and characterization of a human pancreatic cancer cell line (SUIT-2) producing carcinoembryonic antigen and carbohydrate antigen 19-9. Japanese journal of cancer research: Gann vol. 78 (1987).
- 20. Trietsch, S. J., Iśraëls, G. D., Joore, J., Hankemeier, T. & Vulto, P. Microfluidic titer plate for stratified 3D cell culture. Lab on a Chip 13, 3548–3554 (2013).
- 21. Schindelin, J. et al. Fiji: An open-source platform for biological-image analysis. Nature Methods 9, 676–682 (2012).
- 22. Sternberg. Biomedical Image Processing. Computer 16, 22–34 (1983).
- 23. Vriend, J. et al. Screening of Drug-Transporter Interactions in a 3D Microfluidic Renal Proximal Tubule on a Chip. The AAPS Journal 20, (2018).

24. Vulto, P. et al. Phaseguides: a paradigm shift in microfluidic priming and emptying.

Lab on a chip 11, 1596–602 (2011).

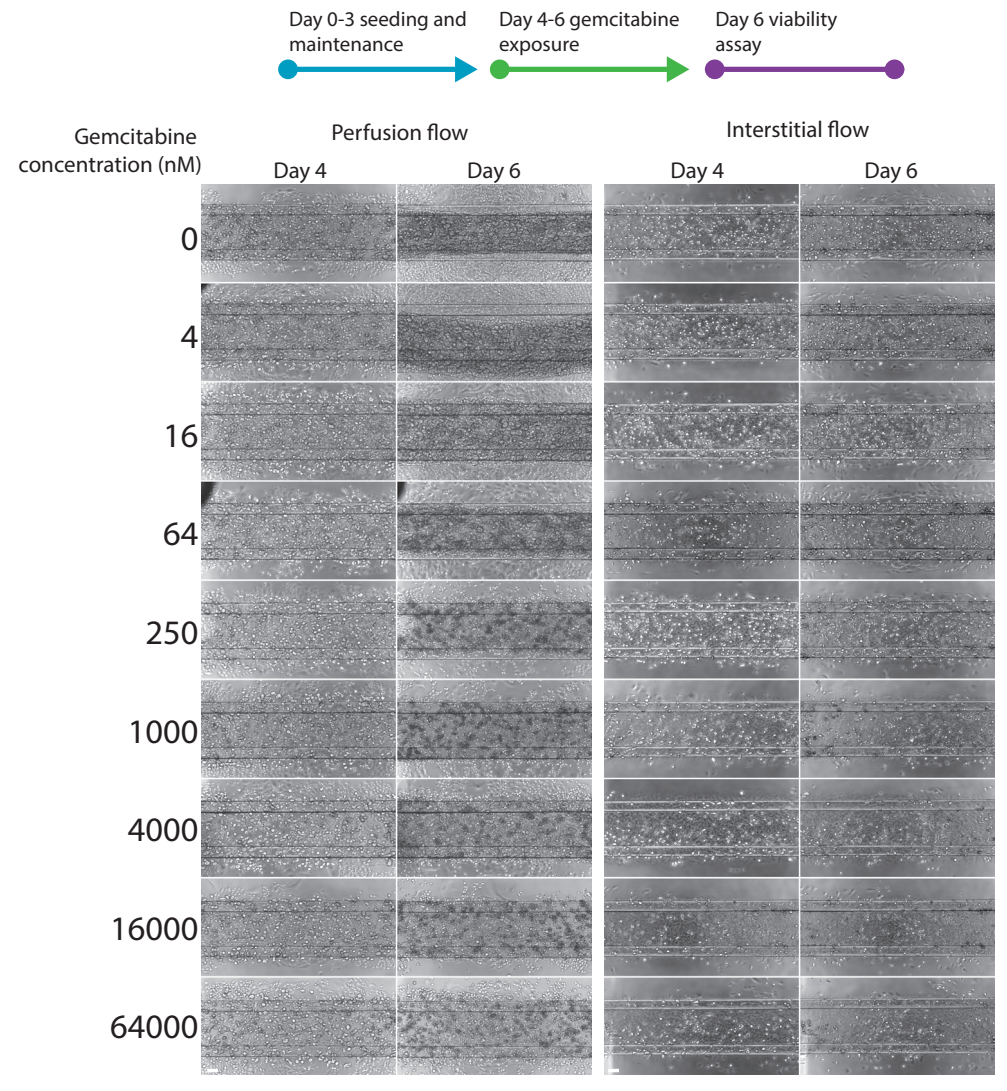
25. Dafni, H., Israely, T., Bhujwalla, Z. M., Benjamin, L. E. & Neeman, M. Overexpression of vascular endothelial growth factor 165 drives peritumor interstitial convection and induces lymphatic drain: Magnetic resonance imaging, confocal microscopy, and histological tracking of triple-labeled albumin. Cancer Research 62, 6731–6739 (2002).

26. Amrutkar, M. & Gladhaug, I. P. Pancreatic cancer chemoresistance to gemcitabine.

Cancers 9, 1-23 (2017).

- 27. Miyamoto, H. et al. Tumor-Stroma Interaction of Human Pancreatic Cancer: Acquired Resistance to Anticancer Drugs and Proliferation Regulation Is Dependent on Extracellular Matrix Proteins. Pancreas 28, 38–44 (2004).
- 28. Szakács, G., Paterson, J. K., Ludwig, J. A., Booth-Genthe, C. & Gottesman, M. M. Targeting multidrug resistance in cancer. Nature Reviews Drug Discovery 5, 219–234 (2006).
- 29. Gutmann, H. et al. Modulation of multidrug resistance protein expression in porcine brain capillary endothelial cells in vitro. Drug Metabolism and Disposition 27, 937–941 (1999).
- 30. Fang, Y. & Eglen, R. M. Three-Dimensional Cell Cultures in Drug Discovery and Development. SLAS Discovery 22, 456–472 (2017).
- 31. Abbott, A. Cell culture: biology's new dimension. Nature vol. 424 870–872 Preprint at https://doi.org/10.1038/424870a (2003).
- 32. Jiang, X., Galettis, P., Links, M., Mitchell, P. L. & McLachlan, A. J. Population pharmacokinetics of gemcitabine and its metabolite in patients with cancer: Effect of oxaliplatin and infusion rate. British Journal of Clinical Pharmacology 65, 326–333 (2008).
- 33. Jiang, P. H., Motoo, Y., Sawabu, N. & Minamoto, T. Effect of gemcitabine on the expression of apoptosis-related genes in human pancreatic cancer cells. World Journal of Gastroenterology 12, 1597–1602 (2006).
- 34. Hagmann, W., Jesnowski, R. & Löhr, J. M. Interdependence of Gemcitabine Treatment, Transporter Expression, and Resistance in Human Pancreatic Carcinoma Cells. Neoplasia 12, 740–747 (2015).
- 35. Rudin, D. et al. Gemcitabine Cytotoxicity: Interaction of Efflux and Deamination. Journal of drug metabolism & toxicology 2, 1–10 (2011).
- 36. Falasca, M. & Linton, K. J. Investigational ABC transporter inhibitors. Expert opinion on investigational drugs 21, 657–666 (2012).
- 37. Chen, Z.-S. & Tiwari, A. K. Multidrug resistance proteins (MRPs/ABCCs) in cancer chemotherapy and genetic diseases. The FEBS journal 278, 3226–3245 (2011).
- 38. Yao, Ĺ. et al. Dynamic quantitative detection of ABC transporter family promoter methylation by MS-HRM for predicting MDR in pancreatic cancer. Oncology Letters 15, 5602–5610 (2018).
- 39. Waldeland, J. O. & Evje, S. Competing tumor cell migration mechanisms caused by interstitial fluid flow. Journal of Biomechanics 81, 22–35 (2018).
- 40. Banyard, J. et al. Identification of genes regulating migration and invasion using a new model of metastatic prostate cancer. BMC cancer 14, 387 (2014).

# Supplementary materials



Supplementary Figure 1. Phase contrast images of S2-028 cell line after 72 hour gemcitabine exposure under perfusion or interstitial flow. Decrease in cell density and cell death can be observed in the perfusion flow condition upwards from 64 nM gemcitabine. When S2-028 cells are cultured under interstitial flow these effects are observed upwards from 250 nM gemcitabine. Scalebar =  $100 \, \mu m$ 

Gene	Forward primer	Reverse primer	
TBP	TGCACAGGAGCCAAGAGTGAA	CACATCACAGCTCCCCACCA	
ABCC1	GCCGAAGGAGAGATCATC	AACCCGAAAACAAACAGG	
ABCC2	AGAGCTGGCCCTTGTACTCA	AGGGACAGGAACCAGGAGTT	
ABCC3	GTGGGGATCAGACAGAGAT	TATCGGCATCACTGTAAACA	
ABCC4	TGTTTGATGCACACCAGGAT	GACAAACATGGCACAGATGG	
ABCC5	CAGCCAGTCCTCACATCA	GAAGCCCTCTTGTCTTTTT	
ABCC6	AGGAGGCCCGAGCTTAGAC	CCTGCCGTATTGGATGCTGT	
ABCC10	GTCCAGATTACATCCTACCCTGC	GCCAACACCTCTAGCCCTATG	
ABCC12	ATGCGGTTGTCACTGAAG	GTTGCCTCATCCATAATAAGAAT	

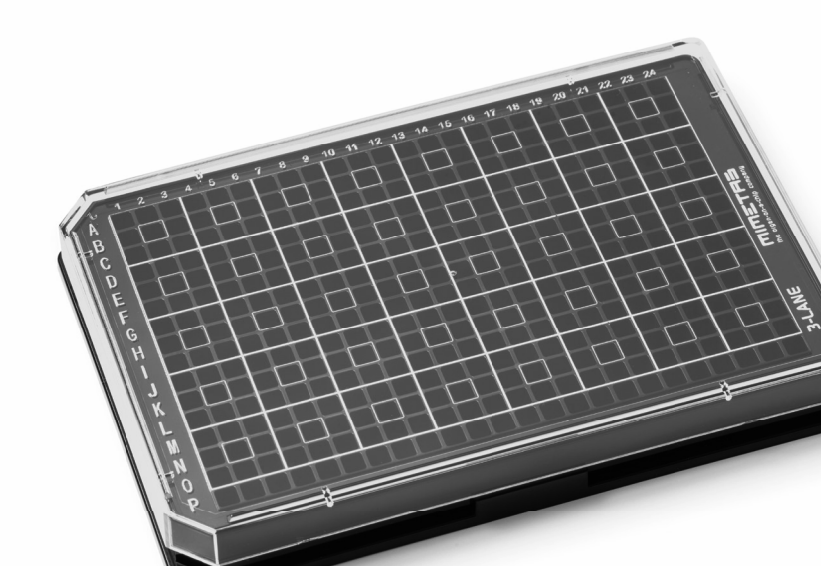
Supplementary table 1. Primer sequences used for qPCR

# Chapter 3

3D human microvessel-on-a-Chip model for studying monocyte-toendothelium adhesion under flow – application in systems toxicology

Carine Poussin\*, Bart Kramer\*, Henriette L. Lanz\*, Angelique van den Heuvel, Alexandra Laurent, Thomas Olivierb, Marjolein Vermeer, Dariusz Peric, Karine Baumer, Rémi Dulize, Emmanuel Guedj, Nikolai V. Ivanov, Manuel C. Peitsch, Julia Hoeng, and Jos Joore

Published in: Alternatives for Animal Experimentation (2020) 37



# **Abstract**

Lifestyle and genetic factors can lead to the development of atherosclerosis and, ultimately, cardiovascular adverse events. Rodent models are commonly used to investigate mechanism(s) of atherogenesis. However, the 3Rs principles, aiming to limit animal testing, encourage the scientific community to develop new physiologically relevant in vitro alternatives. Leveraging the 96-chip Organo Plate®, a microfluidic platform, we have established a three-dimensional (3D) model of endothelial microvessels-on-a-chip under flow using primary human coronary arterial endothelial cells. As functional readout, we have set up an assay to measure the adhesion of monocytes to the lumen of perfused microvessels. For monitoring molecular changes in microvessels, we have established the staining and quantification of specific protein markers of inflammation and oxidative stress using high content imaging, as well as analyzed transcriptome changes using microarrays. To demonstrate its usefulness in systems toxicology, we leveraged our 3D vasculature-on-a-chip model to assess the impact of the Tobacco Heating System (THS) 2.2, a candidate modified risk tobacco product, and the 3R4F reference cigarette on the adhesion of monocytic cells to endothelial microvessels. Our results show that THS 2.2 aerosol-conditioned medium had a reduced effect on monocyte-endothelium adhesion compared with 3R4F smoke-conditioned medium. In conclusion, we have established a relevant 3D vasculature-on-achip model for investigating leukocyte-endothelial microvessel adhesion. A case study illustrates how the model can be used for product testing in the context of systems toxicology-based risk assessment. The current model and its potential further development options also open perspectives of applications in vascular disease research and drug discovery.

## Introduction

The endothelium is a single layer of cells at the interface between circulating blood and organ tissues that plays critical roles in vascular processes, such as barrier permeability,<sup>1</sup> vasotone regulation, leukocyte adhesiveness and extravasation, blood clotting, and angiogenesis.<sup>2</sup> Endothelial dysfunction that increases permeability, adhesiveness, and transmigration of leukocytes as well as the accumulation of fatty streaks in the subendothelial compartment<sup>3</sup> are a hallmark of atherosclerosis, characterized by the development of plaques that can become unstable and rupture, resulting in cardiovascular adverse events.<sup>2</sup>

The development of atherosclerosis and its prevention by therapeutic interventions is studied extensively in humans and in rodent models. Although highly relevant, the use of in vivo models remains technically challenging for indepth and rapid mechanistic investigations, such as the deconvolution of the effects on endothelial cells of different molecules present in a milieu. Moreover, the identification of potent drug compounds for therapeutic intervention and the testing of compounds/products for toxicological safety or risk assessments require high-throughput settings for a pre-screening phase that is generally not conducted in vivo. The perspective of the 3Rs principle, "replacement, reduction,

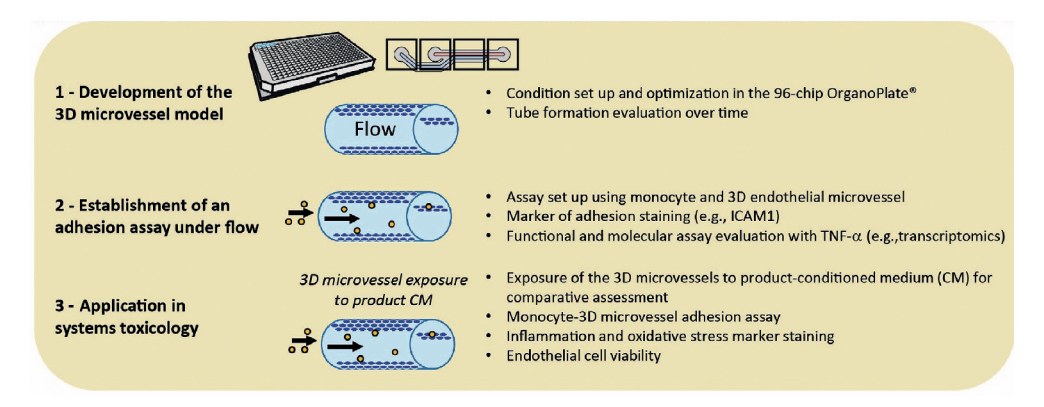


**Figure 1.** Overview of the steps for the development, functional evaluation, and real-case application in systems toxicology of our 3D vasculature-on-a-chip model for studying monocyte-endothelial adhesion under flow.

and refinement," which aims to limit animal testing,<sup>4</sup> encourages the scientific community to develop relevant in vitro alternatives. So far, two-dimensional (2D) and static endothelial in vitro models have been used extensively, but more physiologically relevant models are required that integrate the three-dimensional (3D) geometry of vessels and hemodynamic flow. These properties play important mechanical roles through mechano-transduction signaling that influence vascular differentiation and proliferation as well as endothelial cell morphology and response to stimuli.<sup>5,6</sup> Along with other factors, flow patterns and the magnitude of shear stress promote anti- or pro-atherogenic effects on endothelial cells that contribute to the protection or promotion of vascular diseases.<sup>6,7</sup>

The emergence of a wide range of engineered microfluidic systems and techniques enabling the culture of cells under flow and in a 3D space has accelerated the innovation of advanced perfusable in vitro vascular models. These models vary in complexity and physiological relevance, from a simple planar endothelial cell layer, on top of which controlled shear stress can be applied, to 3D microvessels or even more complex vasculature networks. <sup>8,9</sup> Models are classified according to their method of fabrication and constitute a toolbox for studying different aspects of vascular biology. <sup>9</sup> Each model offers advantages (e.g., high physiological relevance, high-throughput capacity, easy setup) and possesses limitations (e.g., time-consuming to manufacture, low throughput, lower physiological relevance). <sup>9</sup> Therefore, it is important to define the biological mechanism(s) of interest, the extension potential of the model, and the capacity needed to select or develop a vascular model that adequately balances experimental feasibility, physiological relevance, and throughput capacity for larger experimental condition screening.

Lifestyle and genetic predisposition affect the development of vascular disorders that result in atherogenesis.<sup>10</sup> Smoking, for instance, is a recognized major risk factor for the development of cardiovascular diseases.<sup>11</sup> Over time, smokers develop low-grade inflammation and oxidative properties in the systemic compartment that can alter endothelial function, resulting in the initiation and

progression of atherosclerosis. 12 The health risks associated with cigarette smoking are attributable to toxicants that are generated in the smoke through tobacco combustion.<sup>13</sup> Therefore, reducing exposure to smoke constituents is crucial for risk reduction,14 for which the development of modified risk tobacco products (MRTP) is necessary.<sup>15</sup> Potential MRTPs that heat tobacco rather than burning it have been developed, offering significant decreases in the complexity and number of toxicants generated in the aerosol during use.<sup>16</sup> Pre-clinical and clinical studies aimed to assess these products have compared them with cigarettes to determine whether this reduction in exposure translates into a reduction in health risk in both laboratory models and humans.<sup>14</sup> Overall, the results indicated that the Tobacco Heating System (THS) 2.2, a candidate MRTP, and the Carbon-Heated Tobacco Product (CHTP) 1.2, a potential MRTP, exert reduced effects on respiratory and cardiovascular functional and molecular endpoints in both in vitro and in vivo laboratory models.<sup>17-20</sup> Human studies showed significant reduction in biomarkers of exposure and potential harm after switching from cigarettes to THS 2.2.21

The present work aimed to develop a 3D vasculature-on-a-chip model under flow to study monocyte-endothelium adhesion and provide a use case application by leveraging this model for tobacco product testing in a systems toxicology framework (Figure 1). Using the OrganoPlate®, a standardized 96-chip microfluidic cell culture plate, we optimized conditions to grow endothelial microvessels with disease-relevant primary human coronary artery endothelial cells (HCAEC, Figure 1, Step 1). This microfluidic platform has been used previously to develop perfusable human umbilical vein endothelial cells, VeraVec human endothelial cell vessels, for studying vascular permeability.8 To evaluate the functionality and relevance of the HCAEC microvessel model, we developed an assay to quantify (i) the adhesion of monocytic cells under flow to the lumen of HCAEC microvessels as a functional readout and (ii) the intercellular adhesion molecule 1 (ICAM1; also known as CD54) protein in HCAECs as a molecular readout for adhesion (Figure 1, Step 2). We used tumor necrosis factor α (TNFα), a prototypical inflammatory

stimulus known to trigger monocyte-endothelium adhesion, and also investigated concentration-dependent gene expression changes in HCAEC microvessels using transcriptomics. As a real-case application of our 3D vasculature-on-a-chip model, we assessed the comparative impact of THS 2.2 aerosol and 3R4F cigarette smoke in the form of conditioned medium on the adhesion of monocytic cells to HCAEC microvessels, a key event in atherogenesis (Figure 1, Step 3). After exposure to conditioned medium, glutathione (GSH) content was also measured to quantify oxidative stress promoted in endothelial microvessels similarly to smokers' blood that acquired oxidative properties over time and may contribute to endothelial dysfunction.<sup>22</sup>

## Material and methods

#### **Cell culture**

Primary HCAECs (PromoCell 12221; Heidelberg, Germany) were cultured in pre-coated tissue culture flasks (Nunc Easyflask; Roskilde, Denmark) with MV2 endothelial cell growth medium (PromoCell C-22-22) containing 5% fetal bovine serum (FBS, Gibco 16140-071; Waltham, MA, USA) and 1% penicillin/streptomycin (Sigma-Aldrich P4333; St. Louis, MO, USA). Mono-Mac-6 (MM6) cells (DSMZ, ACC-No.124; Braunschweig, Germany) were maintained in Roswell Park Memorial Institute (RPMI) 1640 medium (Sigma-Aldrich R0883) containing 10% FBS and 1% penicillin/streptomycin.

## **OrganoPlate® culture**

We used two-lane OrganoPlates® with 400  $\mu$ m  $\times$  220  $\mu$ m (w  $\times$  h) channels (MIMETAS 9603-400B, Leiden, The Netherlands). Gel and perfusion channel lengths were 9 mm and 12.2 mm, respectively. Before seeding, 50  $\mu$ L of Hank's Balanced Salt Solution (HBSS) were dispensed into the observation window to

prevent evaporation and enhance optical clarity. Two microliters of gel composed of 4 mg/mL collagen I (Cultrex rat collagen 1, 5 mg/mL; Trevigen, Gaithersburg, MD, USA), 100 mM HEPES (Gibco 15630-056), and 3.7 mg/mL Na2HCO3 (Sigma-Aldrich S5761) were dispensed in the gel inlet and incubated for 30 minutes at 37 °C allowing gelation of the extracellular matrix (ECM). HCAECs at passage three were trypsinized using 0.025% trypsin in phosphate-buffered saline (PBS)/ethylenediaminetetraacetic acid (Lonza CC-5012; Basel, Switzerland) and resuspended in the appropriate volume (106 cells/mL) in MV2 medium. Two microliters of cell solution were dispensed in the perfusion channel inlet of the OrganoPlate®. After addition of the cells, 50 µL of MV2 medium were dispensed in the perfusion inlet to prevent dehydration of the cell suspension. The plate was incubated on its side for two hours to allow the cells to attach to the ECM. Subsequently, 50 µL of MV2 medium were dispensed in the perfusion outlet, and the plate was placed in the incubator (37 °C, 5% CO2) on a rocking platform (four-minute intervals at an angle of 7°) resulting in a bidirectional flow. For the culture optimization step, we used 9.1 mg/mL of Matrigel growth factor reduced basement membrane matrix (Corning 356231; Corning, NY, USA) and endothelial medium from Cell Biologics (H1168; Chicago, IL, USA). ECM and medium were mixed at a 1:1 (v/v) ratio. The medium was changed three times per week.

#### **Barrier integrity assay**

Medium in the perfusion channel was replaced by MV2 medium containing 0.5 mg/mL 20 kDa fluorescein isothiocyanate (FITC)-dextran (Sigma-Aldrich FD20S) and 0.5 mg/mL 155 kDa tetramethylrhodamine isothiocyanate (TRITC)-dextran (Sigma-Aldrich T1287) (40  $\mu$ L on perfusion inlet, 30  $\mu$ L on perfusion outlet). Ten microliters of MV2 medium were dispensed on the gel inlet. Leakage of the fluorescent probe from the lumen of the endothelial microvessel into the ECM compartment was captured using an ImageXpress XLS Micro HCI system (two-minute intervals, 14 minutes total; Molecular Devices, San Jose, CA, USA). The ratio between the fluorescent signal in the perfusion channel and the ECM channel

was analyzed using Fiji (ImageJ, NIH, Bethesda, MD, USA). The permeability of the membranes was analyzed by measuring the number of molecules that leaked though the membrane into the adjacent gel lane over time. From these measurements, the apparent permeability index (Papp: initial flux of a compound through a membrane, normalized by membrane surface area and donor concentration) was calculated using the following formula:

$$P_{app} = \frac{\Delta C_{receiver} \times V_{receiver}}{\Delta t \times A_{barrier} \times C_{donor}} \left(\frac{cm}{s}\right)$$

where  $\Delta C_{receiver}$  is the measured normalized intensity difference of the ECM to the donor channel at  $t_{0min}$  and  $t_{10min}$ , Vreceiver is the volume of the measured region in the ECM channel,  $\Delta t$  is the time difference,  $A_{barrier}$  is the surface of the ECM interface with the medium channel, and  $C_{donor}$  is the donor concentration of the dextran dye (0.5 mg/mL).

### Monocyte-endothelial microvessel adhesion assay under flow

MM6 monocytes (passage 12) were harvested and suspended at a density of 105 cells/mL in RPMI medium containing 0.5  $\mu$ g/mL calcein AM (Life Technologies C3099; Carlsbad, CA, USA) for 15 minutes at 37 °C. The monocytes were spun down at 200  $\times$  g for five minutes, the calcein AM-containing medium was aspirated, and the cells were resuspended in a density of 105 cells/mL in MV2 medium. Simultaneously, the nuclei of the endothelial microvessels were stained with Hoechst 33342 (1:2,000, Thermo Fisher Scientific H3570; Waltham, MA, USA) for 20 minutes at 37 °C. After washing the endothelial tube for five minutes with MV2 medium, the monocyte suspension was added to the perfusion channel and incubated at 37 °C and 5% CO2 for 15 minutes on a rocking platform (eightminute intervals at a 7° angle). After washing twice with HBSS for five minutes, the endothelial vessel was imaged using an ImageXpress XLS-C HCI system. The number of endothelial nuclei in the microvessels was extracted using an approach based on morphological shape filtering using built-in tools available in Fiji (version

2) / ImageJ (1.52e build). $^{23}$  Endothelial cells nuclei were extracted by removing the background signal via a Rolling Ball method in the blue Hoechst channel. $^{24}$  After the remaining signal was thresholded to highlight the nuclei, a particle detection was subsequently performed to count the number of nuclei. The number of adhering monocytes was extracted using methods based on intensity thresholding and particle detection in the green calcein AM channel. $^{25}$  The method used was nearly identical to the method described for obtaining the number of endothelial nuclei. The expected minimum size for a monocyte was adjusted, because monocytes are larger than nuclei. (5-9 $\mu$ m for nuclei, more than 10 $\mu$ m for monocytes). The ratio of monocytes to endothelial cells was subsequently calculated and used as standardized expression of monocyte adhesion to the endothelial microvessel.

#### **Immunohistochemistry**

Endothelial microvessels were fixed using 3.7% formaldehyde (Sigma-Aldrich 252549) in HBSS (Sigma-Aldrich H6648) for 20 minutes, washed twice with HBSS for five minutes, and permeabilized with 0.3% Triton X-100 (Sigma-Aldrich T8787) in HBSS for 10 minutes. After washing with 4% FBS in HBSS for five minutes, the HCAECs were incubated with a blocking buffer (2% FBS, 2% bovine serum albumin [Sigma-Aldrich A2153]) and 0.1% Tween 20 (Sigma-Aldrich P9416) in HBSS for 45 minutes. After blocking, cells were incubated for 90 minutes with a primary antibody solution, washed three times with 4% FBS in HBSS, and incubated with a secondary antibody and nuclear staining for 30 minutes. All steps were performed at room temperature. The primary antibodies used were mouse antihuman antibodies for ICAM-1 at 5 µg/mL (1:100, Bio-Techne BBA3; Minneapolis, MN, USA) and CD31 at 10 µg/mL (Dako M0823) and rabbit anti-human antibodies for VE-cadherin at 1 µg/mL (Abcam, Ab33168; Cambridge, UK). The secondary antibodies were goat anti-mouse Alexa Fluor 488 at 8 µg/mL (Invitrogen A11001; Carlsbad, CA, USA) and goat anti-rabbit Alexa Fluor 488 at 8 µg/mL (Invitrogen A11008). For nuclear staining, Hoechst 33342 (Thermo Fisher Scientific H3570) at 5 μg/mL was used.

Images were captured using an ImageXpress XLS-C HCI system. For quantification of the immunofluorescent staining, z-series were captured, and the sum projection was saved. Quantification was performed by calculating the mean intensity of the captured image in Fiji divided by the number of nuclei observed.

# Transcriptomic analysis of endothelial microvessels stimulated by TNFα

## **Microvessel lysis**

HCAEC microvessels were lysed by applying 40  $\mu$ L of lysis buffer (consisting of 1% beta-mercaptoethanol [Sigma-Aldrich M6250] in Buffer RLT [QIAGEN 79216; Hilden, Germany]) to the perfusion inlet and 10  $\mu$ L lysis buffer to the perfusion outlet, creating a flow through the microfluidic channel. After 30 seconds, the lysate was collected in a polymerase chain reaction clean tube (VWR 211-2120; Radnor, PA, USA). Seven microfluidic chips were pooled into a total volume of 240  $\mu$ L lysis buffer and stored at  $-80^{\circ}$ C for transcriptomics analysis.

#### RNA extraction and profiling

Samples from pooled HCAEC microvessel lysates from four independent experiments were randomized, and RNA was extracted on a QIAcube robot (batch of 12 samples) using the RNeasy Micro Kit (QIAGEN 74004) and then stored at  $-80^{\circ}$ C. Purified RNA was quantified using a Nanodrop ND-1000 (Thermo Fisher Scientific). The RNA integrity number was determined using an Agilent 2100 Bioanalyzer with the Agilent RNA 6000 Pico Kit (Agilent Technologies 5067-1513; Santa Clara, CA, USA); RNA integrity number values ranged from 6.8 to 10 (mean: 9.58). RNA was processed in a 96-chip plate (same batch) and required 50 ng of total RNA on a fully automated Biomek FXp robot (Beckman Coulter, Brea, CA, USA) with the NuGEN Ovation RNA amplification system V2 protocol (3100-A01; San Carlos, CA, USA). Single-primer isothermal amplification was followed by fragmentation and biotinylation of the cDNA. Hybridization was performed overnight (16 hours)

at 60 rpm in a 45°C GeneChip® Hybridization Oven 645 (Affymetrix, Santa Clara, CA, USA) on a GeneChip Human Genome U133 Plus 2.0 Array (Affymetrix), which measures the expression of more than 47,000 transcripts. The sequences from which these probe sets were derived were selected from GenBank™, dbEST, and RefSeq sequence databases. Arrays were washed and stained on a GeneChip® Fluidics Station FS450 DX (Affymetrix) using the Affymetrix GeneChip™ Command Console Software (AGCC software version 3.2, protocol FS450\_0004).

### Transcriptomic data processing and pairwise comparisons

Summarization and normalization of probes in the raw data (CEL files with access ID E-MTAB-7555 are available in the ArrayExpress public repository database) were performed using Entrez-based probe annotation HGU133Plus2\_Hs\_ENTREZG cdf version 16.0.0<sup>26</sup> and frozen robust microarray analysis (fRMA),<sup>27</sup> respectively. The normalization vector HGU133Plus2 fRMAvecs version 1.3.0 was used with the R package fRMA version 1.18.0. Quality controls, including log intensities, normalized unscaled standard error, relative log expression, median absolute value of relative log expression, and pseudo-images and raw image plots, were performed with the affyPLM package version 1.42.0 (Bioconductor suite).<sup>28</sup> After quality control, pairwise comparisons at the gene level, called systems response profiles (SRP), were computed by comparing each concentration treatment with its respective vehicle control (VC) using the Bioconductor Limma R package version 3.22.1.<sup>29</sup> No gene was filtered out at any step of the computational analysis. Genes with a false discovery rate (FDR) below 0.05 (p-value adjustment using the Benjamini and Hochberg method) were considered differentially expressed.<sup>30</sup> For biological interpretation, SRPs including all genes (18,604) were analyzed using p-value threshold-free computational approaches (gene set enrichment analysis and network perturbation amplitude (NPA) analyses described below). Most R packages used to conduct the data analysis were included in Bioconductor version 3.0. The R version used was 3.1.2.

#### **NPA** analysis

Using transcriptomic data and biological cause-and-effect network models, we applied a computational approach that quantifies a response to a stimulus to analyze network perturbation<sup>31</sup> in HCAEC microvessels. A network is an assembly of directed and signed causal relationships between molecular biological entities that collectively model a specific biological process in a defined context (e.g., lung or vascular). The causal relationships have been curated from the scientific literature and encoded in Biological Expression Language syntax. The network is composed of functional (backbone) and transcript (gene expression) layers. The backbone node-level and network-level perturbation amplitudes can be calculated by considering the measured gene expression changes and the network topology using a backward-causal reasoning algorithm. Three statistics are computed to assess the significance of an NPA score with respect to biological variation (confidence interval) and its specificity to the given two-layer network structure (O and K statistics). A collection of biological networks representative of the main processes of cell fate, inflammation, repair, stress, and proliferation has been published and is accessible at http://causalbionet.com.<sup>32,33</sup> We report here the NPA scores for the vascular inflammatory processes/endothelial cellmonocyte interaction network model in the scope of this manuscript.

### Principal component (PC) analysis (PCA) and pathway enrichment analysis

Gene set enrichment analysis was conducted to identify biological pathways/ processes associated with genes that drive the discrimination of concentration and exposure time of HCAEC microvessels to TNFα. After performing PCA of the gene expression fold-change (FC) matrix, genes were ranked by their contribution to PCs that explained the maximum of variance. Gene set enrichment analysis was performed using the MSigDB C2-CP gene set collection to identify enriched gene sets representative of biological canonical pathways/processes.<sup>34</sup> Gene resampling (Q1) was performed to generate the null hypothesis distribution and compute the significance associated with each gene set.<sup>35</sup>

## Preparation of THS 2.2- and 3R4F-conditioned media from MM6 cells

#### Generation of fresh aqueous extracts from THS 2.2 aerosol or 3R4F smoke

Mainstream smoke from the 3R4F reference cigarette (Kentucky Tobacco Research Center, University of Kentucky, Lexington, KY, USA) was generated on a 20-port rotary Borgwaldt smoking machine (Hamburg, Germany) according to the Health Canada Intense protocol: 55 mL puff volume, 30-second puff interval, with all ventilation holes blocked.<sup>36</sup> The smoke generated from six reference cigarettes was bubbled through 36 mL of ice-cold RPMI 1640 culture medium to trap the water-soluble fraction, resulting in a stock solution concentration of approximately 1.8 puffs/mL, corresponding to about 10.7 puffs per cigarette, on average. Mainstream aerosol from the candidate MRTP THS 2.2, developed by Philip Morris International, was produced using a pre-defined puff count of 12 puffs per stick on a 30-port rotary aerosol generator (type SM 2000 P1), according to the Health Canada protocol. The aerosol was bubbled into ice-cold RPMI 1640 culture medium to trap the water-soluble fraction (10 HeatSticks/40 mL; stock solution concentration: three puffs/mL). Previous analysis of aqueous extracts showed that the concentrations of carbonyls decreased significantly in THS 2.2 aqueous extract compared with concentrations in 3R4F aqueous extract, while nicotine remained at comparable concentrations in both extracts. 17,18

# Exposure of MM6 cells to fresh THS 2.2 or 3R4F aqueous extracts to generate conditioned media

An MM6 cell suspension was adjusted to  $2 \times 10^6$  cells/mL in RPMI 1640 medium supplemented with 10% FBS, and 0.5 mL/well was seeded in a 24-well plate. MM6 cells were exposed to various concentrations of 3R4F/THS 2.2 aqueous extract or culture medium/10% FBS (VC) for two hours. Culture supernatants, namely conditioned media, were collected and stored at -80 °C for the adhesion assay.

Treatment of endothelial microvessels with TNF $\alpha$  or 3R4F/THS 2.2-conditioned medium prior to adhesion assay and marker staining

On the fourth day after seeding, endothelial microvessels were treated with TNFα (ImmunoTools 11343015; Friesoythe, Germany) as a positive control for inflammation, with L-buthionine-sulfoximine (25 μM, Sigma-Aldrich B2515) or ethacrynic acid (25 µM, Sigma-Aldrich E4754) as positive controls for GSH depletion, or with 3R4F- or THS 2.2-conditioned medium for four or 16 hours. The four hours time point was used for comparison with previous results obtained in a static 2D endothelial cell model. 18,37 Adhesion proteins, such as SELE, are already maximally expressed after four hours in endothelial cells, and their expression may be transient and decrease at later time points, while the expression of other adhesion proteins, such as vascular cellular adhesion molecule 1, is maintained or triggered at later time points (i.e., 16 hours).<sup>38</sup> At the four hours time point, primary effects of a stimulus can be investigated, while at later time points, secondary activation occurs via feedback loops. At the end of the treatment, endothelial microvessels were either fixed for specific marker immunohistochemistry staining, lysed for transcriptomic analysis (only for TNFα treatment), or directly nuclear stained and used for the adhesion assay under flow.

#### **Measurement of GSH content**

Endothelial microvessels were incubated with MV2 medium containing 0.125 mg/mL monochlorobimane (Sigma-Aldrich 69899) and 5 μM DRAQ5 (Abcam ab108710) for 30 minutes at 37 °C and 5% CO2 on a rocking platform (eight-minute intervals at a 7° angle). After washing with HBSS, the z-series were captured on an ImageXpress XLS-C HCI system. Quantification of the intensity of the fluorescent signal was performed in Fiji. Sum projections were acquired from the z-series, and the mean intensity was calculated after subtracting the background. Subsequently, the intensity per counted nucleus was calculated.

#### Water-soluble tetrazolium salt (WST-8) viability assay

Medium in endothelial microvessels was replaced with MV2 medium containing Cell Counting Kit-8 solution (1:11 dilution, Sigma-Aldrich 96992) and incubated at 37 °C and 5% CO2 for 30 minutes on a rocking platform (eight-minute intervals at a 7° angle). After incubation, the absorbance was measured at 450 nm on a plate reader (Multiskan FC, Thermo Fisher Scientific). The measurements of the gel inlet, perfusion inlet and outlet, and observation window were adjusted for volume differences and combined after background subtraction of the positive cell free control. Analysis was performed in Microsoft Excel (Redmond, WA, USA). Data was normalized to the negative control (MV2 MV2 0 pg/mL TNF $\alpha$  for the "starvation experiment" and the conditioned medium vehicle control (corresponding to supernatant of MM6 cells exposed to 0 puffs/ml smoke/aerosol aqueous extract) for the "conditioned medium exposure experiment".

#### **Statistical analysis**

Statistical analysis was conducted in GraphPad Prism (La Jolla, CA, USA). The mean values for all within-OrganoPlate® chip replicates were calculated and normalized to the control (ratio value/control). Statistical analysis was performed with a one- or two-way analysis of variance (ANOVA) followed by post-hoc Dunnett's pairwise comparisons. The number of replicates for chips within an OrganoPlate® (n) and independent experiments (N) is indicated in the figure legends for each experiment.

## Results

# Development and optimization of conditions for the formation of endothelial microvessels

Endothelial microvessels were cultured in the two-lane 400-µm OrganoPlate® (Figure 2A). HCAEC vessel formation was optimized for seeding density (Figure 2B), ECM (Figure 2C), and medium composition (Figure 2D). Rapid vessel formation and vessel stability for at least eight days without ingrowth of HCAECs into the ECM were achieved with a seeding density of 106 cells/mL together with collagen 14 mg/mL ECM cultured in MV2 medium. All further experiments were conducted using this optimized seeding protocol. To show stable vessel formation and endothelial marker expression, endothelial microvessels were fixed at different time points; 3D reconstructions show the reproducible formation of a complete vessel after two days. The vessel remained stable with regards to the expression of CD31 (PECAM-1), VE-cadherin at the junctions (Figure 2E) and low expression of the apoptosis markers caspase 3/7 (supplementary Figure 1) for at least eight days (Figure 2E).

# Barrier integrity increases in the course of endothelial microvessel formation and remains stable up to eight days

To assess barrier formation in the HCAEC microvessels, a barrier integrity assay was performed (Figure 3A). Briefly, a fluorescent reporter molecule was perfused through the lumen of the vessel (perfusion channel) and followed over time to assess the diffusion of the reporter into the gel channel. The fluorescence intensity of the medium and gel channel was measured to calculate the apparent permeability coefficient. The barrier integrity assay was performed with three sizes of dextran molecules (4.4, 20 and 155 kDa). Representative images of microvessels at different time points are shown in Figure 3B. Figure 3C shows barrier formation over time. One day after introducing the HCAECs into the microfluidic channels, the diffusion of both 4.4-kDa and 20-kDa dextran through the barrier began

to decrease compared with diffusion in controls without cells, indicative of the formation of an endothelial cell barrier that remained stable for up to eight days.

# Establishment of a monocyte-endothelial microvessel adhesion model under flow

To test the endothelial microvessel model for monocyte attachment, fluorescently labeled MM6 monocytes were introduced into the endothelial microvessels after vessel stimulation with increasing concentrations of TNFα for four or 16 hours under flow. After 15 minutes of incubation under perfusion flow, nonattached monocytes were washed away, and the adherent monocytes were quantified. Representative images are shown in Figure 4A. Quantification shows a significant concentration-dependent upregulation of monocyte attachment after stimulation for four and 16 hours for all tested concentrations of TNFa compared with attachment in the VC (Figure 4B). At the four hours time point, the FC of adherent monocytes reached a plateau at concentrations of 50–100 pg/mL (Figure 4B). At the 16 hours time point, the FC of adherent monocytes tended to decrease at the lowest tested concentrations (100 and 500 pg/mL) of TNFa, but was maintained at higher concentrations (500 and 1,000 pg/mL) and increased at the highest concentration (10,000 pg/mL), compared with the FCs at the four hours time point (Figure 4B). In parallel to monocyte adhesion, ICAM1, an adhesion molecule expressed by endothelial cells to which monocytes bind (Figure 4C), was quantified in endothelial microvessels. Stimulation of the endothelial microvessels with TNFa significantly upregulated ICAM1 protein levels in HCAECs in a concentration-dependent manner compared with levels in the VC. Representative images are shown in Figure 4D, and quantification of the immunofluorescent images is shown in Figure 4E. Longer stimulation with high concentrations of TNFa (more than 500 pg/mL) resulted in higher ICAM1 levels. The profiles of concentration-dependent ICAM1 protein abundance FCs observed at four and 16 hours correlated positively with those of monocyte-endothelial microvessel adhesion at the corresponding time points (Figure 4B and E).

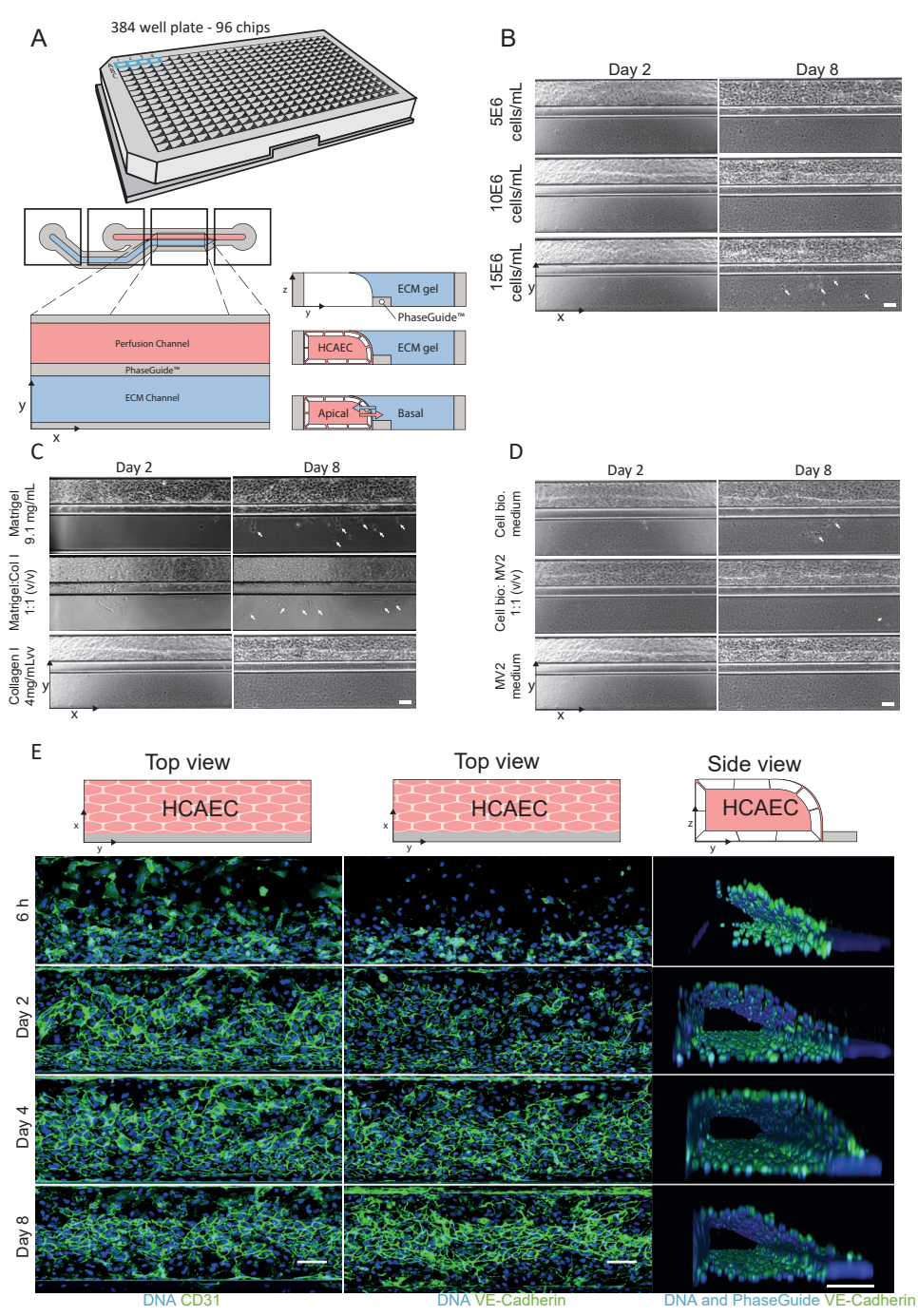
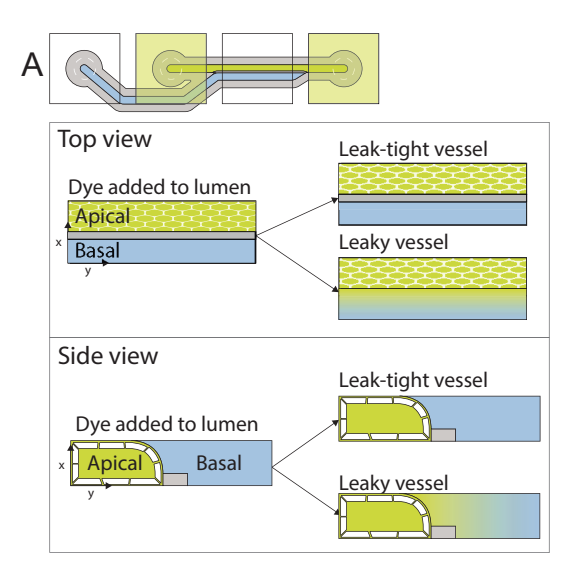


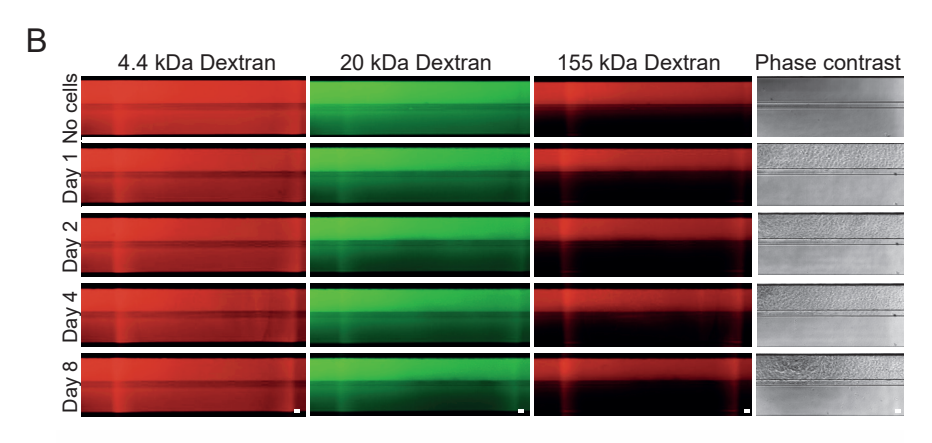
**Figure 2. 3D endothelial microvessel culture formation and optimization. (A)** Schematic overview of the OrganoPlate®. A gel channel (blue) holds an ECM in place

through the PhaseGuide's pressure barrier function. Endothelial cells are seeded in the adjacent medium perfusion channel (red). Upon the addition of perfusion flow, a tubular structure is formed in the medium channel. (B–D) 3D culture optimization of primary human coronary artery endothelial cells on the OrganoPlate® platform. The platform was optimized for cell seeding density (B), ECM composition (C), and medium composition (D) to select the optimal cell culture conditions. Phase contrast pictures were taken two and eight days after seeding, and the optimal conditions (barrier formation and no invasion of the ECM) were selected for subsequent experiments. White arrows indicate invasion of cells into the ECM on day eight. (E) Maximum projection and 3D reconstruction of a confocal z-stack of the cells in the tissue chips using the optimized seeding conditions (106 cells/mL, collagen I at 4 mg/mL ECM, and MV2 medium). HCAEC microvessels were fixed six hours and two, four and eight days after seeding and stained for DNA and the adherens-junction markers CD-31 and VE-cadherin. The maximum projections and 3D reconstruction show barrier formation and stable tubular morphology with a lumen two to eight days after seeding. Scale bar = 100 µm. Abbreviations: h, hours.

# Transcriptomic analyses of HCAEC microvessels stimulated by TNF $\alpha$ for four and 16 hours

Transcriptome analysis of HCAEC microvessels enabled the investigation of molecular changes at the mRNA transcript level following treatment with TNFa for four and 16 hours. SRPs (or contrasts) were computed by comparing each TNFa treatment group with its respective VC using linear modeling. A PCA plot of the FC matrix visualized the sources of variation in gene expression data. Scores (treatment groups) and loadings (genes contributing to the discrimination of treatment groups) were visualized on a biplot for PC1-PC2 sub-space, both PCs explaining 73.1% of the total variance (Figure 5A and B), and revealed time and concentration effects, with a clear separation of SRPs mostly along PC1 and PC2, respectively. Top genes with the largest positive and negative loading values for PC1 and PC2 (Figure 5B) showed specific FC expression patterns across concentrations and time points (Figure 5C). For biological interpretation, all genes were ranked by their contribution to PC1 or PC2, and gene set enrichment analysis was performed using the MSigDB C2-CP gene set collection representative of canonical pathways/biological processes. Gene sets grouped by their positive and negative enrichment scores were scattered in the four quadrants of the PCA biplot. The top five significant (FDR < 0.05 for at least one PC) gene sets for each quadrant are highlighted in Figure 5D. The results show an enrichment of gene sets reflective





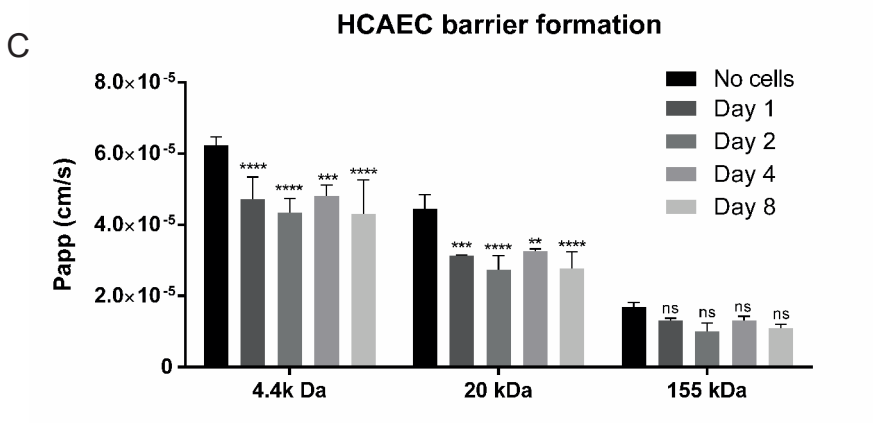


**Figure 3. Barrier formation in HCAECs. (A)** Principle of the barrier integrity assay in the OrganoPlate®. A fluorescent dye is added to the lumen of the vessel, and the integrity of the barrier is quantified by measuring the intensity of fluorescent dye diffusing into the adjacent gel channel. **(B)** Fluorescent images show HCAEC barriers for both 4.4 kDa FITC-dextran, 20 kDa FITC-dextran and 155 TRITC-dextran one to eight days after seeding. The fluorescent images were taken 14 minutes after addition of the dye. Scale bar = 100  $\mu$ m **(C)** Papp index of the HCAEC barrier over time. Plot bars represent the mean + standard deviation (N = 3, n  $\ge$  7). ns = not significant, \*\*p < 0.01, \*\*\*\*p < 0.001, \*\*\*\*p < 0.0001 (two-way ANOVA).

of inflammation (e.g., KEGG CYTOKINE CYTOKINE RECEPTOR INTERACTION, PID CD40 PATHWAY), protein post-translational modification (e.g., REACTOME BIOSYNTHESIS OF THE N GLYCAN PRECURSOR DOLICHOL LIPID LINKED OLIGOSACCHARIDE LLO AND TRANSFER TO A NASCENT PROTEIN), cycle/DNA replication (e.g., REACTOME E2F MEDIATED REGULATION OF DNA REPLICATION), and mitosis (e.g., PID AURORA B PATHWAY, REACTOME MITOTIC PROMETAPHASE) pointed in the direction of the Q1, Q2, Q3, and Q4 quadrants, respectively (Figure 5D and Supplementary Table 1). The selection of differentially expressed genes (DEG) (FDR < 0.05) revealed a TNFα concentration-dependent increase of significantly upregulated and downregulated genes with a lower effect at 16 hours than at four hours (Figure 5E). To verify consistency between molecular changes and functional readouts, we conducted a network perturbation analysis, leveraging each SRP and a causal network model representative of monocyteendothelial cell adhesion mechanisms. Figure 5F shows a TNFα concentrationdependent increase in the NPA similar to the readout observed with the MM6 cell-HCAEC microvessel adhesion assay (Figure 4B). Interestingly, the nodes with the larger significant amplitude scores across SRPs were "p(HGNC:ICAM1)" and "path(SDIS:monocyte\_adherence)," corresponding to predicted activation of the protein ICAM1 and the adhesion of monocytes to the endothelium, respectively (Supplementary Table 2). This result was supported by an increased expression of mRNA transcripts coding for adhesion molecules as measured by Affymetrix microarray (Supplementary Figure 2). We then compared the response to TNFα in our 3D model and a 2D model to assess whether a similar biology was perturbed. For this purpose, we retrieved an SRP from a previous study, corresponding to the

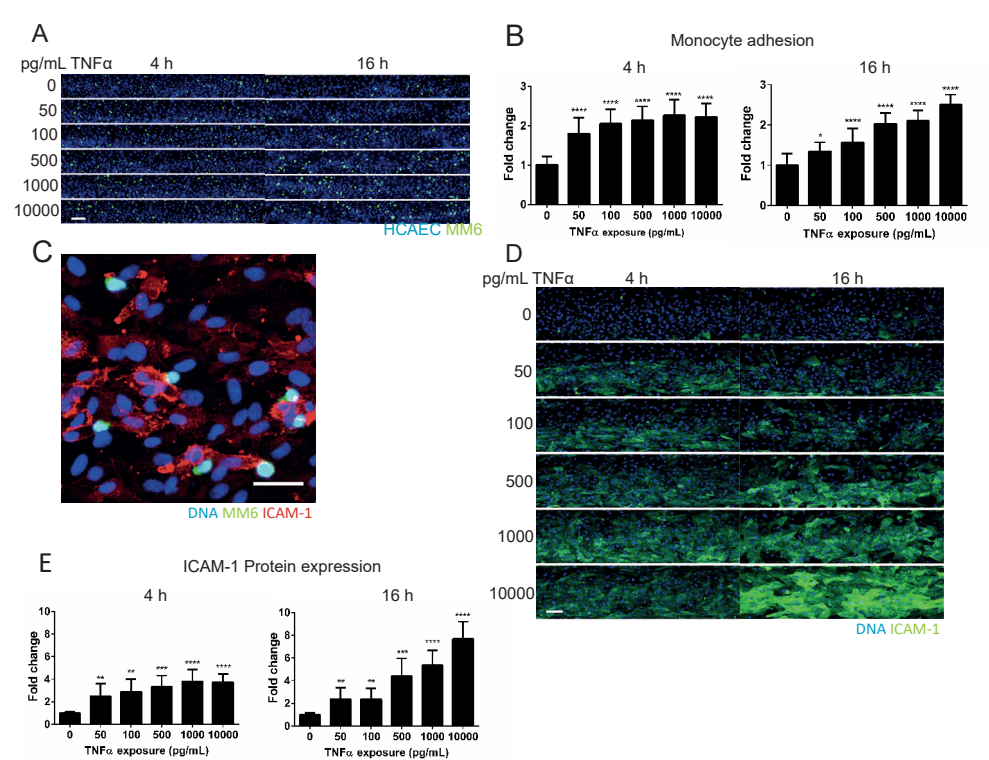


**Figure 4. Establishment of a monocyte-endothelial microvessel adhesion model under flow.** (A) Monocyte adhesion after four or 16 hours of TNFα exposure. MM6 monocytes labeled with live stain calcein AM were added under flow to the endothelial microvessel (pre-stained with the nuclear dye Hoechst 33342) for 15 minutes. After washing, fluorescent images were captured (scale bar = 50 μm) and the number of attached monocytes (green) per nucleus (blue) was calculated. (B) The plot shows the mean increase compared to the VC + standard deviation. \*p < 0.05, \*\*\*\*p < 0.0001 (one-way ANOVA followed by post-hoc Dunnett's pairwise comparisons) compared with VC. N = 2–3, n = 6. (C) High magnification of monocyte-endothelial attachment (scale bar = 50 μm). (D and E) Images and quantification of the protein adhesion marker ICAM1 in the endothelial microvessel after four or 16 hours of exposure to TNFα. The intensity of the immunofluorescent ICAM1 staining was measured per nucleus of HCAECs. N = 3, n = 3. The plots show the fold change relative to the VC corresponding to the condition with no TNFα (mean + standard deviation). \*\*p < 0.01, \*\*\*\*p < 0.001, \*\*\*\*\*p < 0.0001 (one-way ANOVA followed by post-hoc Dunnett's pairwise comparisons). Abbreviations: h, hours.

conditions of 2D monolayer HCAECs treated with 10 ng/mL of TNF $\alpha$  for four hours and the respective VC.<sup>17</sup> Leveraging the same conditions using our 3D model, a comparison of gene expression FCs and pathway-based gene set enrichment scores revealed a high consistency between the 3D and 2D models (Figure 5G and H; Supplementary Table 3). The correlation increased notably when selecting

significant genes (FDR < 0.05) and gene sets (FDR < 0.10), highlighted as red dots on the scatter plots (Figure 5G and H). A subset of gene sets was inversely correlated with the enrichment scores, which were not significant (Figure 5H).

# Model application for product toxicological assessment: use case with a heat-not-burn tobacco product compared with a reference product

As an application of the established monocyte-endothelial microvessel adhesion model, we assessed the impact of a candidate MRTP, THS 2.2, compared with that of the 3R4F reference cigarette on the adhesion of monocytic cells to endothelial microvessels, a key step in the initiation of atherogenesis. In a previously established 2D and static adhesion assay, HCAECs were exposed to conditioned medium generated from human monocytic MM6 cells treated with various concentrations of aqueous extract of 3R4F smoke or THS 2.2 aerosol.<sup>18</sup> We used the same type of endothelial microvessel exposure.

# Reduced effect of THS 2.2 aqueous extract compared with that of 3R4F aqueous extract on TNFα release by MM6 cells

Cigarette smoke-derived chemicals that are water-soluble can interfere with serum proteins present in the culture medium, potentially reducing the effect of the smoke/aerosol aqueous extract.<sup>39</sup> To limit this, conditioned medium is, in principle, generated using starvation medium by reducing the percentage of FBS from 10% to 0.5%. The supplementary Figure 3 shows that the adaptation of HCAEC microvessels to medium with low serum content (0.5% FBS) affected HCAEC viability/proliferation and number of cells, as measured by WST-8 enzymatic activity (panels A – D) and nuclei count (panels E – H), respectively, after four and 16 hours. Therefore, we decided to generate conditioned medium by maintaining the serum content at 10% FBS and measure the levels of TNFα

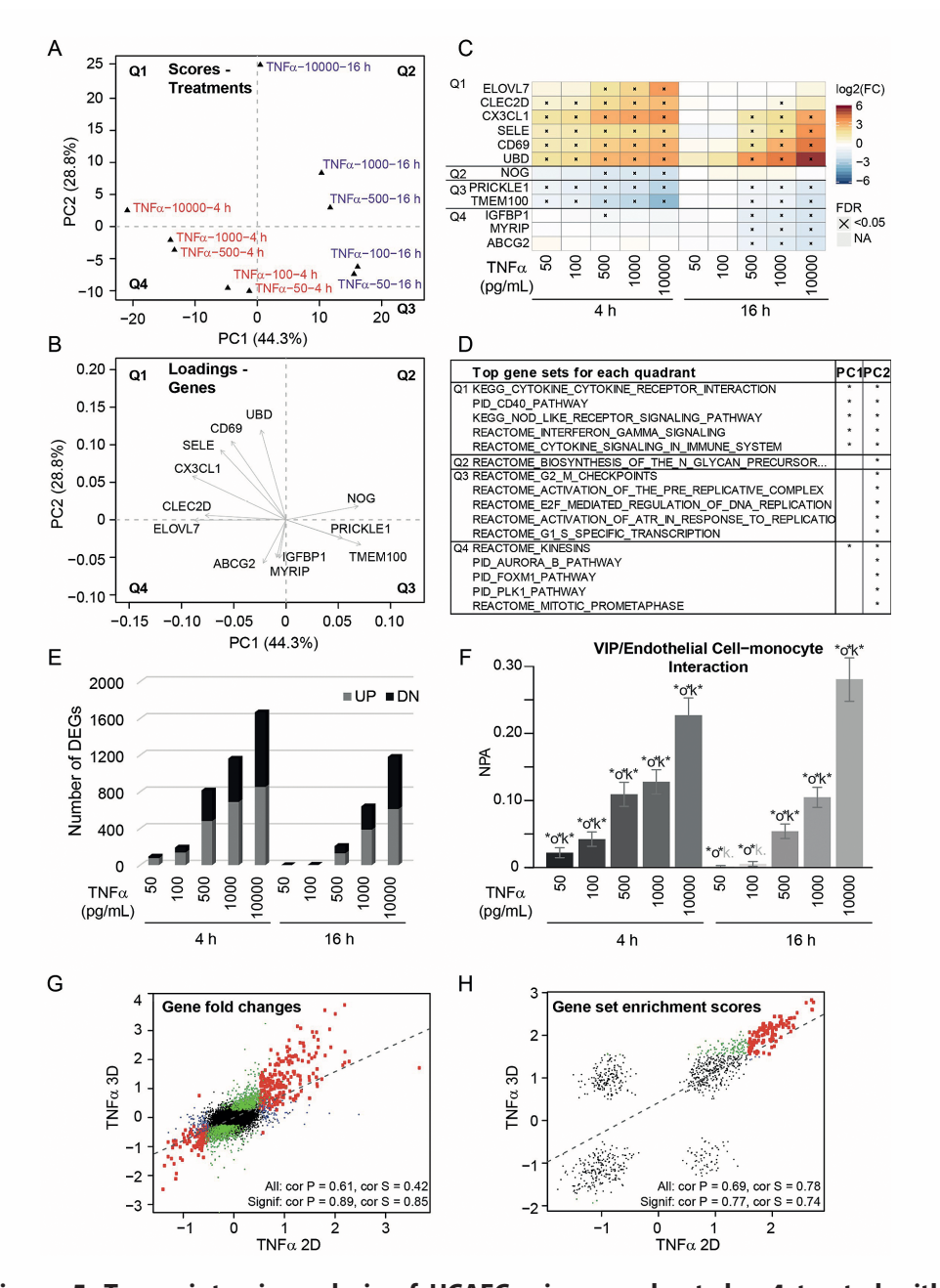
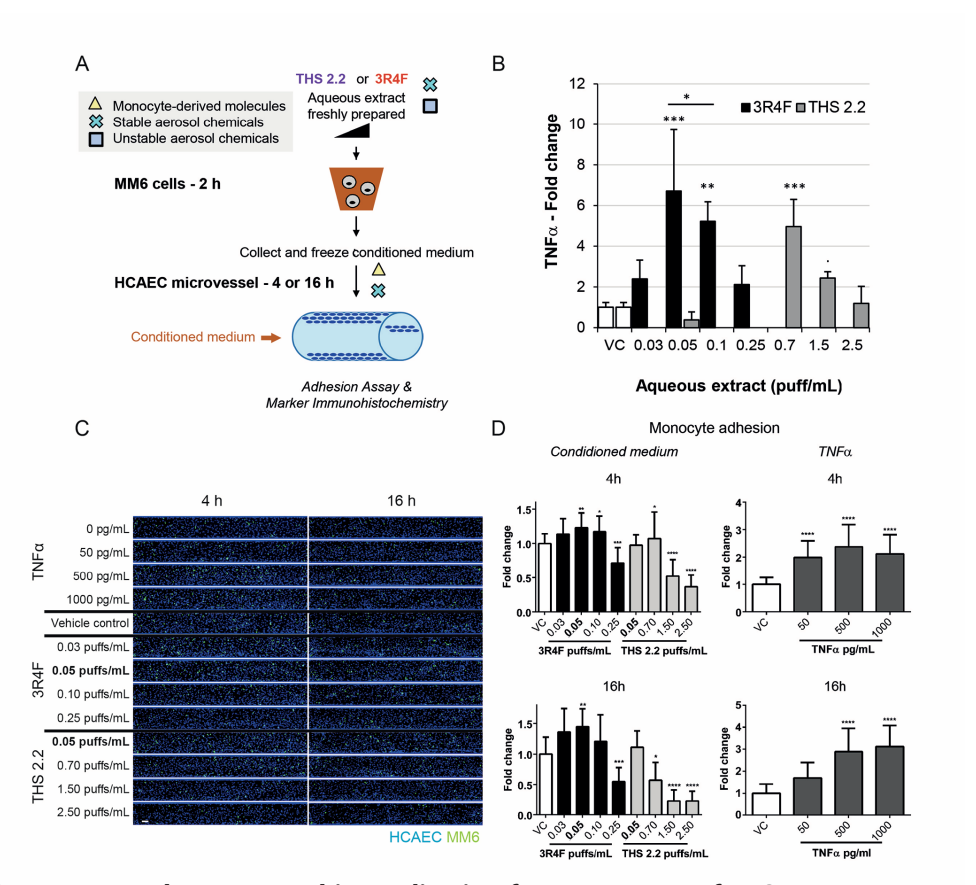


Figure 5. Transcriptomic analysis of HCAEC microvessels at day 4 treated with various concentrations of TNFα for 4 and 16 hours. PC1-PC2 sub-space scatterplots of (A) treatment group scores and (B) gene loadings following principal component analysis of FC gene expression matrix. (C) Heatmap of expression FCs (in log2 scale) of the top six genes per principal component contributing the most to the separation of

treatment groups. (D) Top gene sets associated with genes pointed in the direction of the four quadrants of the PC1-PC2 sub-space scatterplot. Gene sets were ranked by their average FDRs associated with PC1 and PC2 enrichment scores, and the top five gene sets (if more than five gene sets appeared on the list) were extracted and displayed. The full list of significant gene sets is provided in Supplementary Table 1. (E) Barplot of DEGs (FDR < 0.05) for all systems response profiles. (F) Barplot of NPA scores for microvessel systems response profiles graphed using the vascular inflammatory processes/endothelial cellmonocyte interaction network model. Scores are shown with their confidence intervals accounting for experimental variation. A network is considered perturbed if, in addition to the significance of the NPA score with respect to the experimental variation, the two companion statistics (O and K) derived to inform the specificity of the NPA score with respect to the biology described in the network are significant. \*O and K statistic p-values below 0.05 and NPA significance with respect to the experimental variation, p-values between 0.05 and 0.1 for "O" and "K" (in grey). (G) Scatterplot of gene expression FCs in log2 2D vs. 3D models (TNFa, 10 ng/mL, four hours exposure). (H) Scatterplot of gene set enrichment scores for 2D and 3D models (TNFa, 10 ng/mL, four hours exposure). For panels G and H, data points highlighted in red, green, and blue correspond to genes or gene sets that are significant in both 3D and 2D models, in the 3D model only, and in the 2D model only, respectively. The dotted line corresponds to the regression line when considering all genes or gene sets for the linear model. All Spearman and Pearson correlation coefficients were computed using all genes/gene sets; significant genes/gene sets were highly significant (p < 0.0001). The full list of significant gene sets is provided in Supplementary Table 3. For the 3D model, N = 4 independent experiments, n = 7 microvessels pooled in one lysate. Abbreviations: cor P, Pearson's correlation coefficient; cor S, Spearman's correlation coefficient; DN, downregulated; Signif, significant; UP, upregulated; h, hours.

released by monocytic cells in conditioned medium as a quality check showing similar results to previous work done in low serum content conditions. 17,18

We previously showed that TNF $\alpha$ , a surrogate inflammatory marker, was released by MM6 cells in the starvation medium following a two-hour treatment with 3R4F aqueous extract.<sup>37</sup> Therefore, the concentration of TNF $\alpha$  was determined in 3R4F-and THS 2.2-conditioned media containing 10% FBS (Figure 6B). The results show a concentration-dependent augmentation of TNF $\alpha$  reaching a maximum at 0.05 puffs/mL of 3R4F aqueous extract and then decreasing at higher concentrations (0.1 and 0.25 puffs/mL). At the concentration of 0.05 puffs/mL of 3R4F aqueous extract at which a TNF $\alpha$  peak was measured, no significant TNF $\alpha$  release was observed for the THS 2.2 aqueous extract exposure. It was necessary to enhance the concentration of THS 2.2 aqueous extract (0.7 puffs/mL) by a factor of approximately 14 to measure TNF $\alpha$  levels in the conditioned medium that were similar to those obtained with the 3R4F aqueous extract exposure (Figure 6B).



**Figure 6. Vasculature-on-a-chip application for assessment of THS 2.2: monocyte-to-endothelial microvessel adhesion under flow. (A)** Scheme of experimental design. **(B)** TNFα release in conditioned medium following a two-hour exposure of MM6 cells to freshly generated aqueous extract from 3R4F cigarette smoke or THS 2.2 aerosol. N=4, n=2. **(C)** Representative images of monocyte attachment to 4 day-HCAEC microvessels after exposure to TNFα or conditioned medium for four and 16 hours. **(D)** Quantification of monocyte adhesion after conditioned medium exposure. MM6 attachment to the endothelial microvessels was measured four and 16 hours after addition of the conditioned medium. Attachment was quantified as the number of MM6 cells attached per 100 HCAECs and normalized for the VC corresponding to conditioned medium without 3R4F smoke/ THS2.2 aerosol aqueous extracts. N=4, n=4-6. p<0.1, \*p < 0.05, \*\*p < 0.01, \*\*\*p < 0.001 compared with attachment in VC (one-way ANOVA followed by post-hoc Dunnett's pairwise comparisons). Abbreviations: h, hours.

# Reduced effect of THS 2.2-conditioned medium compared with that of 3R4F-conditioned medium on MM6 cell adhesion to HCAEC microvessels

After exposure of HCAEC microvessels to 3R4F-conditioned medium for four and 16 hours, the adhesion of MM6 cells to the lumen of microvessels increased significantly and peaked at a concentration of 0.05 puffs/mL of 3R4F aqueous extract (Figure 6C and D). At this concentration, THS 2.2-conditioned medium did not significantly promote the adhesion of MM6 cells to HCAEC microvessels (Figure 6C and D). The concentration of THS 2.2 aqueous extract (0.7 puffs/mL) in conditioned medium had to be enhanced by a factor of approximately 14 to yield similar adhesion (Figure 6D). At 16 hours, no significant increase in adhesion was measured at any concentration of THS 2.2 aqueous extract in conditioned medium, and adhesion actually decreased significantly at the highest concentrations of THS 2.2 aqueous extract (1.5 and 2.5 puffs/mL) (Figure 6D). In parallel, various concentrations of TNFα were included as positive controls and yielded similar results (Figure 6C and D) to those observed (Figure 4) in establishing the adhesion assay with HCAEC microvessels.

# Reduced effect of THS 2.2-conditioned medium compared with that of 3R4F-conditioned medium on ICAM1 protein abundance and GSH content in HCAEC microvessels

ICAM1 protein was stained and quantified in HCAEC microvessels, and patterns of ICAM1 protein abundance changes similar to those observed for MM6-HCAEC microvessel adhesion were measured after four or 16 hours of exposure to conditioned medium (Figure 7A and B). Exposure to conditioned medium did not affect the viability of the microvessel cultures, except at the highest concentration (2.5 puffs/mL) of THS 2.2 aqueous extract (Supplementary Figure 4A). The number of nuclei counted in the vessels was not affected by conditioned medium exposure (Supplementary Figure 4B), indicating low toxicity of the conditioned medium at these incubation time points. In addition to soluble mediators released by MM6 cells, conditioned medium contains chemical constituents derived from cigarette

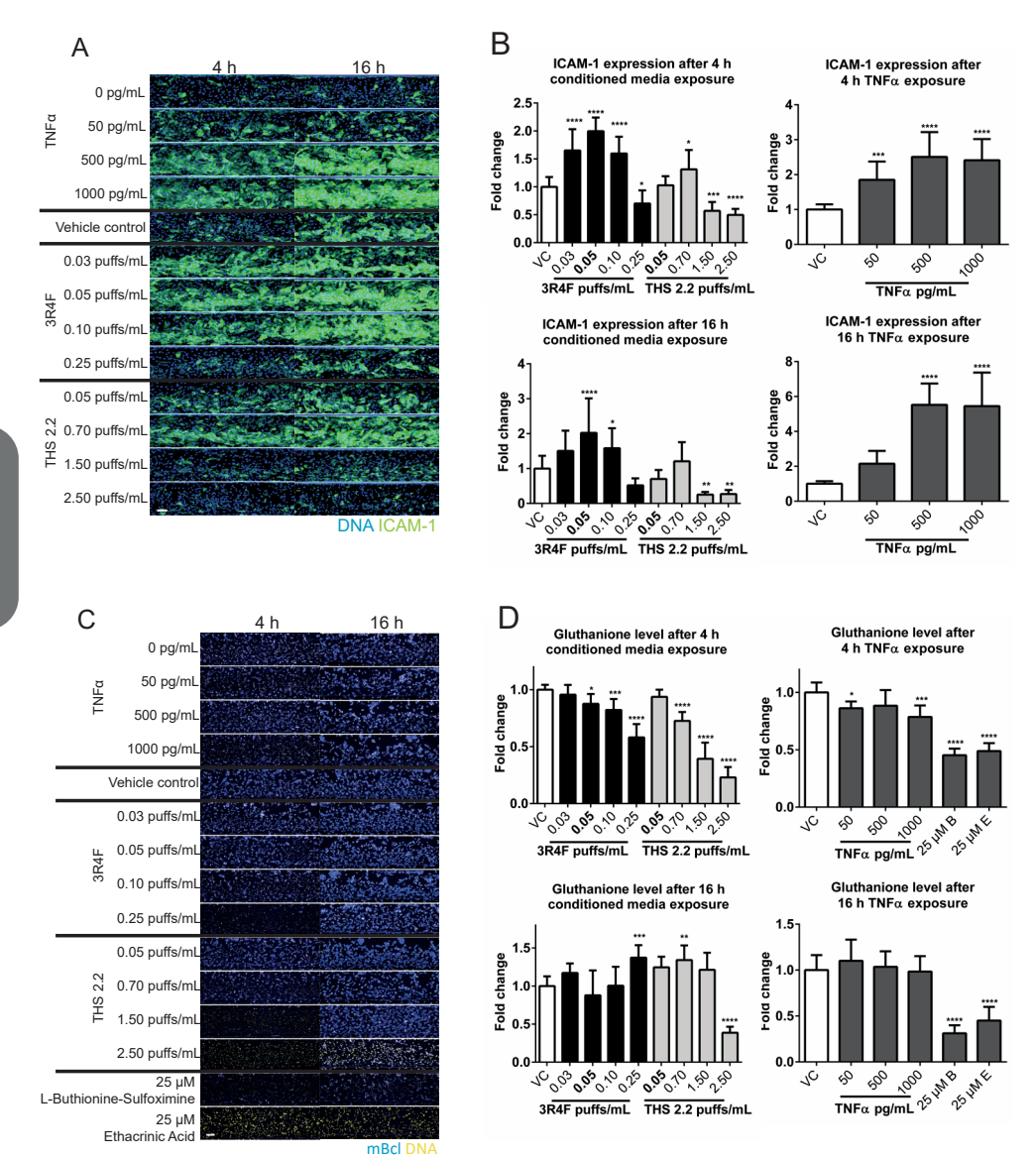


**Figure 7. Vasculature-on-a-chip application for assessment of THS 2.2: quantification of key inflammatory and oxidative stress markers.** HCAEC microvessels at day 4 were treated with 3R4F- and THS 2.2-conditioned media or with TNFα (50-1,000 pg/mL), L-buthionine-sulfoximine [B, 25 μM] and ethacrynic acid [E, 25 μM] as positive controls for four and 16 hours. **(A)** Representative pictures (sum-projections) and **(B)** quantification barplots of ICAM1 protein in HCAEC microvessels. N=4, n=3. **(C)** Representative pictures (sum-projections) and **(D)** quantification barplots of GSH content in HCAEC microvessels. N=3, n=3. The results for both markers are expressed as the FC intensity (calculated per HCAEC nucleus) between treatment and its VC. Statistics: \*=p<0.05, \*\*=p<0.01, \*\*\*\*=p<0.001, \*\*\*\*=p<0.0001 (compared to VC, one-way ANOVA followed by post-hoc

Dunnett's pairwise comparisons). Abbreviations: 3R4F, reference cigarette; THS 2.2, Tobacco Heating System 2.2; h, hours.

smoke. We previously showed that these compounds, which remain stable in conditioned medium, after a freezing/thawing cycle, can trigger oxidative stress in endothelial cells on top of an inflammatory response promoted by MM6-derived soluble mediators. Therefore, we measured GSH levels to assess the magnitude of oxidative stress in HCAEC microvessels (Figure 7C and D). We also exposed HCAEC microvessels to 25  $\mu$ M of L-buthionine-sulfoximine and 25  $\mu$ M of ethacrynic acid as positive controls. The exposure resulted in a significant reduction in GSH levels after four and 16 hours (Figure 7C and D). Depletion of GSH, indicating oxidative stress, was observed with increased concentrations of 3R4F or THS 2.2 aqueous extracts in conditioned medium; however, the effect on GSH levels was measured when concentrations of THS 2.2 aqueous extract in the conditioned medium were approximately 14 times higher than concentrations of 3R4F aqueous extract. After a 16-hour exposure, GSH levels returned to levels similar to those of the VC, with the exception of GSH levels in microvessels exposed to the highest concentration (2.5 puffs/mL) of THS 2.2 aqueous extract (Figure 7C and D).

## Discussion

In this work, we developed and optimized a 3D vasculature-on-a-chip model using the OrganoPlate® platform to investigate the mechanism of leukocyte adhesion to the lumen of endothelial microvessels, a key step in the initiation of inflammation and vascular disorders, such as atherosclerosis. Moreover, we showed how this 3D endothelial vascular model can be leveraged for real-world applications, such as systems toxicology assessments of products in a research and development framework.

In order to establish our 3D model and grow microvessels, we used primary HCAECs, a cellular model particularly relevant in studying cardiovascular diseases. The tubular shape developed within two days only when endothelial cells, adherent to the ECM, were perfused, indicating that the bidirectional and oscillating flow generated by gravity-driven leveling had a mechanical effect on endothelial cells. In this context, cells intermittently undergo a shear stress estimated to rise up to 1.6 dyne/cm2 when the rocker is tilted.<sup>40</sup> In vivo, similar-sized venules are exposed to shear levels between 1 and 5 dyne/cm<sup>2</sup>. The endothelial barrier increased after a few hours and was formed after two days, remaining stable for at least eight days. After two days, permeability to 4.4 and 20 kDa dextran reached levels  $(4.0\times10-5 \text{ cm/s})$  and  $3\times10-5 \text{ cm/s}$ , respectively) comparable with those found in microvessels grown with human umbilical vein endothelial cells.8 HCAEC barrier formation was characterized by positive stainings of the VE-cadherin and CD31 proteins, two major endothelial-junction-associated proteins playing a role in the process of blood vessel tube formation (Vestweber, 2008; Yang et al., 1999). The nature of ECM and microenvironments can influence the growth and migratory phenotypes of endothelial cells.<sup>42,43</sup> Therefore, we optimized the choice of ECM and culture conditions (medium and cell density) to obtain homogeneous and reproducible HCAEC tubes devoid of cell protrusion/migration into the ECM, a characteristic of angiogenic behavior.44

For functional analysis of the model, we set up an adhesion assay by flowing untreated, fluorescently labeled monocytic cells through the lumen of HCAEC microvessels pre-stimulated with TNFα and quantifying the monocytic cells that remained attached to the endothelium. HCAEC microvessels responded to TNFα by promoting the adhesion of monocytic cells to microvessels in a concentration-dependent manner after four hours, with sustained effects at the highest concentrations (500 and 10,000 pg/mL) after a 16-hour treatment. In parallel, the immunohistochemical quantification of ICAM1 in HCAEC microvessels showed a correlation of the adhesion protein with monocyte-endothelium adhesion promoted by TNFα. The kinetic profile of ICAM1 protein expression was consistent with previous findings.<sup>38</sup>

These observations were also supported by TNFα concentration- and timedependent gene expression changes, clearly showing increased transcription of inflammatory genes following the activation of the TNFα/nuclear factor-kappa B signaling pathway. Gene sets that were significantly enriched reflected innate immune/inflammatory pathways, such as cytokine/chemokine signaling, TNFα/ CD40 signaling, and interferon y signaling, in addition to cell cycle processes, such as DNA replication and mitosis. Interestingly, an analysis of time course proteinprotein interaction networks using transcriptomics and genome-wide datasets accompanied by experimental validation has shown that TNFα can promote G1/S transition in the cell cycle in vascular endothelial cells.<sup>45</sup> This may facilitate the cell cycle activation promoted by vascular endothelial growth factor. The comparison in response to TNF $\alpha$  of 3D and 2D endothelial cell models showed high consistency at the levels of gene expression changes and enriched pathways/processes. However, an accurate quantification of differences between both models would require an experiment comparing 3D and 2D cultures simultaneously, using HCAECs from one donor, which was not the case here, although our study was still robust in showing the biology perturbed by TNFa across independent experiments and donors.

Overall, these results indicate that following TNF $\alpha$  stimulation, HCAEC microvessels in vitro can be activated and bind monocytes under flow. The pattern of adhesion correlated with the expression of adhesion molecules, similarly to previous in vivo and in vitro observations in arterial and microvascular endothelial cells. 46-50

For a real-case application in systems toxicology, our HCAEC microvessel model was leveraged to assess the impact of aerosol from THS 2.2, a candidate MRTP, compared with the impact of 3R4F smoke in the form of conditioned medium on the process of monocytic cell adhesion to endothelial microvessels. The conditioned medium was generated by collecting the supernatant of MM6 cells exposed to aqueous extracts from 3R4F smoke or THS 2.2 aerosol for two hours. Conditioned medium contains a mixture of soluble mediators released by monocytic cells and chemical-derived compounds from smoke/aerosol, mimicking an in vitro milieu with inflammatory and oxidative properties, such as blood from smokers. 12,37,51 The four-hour exposure of HCAEC microvessels to 3R4F-conditioned medium triggered an inflammatory response that promoted an increase in endothelial adhesion proteins and monocytic cell adhesion to the lumen of the HCAEC microvessels as well as endothelial oxidative stress, observed as depletion of GSH. Although the presence of serum during the exposure of HCAEC microvessels to conditioned medium may potentially reduce the effect of aqueous extracts,<sup>39</sup> these findings are similar to previous ones in HCAECs, also showing that monocyte-released soluble mediators, such as TNF $\alpha$ , are responsible for inducing the inflammatory response, 37,52 while chemical compounds derived from 3R4F smoke induced oxidative stress in HCAECs.<sup>37</sup> At the later time point (16 hours), GSH content was restored, indicating that HCAEC microvessels coped with the oxidative stress, while endothelial inflammation was still observed at some concentrations, suggesting a sustained effect of inflammatory mediators present in 3R4F-conditioned medium and/or possible autocrine feedback loops. At concentrations of 3R4F-conditioned medium at which molecular and functional effects peaked, no significant effect was observed with THS 2.2-conditioned medium. It was necessary to increase the concentration of THS 2.2 aqueous

extract to generate conditioned medium by a factor of approximately 14 to record similar effects to those seen for 3R4F-conditioned medium. These results are in agreement with our previous work in a 2D HCAEC adhesion assay model. Overall, this case study of leveraging a 3D vasculature-on-a-chip model for risk assessment in vitro shows the potential of water-soluble aerosol extract from THS 2.2 to exert a reduced impact on mechanisms that lead to the development of atherosclerosis in a pathological context, compared with extracts from cigarettes. It should be noted, however, that these findings are specific to an atherosclerosis-related context, and effects may differ in other disease models or physiological systems, underscoring the need for broader investigation before general conclusions can be drawn.

The microvessel model was used for acute exposures to TNFa or product-conditioned medium after four days of seeding to ensure the stability of the tube formation. Longer treatments may show different mediator and gene expression profiles more representative of the chronic conditions that lead to the development of vascular disorders. However, evaluations of endothelial microvessel barrier stability for more than eight will be required before conducting longer exposures.

Other microfluidic systems have been developed to study the adhesion of blood cells, such as leukocytes (e.g., neutrophils), erythrocytes and platelets, and cancer cells to endothelial cells in hemodynamic flow.<sup>53–57</sup> Various systems offer the functionality to control shear stress applied on endothelial cells, which are still, however, grown as a 2D monolayer.<sup>53–56</sup> Interestingly, more advanced systems can be fabricated to incorporate a channel containing a stenotic structure for flow characterization<sup>54</sup> or to mimic in vivo microvasculature network for studying the complete adhesion to transmigration cascade.<sup>57</sup> Nevertheless, the format of these microfluidics remains low-throughput due to the complexity of producing and handling.<sup>54,57</sup> A major advantage of the OrganoPlate® over other microfluidic systems is its microtiter format, which enables growing 96 independent microvessels, providing throughput capacity for multiple-condition testing,

useful for drug screening and dose-response studies. Moreover, continuous flow perfusion of media through HCAEC microvessels using gravity leveling instead of pumps facilitates handling and reduces the risk of contamination. The absence of a pump that permits the application of flow with specific shear stress magnitude and profiles (e.g., pulsatile, oscillatory) can be perceived as a limitation of the system. However, the constant evolution of the OrganoPlate® functionality and design may resolve this issue in the future. The availability of a three-lane OrganoPlate® provides significant potential to extend our HCAEC microvessel model to explore further functional aspects of vascular biology and disorders simultaneously using a single model (e.g. transmigration of monocytes). The development of co-cultures from various tissues/organs, such as smooth muscle cells, neuronal cells, or epithelial cells, paves the way to a range of potential applications. Additional experimental setups such as concomitant exposure of leukocytes and endothelium to a treatment under flow offer the flexibility to investigate independent and combined contribution of both cellular types to a mechanism of interest. Moreover, perfusing human blood or serum/plasma and using endothelial cells from donors with atherosclerosis and cardiovascular disorders or donors of various ages provides an opportunity to screen a wider human population and may further contribute to the translatability of our 3D vasculature-on-a-chip model and advance its development as a precision medicine selection tool.

## Conclusions

In the context of the 3Rs principle that encourages the community to create relevant in vitro alternatives that reduce animal use, we developed and optimized a 3D vasculature-on-a-chip model using the microfluidic OrganoPlate® to investigate the process of leukocyte adhesion to the lumen of primary disease-relevant HCAEC microvessels under flow. In addition to functional readouts, we measured various molecular endpoints using high-content imaging and

transcriptomics, providing mechanistic insights into the model. We demonstrated the applicability of the model for real-world research and development projects, such as systems toxicology-based risk assessment of products in vitro. The OrganoPlate® format and its design evolutions provide scalability and potential for extending the model to investigate additional mechanistic aspects of vascular diseases that would complement cardiovascular disease risk assessment and open a wide spectrum of applications in vascular biology research and beyond.

#### **Conflict of interest**

This publication contains original work. The authors CP, AL, DP, KB, RD, EG, NVI, MCP, and JH are employees of Philip Morris International. The authors BK, HL, TO, MV, AvdH, and JJ are or were employees of MIMETAS BV. These affiliations are declared. The OrganoPlate® is a registered trademark of MIMETAS BV.

### Acknowledgements

Philip Morris International is the sole source of funding and sponsor of this research. We thank Pauline Betsch and Dr Remko van Vught for project management support, Didier Goedertier and Claudius Pak for generating the aqueous smoke/aerosol extracts, Dr Alain Sewer for preparing and submitting transcriptomics data to the Array Express repository database and Frederik Schavemaker for support with schematic illustrations. We also thank Dr Dean Meyer from Edanz Medical Writing (www.edanzediting.com/ac), for editing a draft of this manuscript.

## References

- 1. Radeva, M. Y. & Waschke, J. Mind the gap: Mechanisms regulating the endothelial barrier. Acta Physiol (Oxf) 222, (2018).
- 2. Favero, G., Paganelli, C., Buffoli, B. & others. Endothelium and its alterations in cardiovascular diseases: Life style intervention. Biomed Res Int 8018, (2014).
- 3. Insull Jr., W. The pathology of atherosclerosis: Plaque development and plaque responses to medical treatment. Am J Med 122, S3–S14 (2009).
- 4. Burden, N., Chapman, K., Sewell, F. & others. Pioneering better science through the 3rs: An introduction to the national centre for the replacement, refinement, and reduction of animals in research (nc3rs). J Am Assoc Lab Anim Sci 54, 198–208 (2015).
- 5. Lee, J., Packard, R. R. & Hsiai, T. K. Blood flow modulation of vascular dynamics. Curr Opin Lipidol 26, 376–383 (2015).
- 6. Chatterjee, S. Endothelial mechanotransduction, redox signaling and the regulation of vascular inflammatory pathways. Front Physiol 9, 524 (2018).
- 7. Hsieh, H. J., Liu, C. A., Huang, B. & others. Shear-induced endothelial mechanotransduction: The interplay between reactive oxygen species (ros) and nitric oxide (no) and the pathophysiological implications. J Biomed Sci 21, 3 (2014).
- 8. van Duinen, V. et al. 96 perfusable blood vessels to study vascular permeability in vitro. Sci Rep 7, 18071 (2017).
- 9. Bogorad, M. I., DeStefano, J., Karlsson, J. & others. Review: In vitro microvessel models. Lab Chip 15, 4242–4255 (2015).
- 10. Nahrendorf, M. & Swirski, F. K. Lifestyle effects on hematopoiesis and atherosclerosis. Circ Res 116, 884–894 (2015).
- 11. Messner, B. & Bernhard, D. Smoking and cardiovascular disease: Mechanisms of endothelial dysfunction and early atherogenesis. Arterioscler Thromb Vasc Biol 34, 509–515 (2014).
- 12. Yanbaeva, D. G., Dentener, M. A., Creutzberg, E. C. & others. Systemic effects of smoking. Chest 131, 6–2179 (2007).
- 13. General, S. In (eds.), How tobacco smoke causes disease: The biology and behavioral basis for smoking-attributable disease: A report of the surgeon general. (2010).
- 14. Murphy, J., Gaca, M., Lowe, F. & others. Assessing modified risk tobacco and nicotine products: Description of the scientific framework and assessment of a closed modular electronic cigarette. Regul Toxicol Pharmacol 90, 342–357 (2017).
- 15. Food & Administration, D. Modified risk tobacco product applications: Draft guidance for industry. Http://www.Fda.Gov/downloads/tobaccoproducts/guidancecomplianceregulatoryinformation/ucm297751.Pdf (2012).
- 16. Schaller, J. P., Keller, D., Poget, L. & others. Evaluation of the tobacco heating system Part 2: Chemical composition, genotoxicity, cytotoxicity, and physical properties of the aerosol. Regul Toxicol Pharmacol 81, S27–S47 (2016).
- 17. Poussin, C., Laurent, A., Kondylis, A. & others. In vitro systems toxicology-based assessment of the potential modified risk tobacco product chtp for vascular inflammationand cytotoxicity-associated mechanisms promoting adhesion of monocytic cells to human coronary arterial endothelial cells. Food Chem Toxicol 120, 390–406 (2018).
- 18. Poussin, C., Laurent, A., Peitsch, M. C., Hoeng, J. & De Leon, H. Systems toxicology-based assessment of the candidate modified risk tobacco product THS2.2 for the adhesion of monocytic cells to human coronary arterial endothelial cells. Toxicology 339, 73–86 (2016).
- 19. Phillips, B., Veljkovic, E., Boue, S. & others. An 8-month systems toxicology inhalation/cessation study in apoe-/- mice to investigate cardiovascular and respiratory exposure effects of a candidate modified risk tobacco product, ths , compared with conventional cigarettes. Toxicol Sci 149, 411–432 (2016).
- 20. van der Toorn, M. et al. Aerosol from a candidate modified risk tobacco product has

reduced effects on chemotaxis and transendothelial migration compared to combustion of conventional cigarettes. Food and Chemical Toxicology 86, 81–87 (2015).

- 21. Ludicke, F., Picavet, P., Baker, G. & others. Effects of switching to the menthol tobacco heating system smoking abstinence, or continued cigarette smoking on clinically relevant risk markers: A randomized, controlled, open-label, multicenter study in seguential confinement and ambulatory settings. Nicotine Tob Res 20, 173–182 (2018).
- 22. Fratta Pasini Anna AND Albiero, Serum Oxidative Stress-Induced Repression of Nrf2 and GSH Depletion: A Mechanism Potentially Involved in Endothelial Dysfunction of Young Smokers. PLoS One 7, 1–12 (2012).
- 23. Haralick, R. M., Sternberg, S. R. & Zhuang, X. Image analysis using mathematical morphology. IEEE Transactions on Pattern Analysis and Machine Intelligence PAMI- 9, 550–632 (1987).
- 24. Sternberg. Biomedical image processing. Computer (Long Beach Calif) 16, 22–34 (1983).
- 25. Lee, S. U., Chung, S. Y. & Park, R. H. A comparative performance study of several global thresholding techniques for segmentation: Computer Vision. Graphics, and Image Processing 52, 171–190 (1990).
- 26. Dai, M., Wang, P., Boyd, A. D. & others. Evolving gene/transcript definitions significantly alter the interpretation of genechip data. Nucleic Acids Res 33, 175 (2005).
- 27. McCall, M. N., Bolstad, B. M. & Irizarry, R. A. Frozen robust multiarray analysis (frma). Biostatistics 11, 242–253 (2010).
- 28. Bolstad, B. M. Quality assessment of affymetrix genechip data. in (eds (eds. r., G., carey v.J., huber w., irizarry r.A. & dudoit s.) (bioinformatics and computational biology solutions using r and bioconductor. Statistics for biology and health. Springer, 2005). doi:https://doi.org/10.1007/0-387-29362-0 3.
- 29. Smyth, G. K. Linear models and empirical bayes methods for assessing differential expression in microarray experiments. Stat Appl Genet Mol Biol 3, (2004).
- 30. Benjamini, Y. & Hochberg, Y. Controlling the false discovery rate: A practical and powerful approach to multiple testing: Journal of the Royal Statistical Society Series B 57. 289–300 (1995).
- 31. Martin, F., Sewer, A., Talikka, M. & others. Quantification of biological network perturbations for mechanistic insight and diagnostics using two-layer causal models. BMC Bioinformatics 15, 238 (2014).
- 32. sbv IMPROVER project team Ansari, S. B. J. et al. On crowd-verification of biological networks. 7, 307–325 (2013).
- 33. Boue, S., Talikka, M., Westra, J. W. & others. Causal biological network database: A comprehensive platform of causal biological network models focused on the pulmonary and vascular systems. Database (Oxford) 30, (2015).
- 34. Subramanian, A., Tamayo, P., Mootha, V. K. & others. Gene set enrichment analysis: A knowledge-based approach for interpreting genome-wide expression profiles. Proc Natl Acad Sci U S A 10, 15545–15550 (2005).
- 35. Ackermann, M. & Strimmer, K. A general modular framework for gene set enrichment analysis. BMC Bioinformatics 10, 47 (2009).
- 36. of Canada, G. Tobacco products information regulations. Https://www.Canada. Ca/en/health-canada/services/health-concerns/reports-publications/tobacco/tobacco-products-information-regulations.Html (2000).
- 37. Poussin, C., Laurent, A., Peitsch, M. C. & others. Systems biology reveals cigarette smoke-induced concentration-dependent direct and indirect mechanisms that promote monocyte-endothelial cell adhesion. Toxicol Sci 147, 370–385 (2015).
- 38. Granger, D. N. & Senchenkova, E. Inflammation and the microcirculation. (2010).
- 39. Grigoryan, H., Edmands, W., Lu, S. S. & others. Adductomics pipeline for untargeted analysis of modifications to cys34 of human serum albumin. Anal Chem 88, 10504–10512 (2016).
- 40. Vormann, M. K., Gijzen, L., Hutter, S. & others. Nephrotoxicity and kidney transport

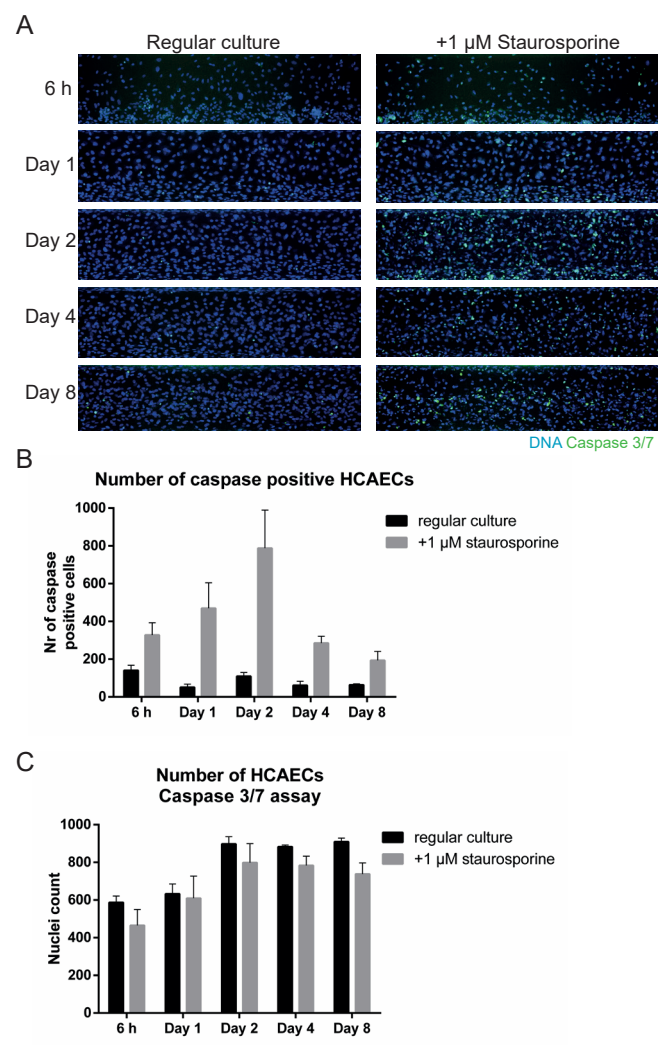
assessment on 3d perfused proximal tubules. AAPS J 20, 90 (2018).

- 41. Cucullo, L., Hossain, M., Puvenna, V., Marchi, N. & Janigro, D. The role of shear stress in Blood-Brain Barrier endothelial physiology. BMC Neurosci 12, 40 (2011).
- 42. Imanaka-Yoshida, K. Extracellular matrix remodeling in vascular development and disease. Etiology and morphogenesis of congenital heart disease: from gene function and cellular interaction to morphology 221–226 (2016).
- 43. Muncie, J. M. & Weaver, V. M. The physical and biochemical properties of the extracellular matrix regulate cell fate. Curr Top Dev Biol 130, 1–37 (2018).
- 44. Mongiat, M., Andreuzzi, E., Tarticchio, G. & others. Extracellular matrix, a hard player in angiogenesis. Int J Mol Sci 17, (2016).
- 45. Chen, Y., Gu, J., Li, D. & others. Time-course network analysis reveals tnf-alpha can promote g1/s transition of cell cycle in vascular endothelial cells. Bioinformatics 28, 1–4 (2012).
- 46. Amberger, A., Maczek, C., Jurgens, G. & others. Co-expression of icam-1, vcam-1, elam-1 and hsp60 in human arterial and venous endothelial cells in response to cytokines and oxidized low-density lipoproteins. Cell Stress Chaperones 2 1, 94–103 (1997).
- 47. Jia, Z., Nallasamy, P., Liu, D. & others. Luteolin protects against vascular inflammation in mice and tnf-alpha-induced monocyte adhesion to endothelial cells via suppressing ikappabalpha/nf-kappab signaling pathway. J Nutr Biochem 26, 293–302 (2015).
- 48. Langert, K. A., Zee, V., L., C. & Stubbs Jr., B. Jr. S. E. Tumour necrosis factor alpha enhances ccl2 and icam-1 expression in peripheral nerve microvascular endoneurial endothelial cells. ASN Neuro 5, (2013).
- 49. Mulligan, M. S., Vaporciyan, A. A., Miyasaka, M. & others. Tumor necrosis factor alpha regulates in vivo intrapulmonary expression of icam-1. Am J Pathol 142, 1739–1749 (1993).
- 50. Zachlederova, M. & Jarolim, P. The dynamics of gene expression in human lung microvascular endothelial cells after stimulation with inflammatory cytokines. Physiol Res 55, 39–47 (2006).
- 51. Zhang, X., Wang, L., Zhang, H. & others. The effects of cigarette smoke extract on the endothelial production of soluble intercellular adhesion molecule-1 are mediated through macrophages, possibly by inducing tnf-alpha release. Methods Find Exp Clin Pharmacol 24, 261–265 (2002).
- 52. Rennert, K., Heisig, K., Groeger, M. & others. Recruitment of cd16(+) monocytes to endothelial cells in response to lps-treatment and concomitant tnf release is regulated by cx3cr1 and interfered by soluble fractalkine. Cytokine 83, 41–52 (2016).
- 53. Conant, C. G., Schwartz, M. A., Nevill, T. & others. Platelet adhesion and aggregation under flow using microfluidic flow cells. vol. 2009 (J Vis Exp).
- 54. Lee, J., Huh, H. K., Park, S. H. & others. Endothelial cell monolayer-based microfluidic systems mimicking complex in vivo microenvironments for the study of leukocyte dynamics in inflamed blood vessels. Methods Cell Biol 146, 23–42 (2018).
- 55. Thompson, T. J. & Han, B. Analysis of adhesion kinetics of cancer cells on inflamed endothelium using a microfluidic platform. Biomicrofluidics 12, 42215 (2018).
- 56. White, J., Lancelot, M., Sarnaik, S. & others. Increased erythrocyte adhesion to vcam-1 during pulsatile flow: Application of a microfluidic flow adhesion bioassay. Clin Hemorheol Microcirc 60, 201–213 (2015).
- 57. Lamberti, G., Prabhakarpandian, B., Garson, C. & others. Bioinspired microfluidic assay for in vitro modeling of leukocyte-endothelium interactions. Anal Chem 86, 8344–8351 (2014).

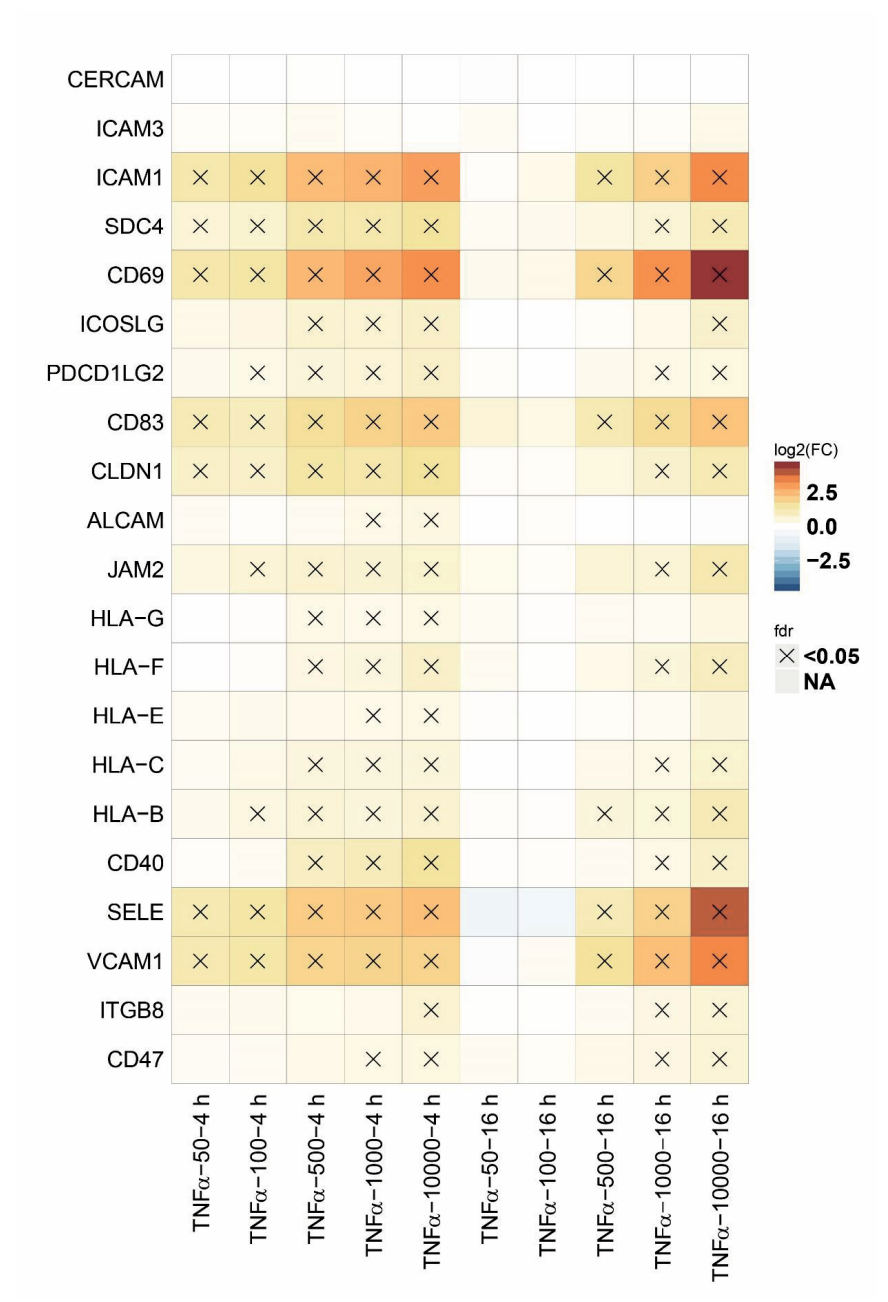
# Supplementary materials

The supplementary tables were not printed due to the length, they are available for download in the orgininal manuscript:

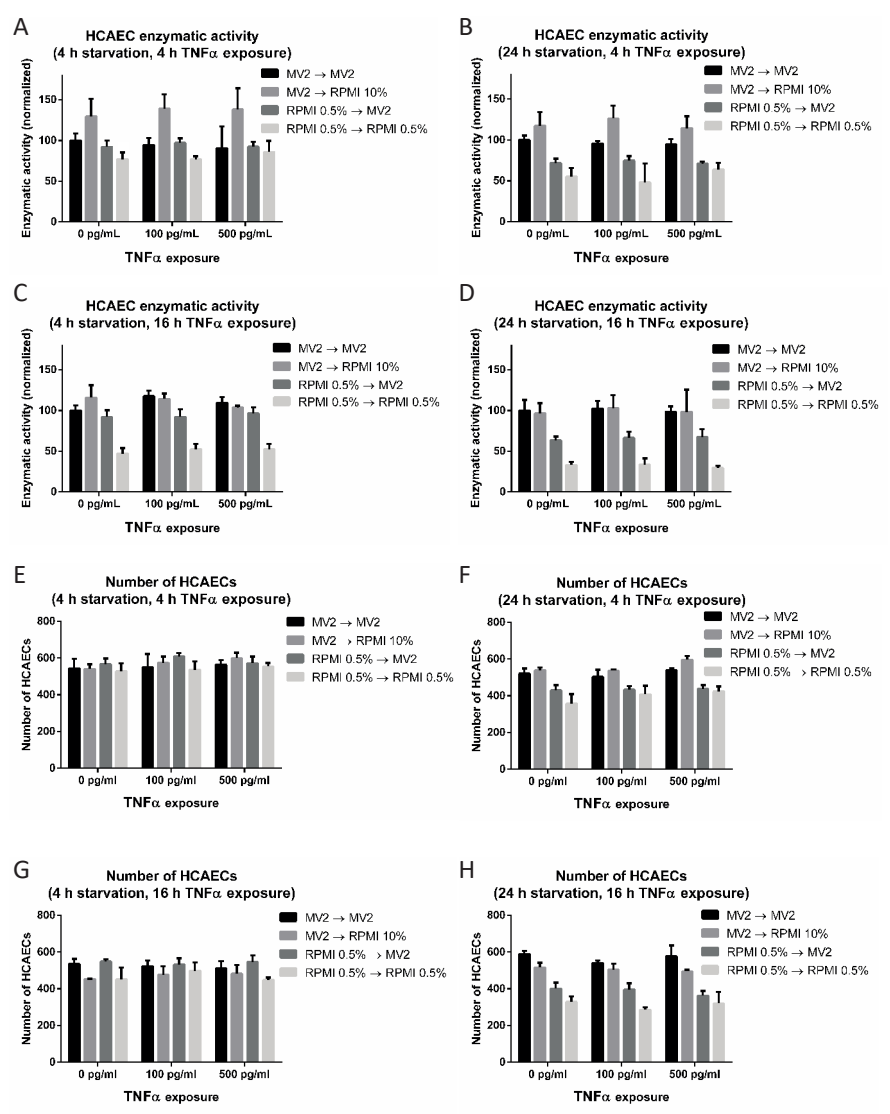
10.14573/altex.1811301



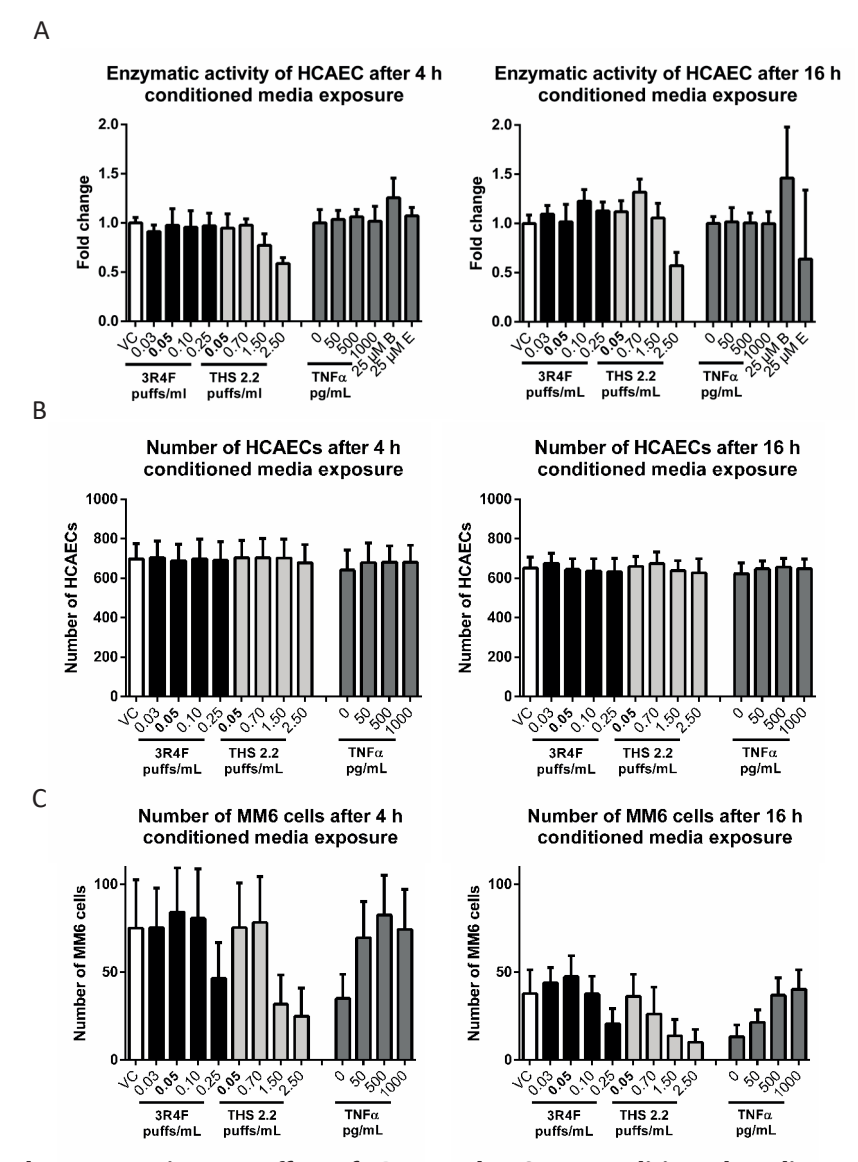
Supplementary figure 1. Quantification of caspase 3/7 activity in HCAEC microvessels up to 8 days culture. (A) HCAEC microvessels were stained for caspase 3/7 at different time points during regular culture (left) or after a 2hour-incubation with 1  $\mu$ M staurosporine. (B) Quantification of the number of caspase 3/7 positive HCAEC cells (N=1, n = 4). (C) Quantification of the total number of HCAEC nuclei (N=1, n = 4). Bars represent average + standard deviation. No statistical analysis given N=1.



Supplementary Figure 2. The FC of mRNA transcripts coding for adhesion molecules in HCAEC microvessels treated with TNF $\alpha$  for four and 16 hours. Heatmap of adhesion molecule-encoding gene expression FCs (as a log2 scale) comparing the effect of TNF $\alpha$  relative to VC. The symbol "X" in the heatmap indicates that the FC is statistically significant (FDR  $\leq$  0.05). Abbreviations: h, hours.



Supplementary Figure 3. Effect of serum content in medium on the viability and number of HCAECs in microvessels. The viability and number of HCAECs within microvessels was assessed using the WST-8 enzymatic assay (A-D) and counting Hoechst-stained nuclei (E-H), respectively, after four and 24 hours exposure to low (0.5%) or normal (5%) serum content in culture medium followed by four or 16 hours exposure to TNF $\alpha$  diluted in low (0.5%), normal (5%) and high (10%) serum content after medium change as illustrated by an arrow. WST-8 absorbance was measured 30 minutes after the addition of the reagent. RPMI medium was supplemented with 0.5% or 10% fetal bovine serum. Bars represent the mean + standard deviation and all WST-8 enzymatic activity values are normalized to the MV2 0 pg/mL TNF $\alpha$  condition. N= 1 independent experiment, n = 3 - 5. Abbreviations: h, hours.



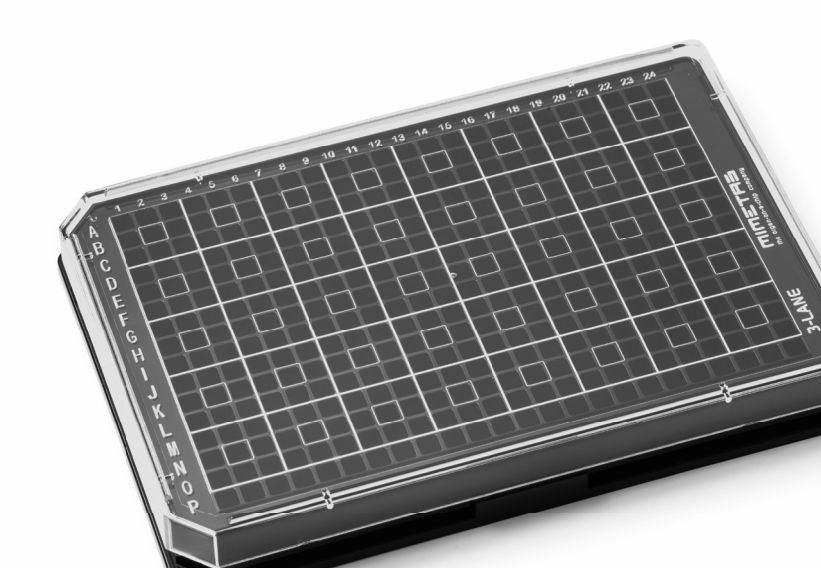
Supplementary Figure 4: Effect of 3R4F- and THS 2.2-conditioned media on the viability and number of HCAECs in microvessels (A) The viability and proliferation of HCAECs forming the microvessels was assessed using the WST-8 enzymatic assay after 4 and 16 h of conditioned medium exposure. WST-8 absorbance was measured 30 min after addition of the reagent (N = 2, n = 3). Data are expressed as fold change relative to the vehicle control (VC) corresponding to conditioned medium with 0 puffs/ml of aqueous extract from 3R4F smoke or THS2.2 aerosol. (B) Hoechst-stained nucleus counts and MM6 (C) in HCAEC microvessels after 4 and 16 h of conditioned medium exposure. Bars represent the mean + SD. N = 4, n = 4-6. 3R4F, reference cigarette; THS 2.2, Tobacco Heating System 2.2; B, L-buthionine-sulfoximine; E, ethacrynic acid.

# Chapter 4

# High-throughput 3D microvessel-on-a-Chip model to study defective angiogenesis in systemic sclerosis

Bart Kramer\*, Claudio Corallo\*, Angelique van den Heuvel, Justin Crawford, Thomas Olivier, Edo Elstak, Nicola Giordano, Paul Vulto, Henriette L. Lanz, Richard A. J. Janssen, Michela A. Tessari

Published in: Scientific Reports (2022) 12, 16930



# **Abstract**

In early Systemic Sclerosis (Scleroderma, SSc), the vasculature is impaired. Although the exact etiology of endothelial cell damage in SSc remains unclear, it is hypothesized that endothelial to mesenchymal transition (EndoMT) plays a key role. To perform physiologically relevant angiogenic studies, we set out to develop an angiogenesis-on-a-chip platform that is suitable for assessing disease parameters that are relevant to SSc and other vasculopathies. In the model, we substituted Fetal Bovine Serum (FBS) with Human Serum without impairing the stability of the culture. We showed that 3D microvessels and angiogenic factorinduced sprouts exposed to key pro-inflammatory and pro-fibrotic cytokines (TNFα and TGFβ) undergo structural alterations consisting of destructive vasculopathy (loss of small vessels). We also showed that these detrimental effects can be prevented by compound-mediated inhibition of TGFβ-ALK5 signaling or addition of a TNF $\alpha$  neutralizing antibody to the 3D cultures. This demonstrates that our in vitro model is suitable for compound testing and identification of new drugs that can protect from microvascular destabilization or regression in disease-mimicking conditions. To support this, we demonstrated that sera obtained from SSc patients can exert an anti-angiogenic effect on the 3D vessel model, opening the doors to screening for potential SSc drugs, enabling direct patient translatability and personalization of drug treatment.

## Introduction

Systemic Sclerosis (Scleroderma, SSc) is a chronic autoimmune connective tissue disease characterized by vasculopathy, inflammation and progressive fibrosis of the skin and internal organs, such as lungs, heart, kidneys and gastrointestinal tract.<sup>1</sup> Vascular alteration is an early and central event in SSc pathogenesis, and it usually precedes the onset of fibrosis.<sup>2</sup> Endothelial cells, as central constituents of the vascular system, play a key role in all aspects of vascular homeostasis as well as in physiological or pathological processes like thrombosis, inflammation, and vascular wall remodeling.<sup>3</sup> Although the etiology of vascular damage in SSc remains unclear, different hypotheses have been formulated to explain this phenomenon.<sup>4</sup> Among these, autoimmunity and the so-called endothelial to mesenchymal transition (EndoMT) appear to play a key role.<sup>5,6</sup> In fact, antiendothelial cell antibodies have been found in numerous autoimmune and/or inflammatory/infectious diseases. These conditions include, in addition to SSc, rheumatoid arthritis, systemic lupus erythematosus, polymyositis, several forms of vasculitis, and cytomegalovirus infection, among others.<sup>7,8</sup> In vitro investigations<sup>9</sup> demonstrate that SSc-specific autoantibodies embedded in immune complexes induce a pro-inflammatory and pro-fibrotic phenotype at the endothelial level. Incubation of endothelial cells with SSc-immune complexes results in modulation of several molecules involved in the three cardinal scleroderma pathophysiological processes. Firstly, it can lead to vascular dysfunction, where a key vascular alteration is represented by the critical imbalance between factors promoting vasoconstriction (e.g., endothelin ET-1) and vasodilation (e.g., nitric oxide). Secondly, SSc-immune complexes can inflame the perivascular space, with aberrant cytokine and chemokine release, and overexpression of adhesion molecules, including intercellular adhesion molecule-1 (ICAM-1) and vascular cell adhesion molecule-1 (VCAM-1).10 Thirdly, microvascular fibroproliferative lesions and other abnormalities associated with altered secretion of growth factors and profibrotic cytokines, such as transforming growth factor-beta (TGFβ), can

develop. TGF $\beta$  is a profibrotic cytokine that plays a key role in the ligand-mediated receptor process that triggers the onset and progression of SSc.<sup>11</sup>

Once activated, endothelial cells contribute to disease pathogenesis by mediating the fibroproliferative vasculopathy characteristic of SSc: the unbalanced production of vasoactive mediators resulting in vasoconstriction; the increased expression of adhesion molecules by damaged endothelial surfaces promoting leukocyte diapedesis, activation, and accumulation; endothelial cell transdifferentiation into myofibroblasts gaining mesenchymal cell markers (EndoMT).<sup>12</sup>

Onset of pathophysiological processes in SSc results in impaired vascular homeostasis, because of which angiogenesis is dysregulated and efficient vascular recovery is impaired.<sup>13</sup> The result is the onset of avascular areas and tissue hypoxia that leads to complications such as digital ulcers,<sup>14</sup> pulmonary arterial hypertension<sup>15</sup> and fibrosis.<sup>16</sup>

Most of the experimental systems for studying angiogenesis in SSc rely on animal models.<sup>17</sup> The first in vitro models were developed using two-dimensional cell culture-based assays.<sup>18</sup> Scientists demonstrated that human microvascular endothelial cells (HMVECs) cultured on a two-dimensional gelatinous protein mixture resembling the extracellular matrix (ECM) can form capillary-like structures upon treatment with pro-angiogenic factors.<sup>19</sup> They also demonstrated that disease relevant cytokines (e.g. ET-1, TGFß) or SSc sera can compromise capillary formation,<sup>20</sup> which could be partially restored using selective compounds.<sup>21,22</sup>

These two-dimensional in vitro models allow the study of fundamental endothelial cell biology, such as migration, proliferation and capillary formation.<sup>23</sup> However, two-dimensional models also have several limitations, including their limited throughput (capillary morphogenesis is usually performed in 6- or 24-well plates) and the short-term stability of the capillary-like structures (24 to 48 hours). This only allows for the study of tubulogenesis, but not the stability of the formed tubules. Additionally, these assays do not recapitulate the angiogenesis process including

its typical hallmarks, such as perfused lumen formation, differentiation into tip and stalk cells, anastomosis and widening of lumen.<sup>24</sup> Progress in tissue engineering and the advent of microfluidic-assisted tissue engineering has resulted in more sophisticated three-dimensional (3D) in vitro models for angiogenesis studies.<sup>25</sup> Although these models better recapitulate the angiogenesis conditions in vivo, they are quite complex to establish. In addition, they are usually implemented on single chips, thus compromising proper experimental design with multiple conditions (e.g. replicates, dilutions, controls).<sup>26</sup> Only few setups are compatible with routine testing and screening requirements, such as high content imaging (HCI)-based multiplexed cellular and molecular analyses, automated liquid handling and real time measurements.<sup>27</sup>

Recently, a gradient-driven, three-dimensional angiogenesis assay in a standardized microfluidic platform was described using immortalized human umbilical vein endothelial cells (HUVECs)<sup>28</sup> or induced pluripotent stem cells (iPS cells).<sup>29</sup> In this assay, angiogenic sprouting is induced from a perfused main vessel through a patterned collagen-1 gel. The resulting angiogenic sprouts have clear lumen, tip-stalk cell hierarchy and undergo anastomosis and vessel widening upon prolonged culture. In this work, we utilize this platform to study angiogenesis in primary human microvascular endothelial cells (HMVECs) and assess disease parameters that are relevant to SSc and other vasculopathies. We show that 3D microvessels and angiogenic factor-induced sprouts exposed to key pro-inflammatory and pro-fibrotic cytokines (TNFα and TGFβ) undergo structural alterations typical of destructive vasculopathy (loss of small vessels). We investigate how compound-mediated inhibition of TGFβ-ALK5 signaling or addition of TNFa neutralizing antibodies can prevent these detrimental effects. In addition, we demonstrate that sera obtained from SSc patients can exert an anti-angiogenic effect on the 3D vessel model, thus opening the doors for direct patient translation and personalization of the assay. Our in vitro model is suited for compound testing and identification of new drugs that can protect from microvascular destabilization and regression in disease-mimicking conditions.

## Material and Methods

### **Cell culture**

Primary HMVEC (Human Microvascular Endothelial Cells) (Lonza CC-2543) were cultured in regular T75 culture flasks (Corning, 734-2705) with EBM2 medium (Lonza CC-3156) containing the EGM-2MV kit (Lonza-4147). HMVEC were passaged one time before being seeded into the OrganoPlate® 3-lane (MIMETAS 4003-400-B, Leiden, The Netherlands). Cell detachment was done with Trypsin/EDTA solution 0.25 mg/mL (Lonza CC-5012) and neutralized with Trypsin Neutralization solution TNS (Lonza CC-5002).

### OrganoPlate culture

We used the OrganoPlate 3-lane with 320  $\mu$ m (top and bottom perfusion channels) x 360  $\mu$ m (middle gel channel) × 220  $\mu$ m (w×h) channels (MIMETAS 4003-400-B, Leiden, The Netherlands). Gel and perfusion channel lengths are 2.2 mm and the Phaseguides have dimensions of 100  $\mu$ m × 55  $\mu$ m (w×h). Before gel seeding, 50  $\mu$ L of Hank's balanced salt solution (HBSS) was dispensed into the observation window to prevent evaporation and enhance optical clarity. A stock solution of 5 mg/mL rat tail collagen type I (Cultrex rat collagen 1, 5 mg/mL; Trevigen, Gaithersburg, MD, USA) was neutralized with 10% 37 g/L NaHCO3 (Sigma, S5761) and 10% 1 M HEPES buffer (Gibco, 15630-056) to obtain a concentration of 4 mg/mL. The neutralized collagen was kept on ice until use and used within 10 minutes. Using a repeater pipette, 2  $\mu$ L of the neutralized collagen was added into the inlet of each gel channel. To polymerize the collagen, the OrganoPlate was incubated for 10 minutes at 37 °C, 5% CO<sub>2</sub>. After incubation, the device was removed from the incubator and 30  $\mu$ L HBSS was added to the gel inlet. The OrganoPlate was stored in the incubator (37 °C, 5% CO<sub>2</sub>) until cell loading next day.

HMVEC were trypsinized with Trypsin/EDTA solution 0.25 mg/mL and neutralized with Trypsin Neutralization solution TNS. Cells were pelleted and resuspended at

a concentration of 10° cells/mL in EBM2 medium containing EGM-2MV kit. HBSS in the gel inlet was aspirated right before cell loading. 2  $\mu$ L of the cell suspension was dispensed into the top perfusion inlet and incubated for 5 hours at 37 °C, 5% CO<sub>2</sub> in the OrganoPlate plate stand to allow the cells to attach to the ECM. After the cells attached to ECM, 50  $\mu$ L of medium was added in the top perfusion inlet and outlet wells. The plates were placed in the incubator (37 °C, 5% CO<sub>2</sub>) on a rocking platform with a 4-minute interval at an angle of 7°. Next day a medium change was performed by replacing the EBM2 medium with EGM-2MV kit for EBM2 medium with adjusted EGM-2MV kit where the FBS in the kit was replaced with 2% (final concentration) Human Healthy Serum (HHS, Tebu-bio, HSER-10ML). The serum consists of 3 donors pooled (1 male, 2 female, average age 35  $\pm$  13.1 years).

### Sprout formation, stimulation with angiogenic factors

HMVEC vessels were cultured for 3 days, in medium with HHS, before a gradient of angiogenic factors was applied. The bottom perfusion channels of the OrganoPlate 3-lane were washed with EBM2 medium (30  $\mu L$  of medium per well) for 10 minutes. Stock solutions of the angiogenic factors were prepared as follows:  $100\,\mu g/mL$  hVEGF-165 (Preprotech, 100-20) in 0.1% BSA in PBS, 1 mM Sphingosine-1-Phosphate (S1P, Sigma, G00918) in 5% 1 M HCl, 95% DMSO, and 10  $\mu g/mL$  Phorbol Myristate Acetate (PMA, Sigma, P1585) in 0.1% DMSO/MilliQ. Angiogenic factors were diluted in EBM2/EGM-2MV/HHS culture medium and used at the following concentrations: 50 ng/mL hVEGF-165, 2 ng/mL PMA, and 500 nM S1P. All medium was aspirated and fresh medium without angiogenic cocktail was added to the top perfusion channel (15  $\mu L$  per in/outlet) while medium with the angiogenic cocktail was added to the bottom perfusion channel (15  $\mu L$  per in/outlet). Angiogenic sprouts were monitored by phase contrast microscopy until ready for assays which was after 4 days of stimulation.

After 4 days of sprout stimulation, the medium with angiogenic cocktail was replaced with basal medium (Lonza CC-3156) without angiogenic cocktail containing antibiotics (GA-1000 from EGM-2MV kit), HHS at 2% or 5% final concentration.

### Sprout stability, exposure, and rescue

### **Stability**

For the stability experiments, after 4 days of sprout formation the angiogenic cocktail medium was replaced by imaging medium (basal medium with antibiotics, HHS (Human Healthy Serum) or HPS (Human Patient Serum) and Calcein-AM) for 30 minutes to establish the baseline and imaged (see sprout visualization and quantification section). After imaging, the imaging medium was replaced with basal medium containing antibiotics (GA-1000) and 2% HHS, 5% HHS or 5% HPS from several donors. After 48 hours, the sprouts were incubated for 30 minutes with basal medium containing Calcein-AM (1:2000, 15  $\mu$ L per top or bottom in/outlet) before imaging and assessing the sprout stability without angiogenic cocktail present in the medium.

### **Exposure and rescue**

For exposure experiments, the medium with angiogenic cocktail was replaced with basal medium without angiogenic cocktail containing antibiotics, HHS at 2% or 5% final concentration, Calcein-AM (1:2000 diluted) and inhibitory compounds for exposure: Alk5i 10mM final concentration (Sigma, S4317) and TNF $\alpha$  neutralizing antibody 0.32 µg/mL final concentration (TNF $\alpha$  iAb, Invivogen Cat# Htnfa-mab1). Medium was applied in top and bottom in- and outlets (15 µL per in/outlet). After 30 minutes incubation, the cultures were imaged and used as timepoint zero for further analysis. After 90 minutes, the pre-incubation medium was exchanged for exposure medium. Exposure medium contained:

basal medium, GA-1000 antibiotics, HHS (5% final concentration), HPS (2% or 5% final concentration) and exposure compounds or proper vehicle controls in different combinations and concentrations. For the triggers, TGF $\beta$  II at 10 ng/mL final concentration (R&D systems, Cat#: 302-B2) and TNF $\alpha$  at 10 ng/mL final concentration (ImmunoTools, Cat#: 11343015) were used as well as a combination of the two at equal concentrations.

#### Patients' enrollment

Serum samples were collected from 8 female patients (age,  $56.9 \pm 13.4$  years; disease duration,  $5.9 \pm 4.5$  years) affected by diffuse-cutaneous-SSc (dSSc) (n=4), by limited-cutaneous SSc (ISSc) (n=3) and by SSc-sine-scleroderma (ssSSc) (n=1) diagnosed in accordance with LeRoy et al. 1988 and who fulfilled the 2013 American College of Rheumatology/European League Against Rheumatism diagnostic criteria for SSc<sup>30</sup>. All patients gave their fully informed, voluntary, written consent according to the principles of the Declaration of Helsinki and in compliance with the ethics committee of the University of Siena, whose institutional review board approved the entire study protocol with code GLPG SSc 16. The major demographic and clinical characteristics of the patients enrolled are shown in Table 1.

Patient	Age (years) Sex	Disease duration (years)	Digital ulcers	PAH	Capillaroscopic pattern	ANA-ENA	Drug treatment
71 dSSc	52 F	10	Yes	No	Active	Antinucleolar-Scl-70	lloprost, Bosentan, glucocorticoids
72 ISSc	34 F	1.5	No	No	Active	Antinucleolar-Scl-70	Glucocorticoids
74 ISSc	42 F	0.5	No	No	Active	Antinucleolar-Scl-70	Nifedipine
75 dSSc	61 F	10	No	No	Active	Antinucleolar-Scl-70	lloprost, glucocorticoids, MMF
77 ssSSc	70 F	10	Yes	Yes	Active	Antinucleolar-Scl-70	lloprost, Bosentan, Nifedipine
79 dSSc	71 F	10	Yes	Yes	Active-late	Antinucleolar-Scl-70	Macitentan, MMF, Nifedipine
SO dSSc	67 F	1	No	Yes	Active	Antinucleolar-Scl-70	Macitentan, MMF, glucocorticoids
83 ISSc	58 F	4	No	No	Active	Antinucleolar-Scl-70	Glucocorticoids, Nifedipine, Azathio- prine
Mean (SD)	56.9 (13.4)	5.9 (4.5)					

**Table 1. The demographic and clinical characteristics of the patients enrolled in this study.** MMF, Mycophenolate mofetil; SD, Standard Deviation

### **Immunohistochemistry**

#### **Fixation**

HMVEC tubes and sprouts were fixated using 3.7% formaldehyde (Sigma, 252549) in HBSS (Sigma H6648) for 15 min, washed twice with HBSS for 5 minutes and stored with 50  $\mu$ L HBSS per well at room temperature until immunofluorescent staining.

#### Staining

HMVEC tubes were washed with washing solution containing 4% Fetal Calf Serum (FCS) (Gibco, cat# A13450) in PBS (Gibco, cat# 70013065) for 5 minutes and permeabilized with 0.3% Triton X-100 (Sigma, T8787) in PBS for 10 minutes. After permeabilization, the cells were washed with washing solution for 5 minutes before the blocking buffer, containing 2% FCS, 2% BSA (Sigma, cat# A2153), and 0.1% Tween20 (Sigma, cat# P9616) in PBS, was added for 50 minutes. After blocking, the cells were immediately incubated for 2 hours with a primary antibody in blocking solution, washed two times for 3 minutes with washing solution and incubated with a secondary antibody in blocking solution, including a nuclear stain, for 30 minutes. All steps were performed at room temperature. Primary antibodies used were Rabbit anti-human VE-Cadherin 1:1000 (Abcam, Ab33168), Mouse anti-human αSMA 1:1000 (Sigma, A2547), Mouse anti-human CD31 1:20 (Dako, M0823) and Rabbit anti-human SM22 (Abcam, Ab14106). The secondary antibodies were donkey-anti-mouse Alexa Fluor 647 (Invitrogen, A31571) and goat-anti-rabbit Alexa Fluor Plus 488 (Invitrogen, A32731). For nuclear staining Hoechst 33342 (Thermo Fisher Scientific H3570) 1:2000 was used.

### Sprout visualization and quantification

All images were captured with an ImageXPress XLS-C HCI system (Molecular Devices) & ImageXPress IXM-XLS micro HCI (Molecular Devices). During cell culture, phase-contrast (4X, 0.13NA) images were obtained on the IXM-XLS to

monitor growth of the HMVEC tubules over time. These images were processed in Fiji<sup>31</sup> to enhance contrast to aid with visual interpretation of the status of the cultures.

To visualize and quantify the growth of the endothelial sprouts, a fluorescent dye (Calcein-AM – FITC excitation & emission) was added to the HMVEC tubules at specific timepoints. These tubules were then imaged on the IXM-C HCI microscope. To accurately capture the 3D-nature of the tubules a 10X 0.5NA, FITC excitation / emission & a Nipkow 60 µm spinning disk was used to capture Z-stacks of the tubules. The separate Z-slices were stored to allow for 3D-reconstruction of the Z-data. Maximum intensity projections (MIP) were also created to quantify the growth of the tubules.

The MIP images were loaded into Fiji and subjected to a rolling ball background correction.<sup>32</sup> The resulting image was subjected to a threshold using Li's Minimum Cross Entropy threshold<sup>33</sup> to extract the area of the image covered by endothelial sprouts. The ratio of area of staining before & after compound addition was then calculated. This metric was then averaged over all replicates of a given condition and compared against the mean of other conditions. Statistics were performed with the 'one-way ANOVA' function in GraphPad Prism version 6.

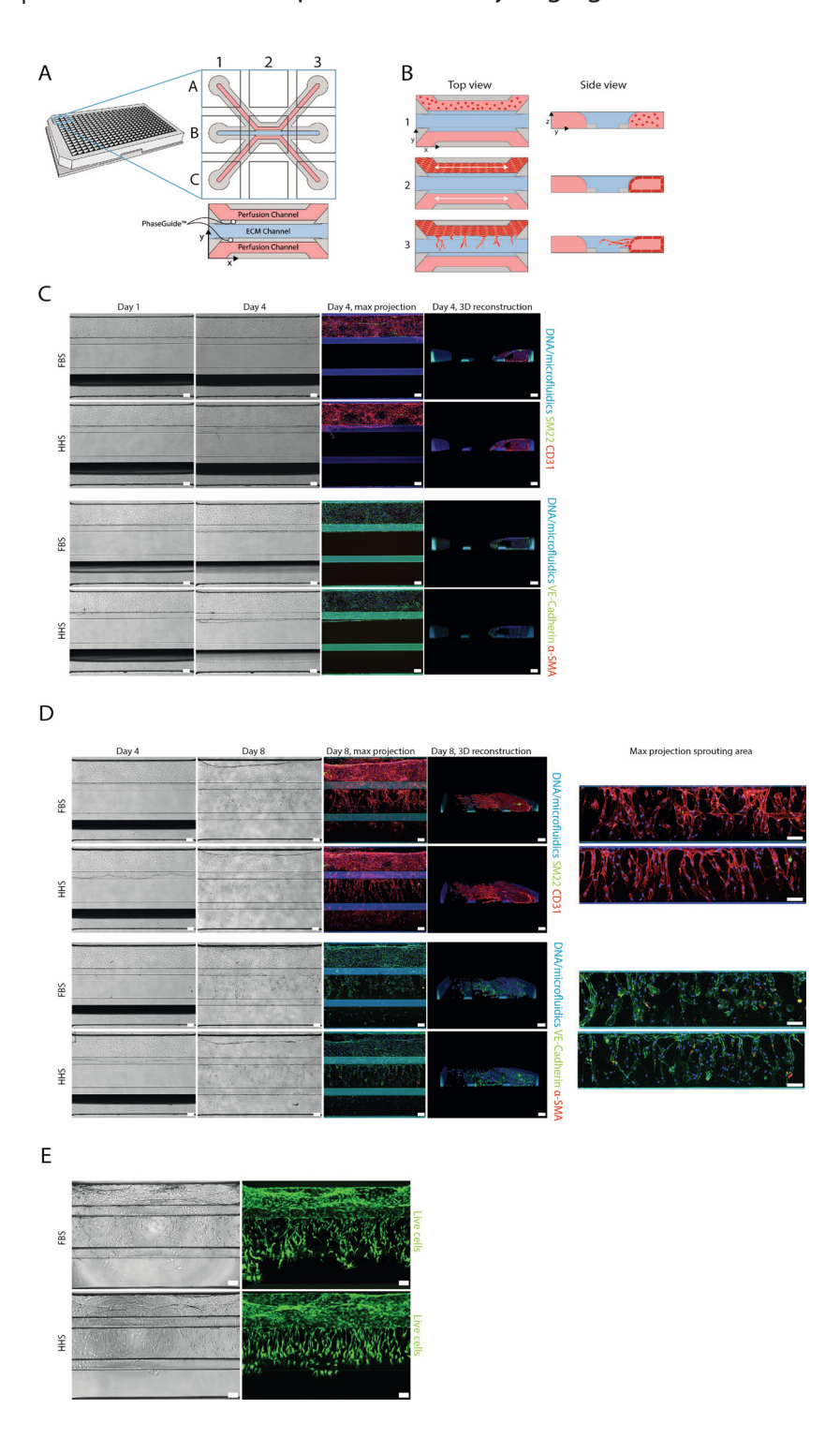


**Figure 1. Endothelial microvessel culture and sprouting. (A)** The microfluidic microtiter plate 'OrganoPlate' was used for a 3D cell culture, based on a 384 well plate interface with 40 microfluidic chips integrated in the bottom. The gel channel (blue) holds the collagen extracellular matrix (ECM) in place through the phaseguide's pressure barrier function. **(B)** Endothelial cells are loaded in the top channel (perfusion lane) to form a microvessel adjacent to the ECM in the middle channel. Bidirectional perfusion of the culture is induced by placing the OrganoPlate on an interval rocking platform. A gradient of an angiogenic cocktail is applied to induce sprout formation. **(C)** Immunofluorescent characterization of HMVEC tubules after 4 days of sprouting with FBS or HHS. On the right, a confocal maximum projection of the middle channel represents the sprouting area in the ECM. **E** Calcein-AM live cell staining of sprouted HMVEC cultures on day 8. All scale bars are 100 μm.

### Results

#### Endothelial microvessel culture and sprouting in a microfluidic platform

HMVECs were cultured in the OrganoPlate® 3-lane (Figure 1A). The process of vessel formation and subsequent angiogenic sprouting is depicted in Figure 1B. First, HMVECs were seeded in the top channel of the chip (1) and allowed to form a three-dimensional tubular structure (2). Bidirectional flow was introduced into the system by placing the plate on a rocking device. To induce angiogenic sprouts, a cocktail of pro-angiogenic factors was introduced into the bottom channel (3).

HMVECs were cultured as tubules for 4 days. The medium was supplemented with FBS or HHS (Figure 1C). The substitution of FBS for HHS prepares the model for the subsequent exposure to patient serum. To verify endothelial phenotype, HMVECs were stained with various markers. Tubules were positive for two endothelial-junction-associated protein markers, vascular endothelial (VE)-Cadherin and CD-31 (PECAM-1), and negative for the myofibroblast markers  $\alpha$ -smooth muscle actin ( $\alpha$ -SMA) and SM22 $\alpha$  by visual assessment. A 3D reconstruction revealed that in both serum conditions, the cells formed a fully confluent tubule without invasion in the collagen-I ECM (not stained).

After the microvessels reached confluency on day 4, an angiogenic sprouting cocktail containing the growth factors hVEGF-165, S1P and PMA, was applied to

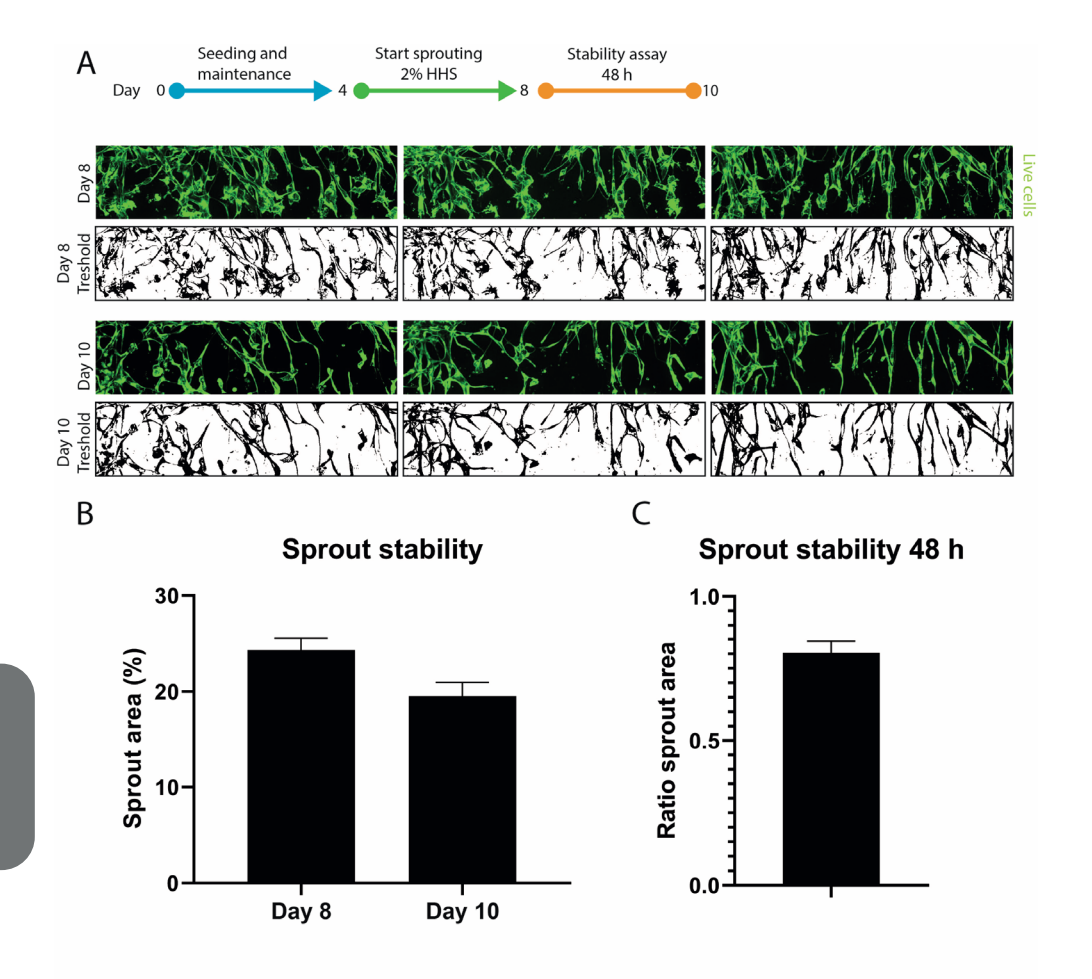


**Figure 2 Stability assessment of sprouted HMVEC microvessels. (A)** Representative maximum projection confocal images (top) and threshold images (bottom) used for quantification of the sprouting area. **(B)** Quantification of the area covered by sprouts at the start (day 8) and end (day 10) of the stability assay (n=9, represented is mean  $\pm$  SEM). **(C)** Ratio of the area covered by sprouts at day 10 versus day 8 (n=9, shown is mean  $\pm$  SEM).

the bottom perfusion channel. Due to the perfusion of the culture by placement of the culture vessel on a rocking platform, a stable gradient of angiogenic factors was formed which stimulated the HMVEC tubules to develop sprouts towards the bottom perfusion channel <sup>28</sup>. Figure 1D depicts the culture after 4 days of sprouting and supplementary Figure 1 shows the whole sprouting process over time. Angiogenic sprouts including tip and stalk cells were observed spanning the full ECM channel directing towards the source of the gradient. A

3D reconstruction reveals that sprouting occurs on different z-levels. No obvious differences in the expression patterns of CD31, VE-Cadherin, SM22 and  $\alpha$ -SMA were observed between cultures treated with FBS or HSS, indicating that in the established model, human serum can be used without affecting the expression of endothelial cell-specific markers. Next, live cultures were stained with the cell-permeant dye Calcein AM. In live cells, the non-fluorescent dye is converted to a green fluorescent calcein, which visualizes all live cells in the culture (see Figure 1E). This allows the observation and quantification of the angiogenic sprouts over time.

### **Quantitative tracking of sprout initiation**

To quantitively follow the angiogenesis process over time, we measured the coverage of calcein stained sprouts in the ECM channel (Figure 2A). To assess the stability of the culture for compound exposure, the angiogenic cocktail was withdrawn from day 8 till day 10 (48 hours) and the sprout area was measured. A small decrease in sprout area was observed (24% area at day 8, 20% area at day 10, Figure 2B, ratio in Figure 2C) related to thinning of vessels, but no regression of sprouts was observed. This provided a 48-hour window that can be utilized for compound or serum exposure.

### Response of sprouted microvessels to cytokines and inhibitors

To induce a diseased in vitro state relevant to SSc and other vasculopathies, we assessed the stability of the established sprouts upon exposure to key proinflammatory (TNF $\alpha$ ) and pro-fibrotic (TGF $\beta$ ) cytokines. Cytokines and inhibitors were added in combination with a low (2%) and high (5%) amount of HHS (Figure 3). TGF $\beta$  has been shown to induce full EndoMT in cultured endothelial cells from different tissues, whereas serum levels of TNF $\alpha$  are elevated in patients with SSc and favor the development of pulmonary fibrosis and pulmonary arterial hypertension. TNF $\alpha$  inhibitors reduce systemic inflammation, improving the endothelial function and decreasing the risk of pulmonary arterial hypertension

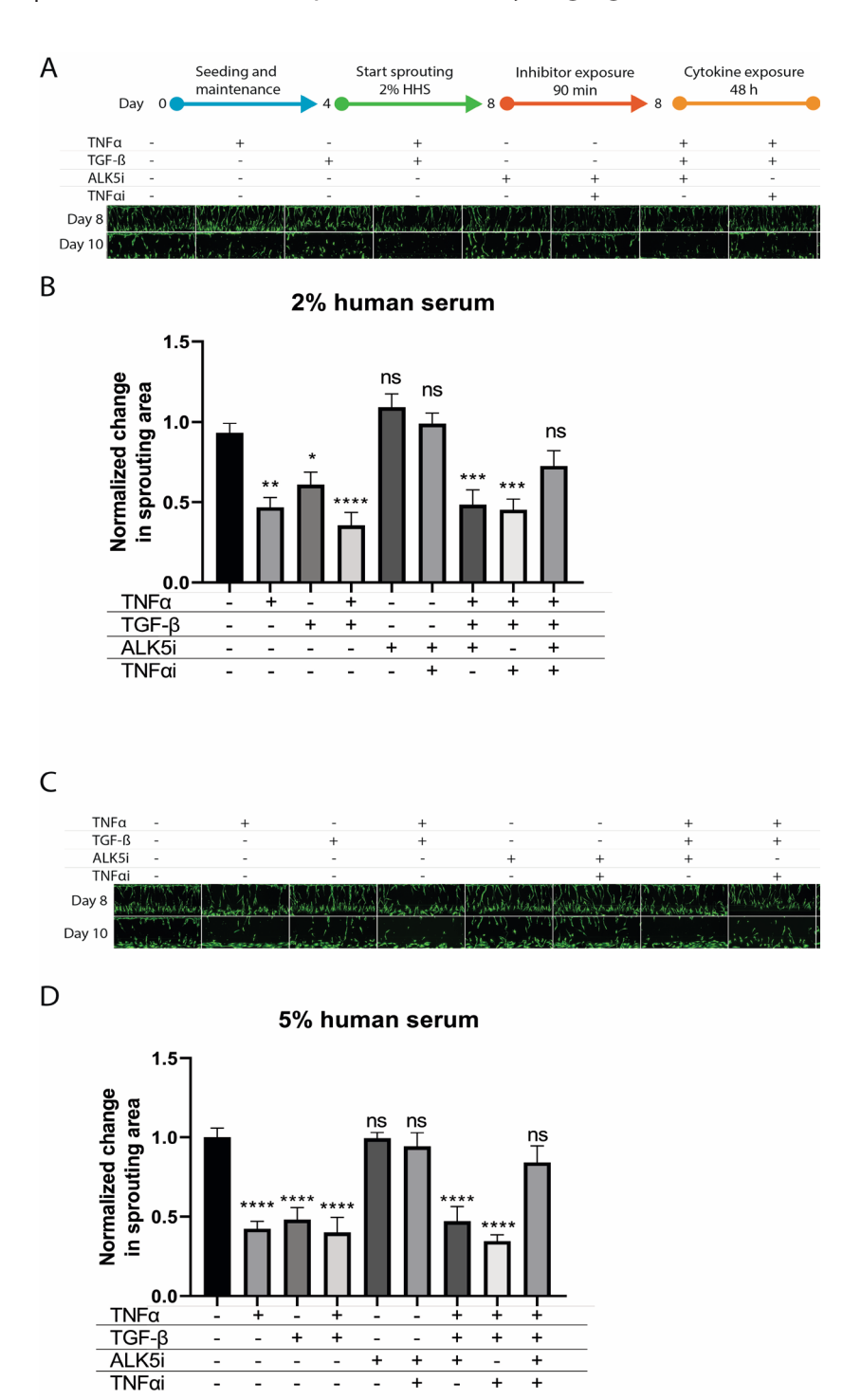


**Figure 3 Response of the sprouted microvessels to cytokines and inhibitors.** Sprouted microvessels were preincubated on day 8 with ALK5i or TNFα iAB for 90 minutes and subsequently exposed to (a combination of) TNFα or TGFß for 48 hours in 2% (panel **A** and **B**) or 5% (panel **C** and **D**) human serum. (**A**) and (**C**) show representative images of cultures exposed to (a combination of) inhibitors and cytokines. (**B**) and (**D**) show quantification plots of the area covered by sprouts of exposed microvessels after exposure. The ratio of the sprouting area before and after the stability assay was normalized to the no exposure condition. n=7-12, shown is the mean  $\pm$ SEM, statistical test – ordinary one-way ANOVA (ns = not significant, \* p < 0.05, \*\* p < 0.01, \*\*\* p < 0.001)

progression.<sup>36</sup> A significant reduction in sprout area was measured when adding TNF $\alpha$  (47%), TGF $\beta$  (42%) or a combination of both cytokines (60%), indicating the degradation of the angiogenic sprouts after additions of these triggers (Figure 3). The effect was observed in both human serum conditions (2% and 5% HHS).

Next, we investigated whether the cytokine-induced destabilization of the vascular structures could be prevented by inhibiting both TNFa and TGFß signaling (Figure 3). TNFa signaling was inhibited by adding a neutralizing monoclonal antibody against human TNFa. TGFB was inhibited with the small molecule SB-431542, which inhibits TGFß-mediated activation of SMAD proteins by the ALK5 receptor. In the presence of the combined TNF $\alpha$  and TGF $\beta$  trigger, the addition of the TNF $\alpha$ neutralizing antibody or SB-431542 alone did not result in any protection of the microvessels. However, when the HMVECs were incubated with both TNFα and TGFß inhibitors before exposure to the trigger, the sprout area was preserved and was found to be comparable to the no trigger control. This effect was observed in presence of both 2% (Figure 3A+B, 2.3-fold reduction) or 5% (Figure 3C+D, 4-fold reduction) healthy human serum in the culture medium, although the rescue effect was slightly larger in the 5% human serum condition. The inhibition and rescue of fresh sprouts of dermal endothelial cells with cytokines showed that the developed assay has an adequate window for exposure, which can be utilized for the routine assessment of compounds and patient samples on angiogenic sprout formation.

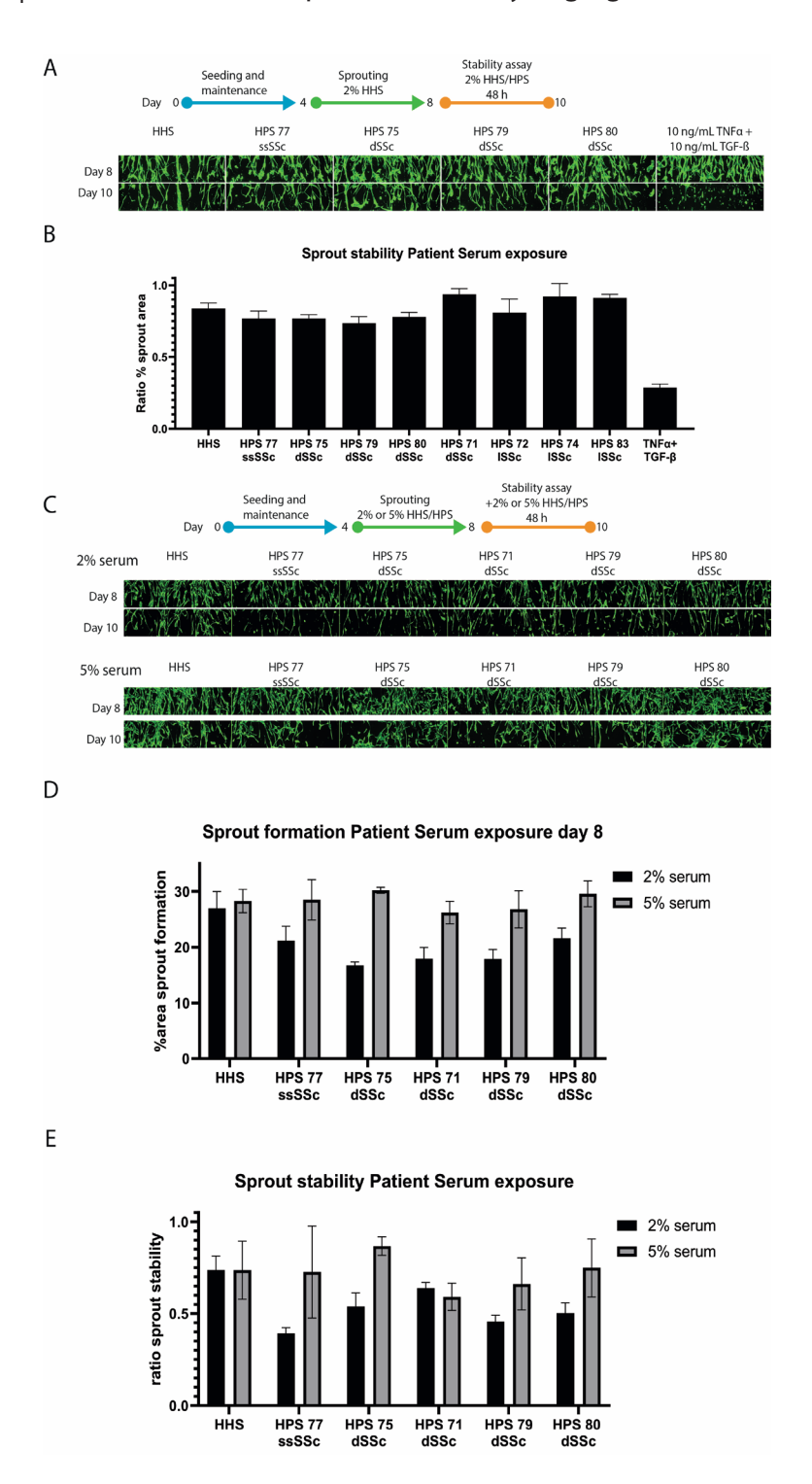


**Figure 4 Exposure of sprouted HMVEC microvessels to sera from patients with systemic scleroderma. (A)** Angiogenic sprouting was induced from day 4 till day 8 including 2% healthy human serum, followed by exposure for 48 hours with 2% patient serum of 8 systemic scleroderma patients. Representative images before and after exposure are shown. **(B)** Bar graph presenting the ratio of the area covered by sprouts after versus before patient serum exposure. n=3-6 shown is mean ± SEM. **(C-E)** Angiogenic sprouting was induced in the presence of 2% or 5% patient serum for 4 days. Subsequently, sprout stability was verified following four days of culture in absence of the sprouting cocktail with the addition of patient serum. Representative images are shown in **(C)**, quantification of sprouting area at day 8 in **(D)** and the ratio of sprout stability in **(E)**. n=3-4, shown are mean ± SD.

### Model application: systemic scleroderma serum assessment

Previous studies have demonstrated that treatment with sera from patients with SSc impairs the tubulogenic performance of human microvascular endothelial cells in an in vitro matrigel assay.<sup>37</sup> As an application of the developed angiogenesis-on-a-chip model, we assessed the effect of different human serum samples from scleroderma patients on the angiogenic sprout formation and stability. Serum samples from eight different SSc patients (Table 1) were interrogated. First, the sprouts were formed in HHS for 4 days. Subsequently, the patient serum was introduced at a 2% concentration to the microfluidic system during the 48-hour stability assay (Figure 4A+B). No significant reduction in sprout area could be observed after 48 hours compared to the HHS control.

As the sprouts were formed from day 4 till day 8 in HHS (Figure 4A+B) before exposure to patient serum, we hypothesized that an effect of the patient serum might be observed on sprout formation. We observed that sprouts formed in all exposure conditions. However, cultures exposed to 2% patient serum formed 31% less dense sprout networks at day 8 compared to the HHS control (Figure 4C+D).

In addition, cultures exposed to 2% patient serum were on average 29% less stable than the healthy serum control after the 48-hour stability assay (Figure 4E). We observed that the cultures exposed with 2% patient serum were on average 28% less stable than cultures exposed with 5% patient serum.

### Discussion

There is a growing need for physiologically relevant assays to model complex diseases in an in vitro setting. Traditionally, animal models have been widely utilized to study disease, but animal models are expensive, labor-intensive, and suffer from ethical and biological limitations.<sup>38,39</sup> To alleviate the need for better models, scientists are increasingly embracing three-dimensional tissue culture to develop more physiologically relevant models.<sup>40</sup> Organ-on-a-Chip technology offers an even higher degree of complexity, where cells are cued to form complex 3D structures in miniaturized channels.<sup>41</sup> The technology has been used to model a wide array of organs and processes, such as the blood-brain barrier,<sup>42</sup> kidnev,<sup>43</sup> cancer<sup>44,45</sup> and vasculature<sup>46,47</sup> and is adopted widely by the pharmaceutical industry.<sup>48</sup> In this work, we developed and optimized a 3D microvessel-on-a-chip on the OrganoPlate platform to study angiogenesis in the context of systemic sclerosis (SSc). We believe this model could represent an optimal solution balancing decent throughput (40 independent samples on a single well plate compatible with automated liquid handlers) with a physiologically relevant model of angiogenesis, overcoming the limitations of 2D models characterized by non-physiologically relevant conditions of cultured cells, and of more complex 3D models restricted by lack of throughput.

We developed a quantitative readout, which allows assessment of both sprout formation and sprout stability. The assays were optimized for human serum culture, replacing the more traditionally used fetal bovine serum. We demonstrated that we could recapitulate typical hallmarks of SSc, such as microvascular destabilization and sprout regression through pro-fibrotic and pro-inflammatory cytokines TGF $\beta$  and TNF $\alpha$ , and showed that addition of inhibitors could prevent the diseased phenotype. Finally, we showed that we could study the effect of human sera derived from SSc patients on sprout formation and stability.

The usage of human serum as an alternative for bovine serum for endothelial cell

culture has been proposed previously,<sup>49–51</sup> but not in the light of an angiogenesis assay. This study optimized the use of human serum in endothelial cell culture thereby allowing us to study the effects of human patient serum on the formation and stability of angiogenic sprouts without a confounding switch from bovine to human serum. In combination with a window for sprout stability of 24 hours, this enabled a unique study on the effect of SSc patient derived serum on the stability of sprouts.

Microvascular destabilization or regression in SSc, leading to consequent dysregulated angiogenesis, could be induced by autoantibodies<sup>9</sup> and by profibrotic and pro-inflammatory cytokines such as TGFß and TNFα. However, it is not clear whether a particular cytokine, or the synergistic actions of groups of cytokines and/or autoantibodies could initiate the endothelial damage.<sup>9</sup> Hence, the need to develop an assay in which one or multiple triggers can be used to recapitulate the onset of the endothelial damage and relative inhibitors can be added to prevent or rescue the phenotype without losing the assay window, becomes fundamental. In our 3D microvessel-on-a-chip model, we managed to obtain an adequate assay window especially when TNFα alone or in combination with TGFß were used as triggers. We observed almost full prevention of 3D microvascular destabilization in presence of a TGFß receptor inhibitor and TNFα blocker, providing the opportunity to assess the effect of novel drugs.

As a proof of concept, we also assessed the effect of different serum samples from SSc patients and observed that patient sera predominantly influenced angiogenic sprout formation and stability when added during the formation of the sprouts. The assay window, however, was shorter compared to purified cytokines.

It needs mentioning though that all sera used in this study were collected from patients undergoing pharmacological treatments. This might have contributed to reduced effects in the angiogenesis assay. The discrepancy in assay window between sprout destabilization by purified cytokines (e.g., TNF $\alpha$  or TGF $\beta$ ) and patients' sera, might also suggest that these cytokines are present in lower

concentrations in sera from patients with prolonged disease and treated with anti-inflammatory or anti-fibrotic drugs.

As a future perspective for further development of this assay, we foresee two improvements in the study design. The first one is the cell source: we used cells from healthy donors and not from SSc patients due to the hurdles of isolating them from skin biopsies. A model containing SSc cells could have been suitable for angiogenesis rescue experiments and would potentially increase the 48-hour exposure window. The second improvement would be to include sera from SSc patients who were naïve to treatments, to potentially increase our assay window for sprouts formation and stability.

In conclusion, we described an angiogenesis-on-a-chip platform which, with 40 chips per microtiter plate, is suitable for high-throughput applications. We optimized the culture protocol to replace FBS with the physiologically more relevant HHS, to allow for assessment of patient sera. As a proof of concept, we investigated the effect of SSc patient serum on our platform and found a destabilizing effect on the angiogenic sprouts. Our in vitro assay allowed us to study and monitor all the stages of angiogenesis, from sprout formation to sprout stabilization and degradation in the presence of different triggers and compounds. We foresee further uptake of the assay in development of novel treatments against scleroderma.

### **Declaration of conflicting interests**

Authors BK, AvdH, TO, PV and HLL are or were employees of MIMETAS and PV is shareholder of that same company. The OrganoPlate® is a registered trademark of MIMETAS BV.

Authors CC, JC, EE, RAJJ and MAT are employees of Galapagos (Leiden, The Netherlands and Milan, Italy). The authors declare no conflict of interest.

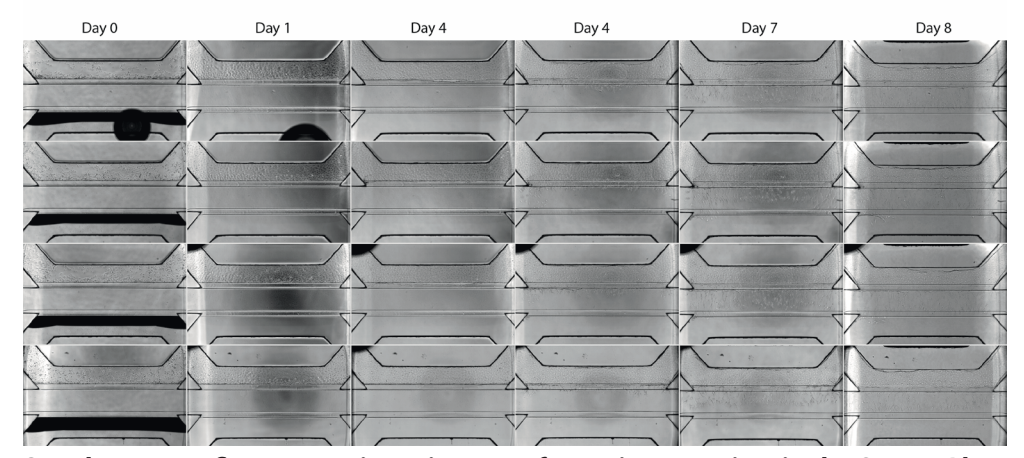
### References

- 1. Denton, C. P. Advances in pathogenesis and treatment of systemic sclerosis. Clin. Med. J. R. Coll. Physicians London 15, s58–s63 (2015).
- 2. Kahaleh, B. Vascular Disease in Scleroderma: Mechanisms of Vascular Injury. Rheum. Dis. Clin. North Am. 34, 57–71 (2008).
- 3. Michiels, C. Endothelial cell functions. J. Cell. Physiol. 196, 430–443 (2003).
- 4. Matucci-Cerinic, M., Kahaleh, B. & Wigley, F. M. Review: Evidence that systemic sclerosis is a vascular disease. Arthritis Rheum. 65, 1953–1962 (2013).
- 5. Cantatore, F. P., Maruotti, N., Corrado, A. & Ribatti, D. Angiogenesis Dysregulation in the Pathogenesis of Systemic Sclerosis. Biomed Res. Int. 2017, (2017).
- 6. Manetti, M. et al. Endothélial-to-mesenchymal transition contributes to endothelial dysfunction and dermal fibrosis in systemic sclerosis. Ann. Rheum. Dis. 76, 924–934 (2017).
- 7. Domiciano, D. S., Carvalho, J. F. & Shoenfeld, Y. Pathogenic role of anti-endothelial cell antibodies in autoimmune rheumatic diseases. Lupus 18, 1233–1238 (2009).
- 8. Meroni, P., Ronda, N., Raschi, E. & Borghi, M. O. Humoral autoimmunity against endothelium: Theory or reality? Trends Immunol. 26, 275–281 (2005).
- 9. Corallo, C. et al. From microvasculature to fibroblasts: Contribution of antiendothelial cell antibodies in systemic sclerosis. Int. J. Immunopathol. Pharmacol. 28, 93–103 (2015).
- 10. Katsumoto, T. R., Violette, S. M. & Sheppard, D. Blocking TGFβ via inhibition of the ανβ6 integrin: A possible therapy for systemic sclerosis interstitial lung disease. Int. J. Rheumatol. 2011, (2011).
- 11. Thuan, D. T. B. et al. A potential link between oxidative stress and endothelial-to-mesenchymal transition in systemic sclerosis. Front. Immunol. 9, 1–14 (2018).
- 12. Raschi, E. et al. Scleroderma-specific autoantibodies embedded in immune complexes mediate endothelial damage: an early event in the pathogenesis of systemic sclerosis. Arthritis Res. Ther. 22, 1–17 (2020).
- 13. Guiducci, S., Giacomelli, R. & Cerinic, M. M. Vascular complications of scleroderma. Autoimmun. Rev. 6, 520–523 (2007).
- 14. Nihtyanova, S. I., Brough, G. M., Black, C. M. & Denton, C. P. Clinical burden of digital vasculopathy in limited and diffuse cutaneous systemic sclerosis. Ann. Rheum. Dis. 67, 120–123 (2008).
- 15. Giordano, N. et al. Pulmonary hypertension: A correct diagnosis for a suitable therapy in scleroderma patients. Clin. Exp. Rheumatol. 33, 182–189 (2015).
- 16. Asano, Y. & Sato, S. Vasculopathy in scleroderma. Semin. Immunopathol. 37, 489–500 (2015).
- 17. Artlett, C. M. Animal models of systemic sclerosis: Their utility and limitations. Open Access Rheumatol. Res. Rev. 6, 65–81 (2014).
- 18. Staton, C. A. et al. Current methods for assaying angiogenesis in vitro and in vivo INTERNATIONAL EXPERIMENTAL. 233–248 (2004).
- 19. Mazzotta, C. et al. Proangiogenic effects of soluble α-Klotho on systemic sclerosis dermal microvascular endothelial cells. Arthritis Res. Ther. 19. (2017).
- 20. Borghini, A. et al. Systemic sclerosis sera impair angiogenic performance of dermal microvascular endothelial cells: Therapeutic implications of cyclophosphamide. PLoS One 10, 1–18 (2015).
- 21. Corallo, C. et al. Bosentan and macitentan prevent the endothelial-to-mesenchymal transition (EndoMT) in systemic sclerosis: In vitro study. Arthritis Res. Ther. 18, 1–9 (2016).
- 22. Romano, E. et al. Bosentan blocks the antiangiogenic effects of sera from systemic sclerosis patients: An in vitro study. Clin. Exp. Rheumatol. 33, 148–152 (2015).
- 23. Liang, C. C., Park, A. Y. & Guan, J. L. In vitro scratch assay: A convenient and

- inexpensive method for analysis of cell migration in vitro. Nat. Protoc. 2, 329–333 (2007).
- 24. Staton, C. A., Reed, M. W. R. & Brown, N. J. A critical analysis of current in vitro and in vivo angiogenesis assays. Int. J. Exp. Pathol. 90, 195–221 (2009).
- 25. Tourovskaia, A., Fauver, M., Kramer, G., Simonson, S. & Neumann, T. Tissue-engineered microenvironment systems for modeling human vasculature. Exp. Biol. Med. (Maywood). 239, 1264–71 (2014).
- 26. Nguyen, D.-H. T. et al. Biomimetic model to reconstitute angiogenic sprouting morphogenesis in vitro. Proc. Natl. Acad. Sci. U. S. A. 110, 6712–7 (2013).
- 27. Junaid, A., Mashaghi, A., Hankemeier, T. & Vulto, P. An End-User Perspective on Organ-on-a-Chip: Assays and Usability Aspects. Curr. Opin. Biomed. Eng. (2017) doi:10.1016/j.cobme.2017.02.002.
- 28. van Duinen, V. et al. Perfused 3D angiogenic sprouting in a high-throughput in vitro platform. Angiogenesis 22, 157–165 (2019).
- 29. van Duinen, V. et al. Robust and scalable angiogenesis assay of perfused 3D human ipsc-derived endothelium for anti-angiogenic drug screening. Int. J. Mol. Sci. 21, 1–9 (2020).
- 30. Van Den Hoogen, F. et al. 2013 classification criteria for systemic sclerosis: An american college of rheumatology/European league against rheumatism collaborative initiative. Arthritis Rheum. 65, 2737–2747 (2013).
- 31. Schindelin, J. et al. Fiji: An open-source platform for biological-image analysis. Nat. Methods 9, 676–682 (2012).
- 32. Sternberg, S. Biomedical Image Processing. Computer (Long. Beach. Calif). 22–35 (1983).
- 33. Li, C. H. & Tam, P. K. S. An iterative algorithm for minimum cross entropy thresholding. Pattern Recognit. Lett. 19, 771–776 (1998).
- 34. Kitao, A. et al. Endothelial to mesenchymal transition via transforming growth factor-β1/smad activation is associated with portal venous stenosis in idiopathic portal hypertension. Am. J. Pathol. 175, 616–626 (2009).
- 35. Cipriani, P. et al. The endothelial-mesenchymal transition in systemic sclerosis is induced by endothelin-1 and transforming growth factor-β and may be blocked by Macitentan, a dual endothelin-1 receptor antagonist. J. Rheumatol. 42, 1808–1816 (2015).
- 36. Murdaca, G. & Contatore, M. Murdaca2014. 6, 283–289 (2014).
- 37. Manetti, M. et al. Systemic sclerosis serum significantly impairs the multi-step lymphangiogenic process: In vitro evidence. Int. J. Mol. Sci. 20, (2019).
- 38. Weinhart, M., Hocke, A., Hippenstiel, S., Kurreck, J. & Hedtrich, S. 3D organ models— Revolution in pharmacological research? Pharmacol. Res. 139, 446–451 (2019).
- 39. Hoarau-Véchot, J., Rafii, A., Touboul, C. & Pasquier, J. Halfway between 2D and animal models: Are 3D cultures the ideal tool to study cancer-microenvironment interactions? Int. J. Mol. Sci. 19, (2018).
- 40. Abbott, A. Biology's new dimension. Nature 424, 870–872 (2003).
- 41. Junaid, A., Mashaghi, A., Hankemeier, T. & Vulto, P. An end-user perspective on Organ-on-a-Chip: Assays and usability aspects. Curr. Opin. Biomed. Eng. 1, 15–22 (2017).
- 42. Wevers, N. R. et al. A perfused human blood–brain barrier on-a-chip for high-throughput assessment of barrier function and antibody transport. Fluids Barriers CNS 15, 23 (2018).
- 43. Gijzen, L. et al. Culture and analysis of kidney tubuloids and perfused tubuloid cells-on-a-chip. Nat. Protoc. 16, 2023–2050 (2021).
- 44. Lanz, H. L. et al. Therapy response testing of breast cancer in a 3D high-throughput perfused microfluidic platform. BMC Cancer 17, 709 (2017).
- 45. Kramer, B. et al. Interstitial flow recapitulates gemcitabine chemoresistance in a 3D microfluidic pancreatic ductal adenocarcinoma model by induction of multidrug

- resistance proteins. Int. J. Mol. Sci. 20, (2019).
- 46. Poussin, C. et al. 3D human microvessel-on-a-chip model for studying monocyte-to-endothelium adhesion under flow Application in systems toxicology. ALTEX 37, 47–63 (2020).
- 47. Zonneveld et al. Standardized and scalable assay to study perfused 3d angiogenic sprouting of ipsc-derived endothelial cells in vitro. J. Vis. Exp. 2019, (2019).
- 48. Vulto, P. & Joore, J. Adoption of organ-on-chip platforms by the pharmaceutical industry. Nat. Rev. Drug Discov. (2021).
- 49. Huang, L., Critser, P. J., Grimes, B. R. & Yoder, M. C. Human umbilical cord blood plasma can replace fetal bovine serum for in vitro expansion of functional human endothelial colony-forming cells. Cytotherapy 13, 712–721 (2011).
- 50. Tancharoen, W. et al. Human platelet lysate as an alternative to fetal bovine serum for culture and endothelial differentiation of human amniotic fluid mesenchymal stem cells. Mol. Med. Rep. 19, 5123–5132 (2019).
- 51. Vianna, L. M. M. et al. Use of human serum for human corneal endothelial cell culture. Br. J. Ophthalmol. 99, 267–271 (2015).

# Supplementary materials



**Supplementary figure 1 Angiogenic sprout formation over time in the OrganoPlate 3-lane.** Cells were loaded into the top channel at day 0 and allowed to form a tubule. At day 4, sprouting was initiated. Shown are 4 representative cultures.

# Chapter 5

# A robust and high-throughput approach for the quantification of three-dimensional vascular beds

Bart Kramer, Marianne Swart, Thomas Olivier, Lenie van den Broek

In preparation for publication



## 5

### **Abstract**

Angiogenesis, the formation of new blood vessels from pre-existing ones, is a complex biological process integral to many physiological and pathological processes. It involves intricate interactions between various cell types, notably endothelial cells and pericytes. In this study, we present an innovative method for studying and quantifying angiogenesis in vitro, leveraging the advantages of high-throughput three-dimensional (3D) imaging. Utilizing the OrganoPlate Graft, we created a controlled environment for vascular bed formation, and subsequently introduced pericytes into the model system to better understand their role in angiogenesis. The application of a fluorescent confocal method for 3D imaging allowed for a more detailed and comprehensive understanding of the vascular bed. Our results demonstrate that 3D analysis is complementary to 2D analysis, but may provide a more precise measurement, offering a robust and efficient approach for studying angiogenesis. This innovative methodology could potentially expedite the development of targeted therapies for diseases characterized by abnormal angiogenesis.

### Introduction

The vascular network is a vital part of the circulatory system responsible for providing the body with necessary nutrients, oxygen, and hormones. It also plays an important role in removal of metabolic waste, maintenance of blood pressure, thermoregulation,<sup>1</sup> and moreover, it is involved heavily in the immune response.<sup>2</sup> Endothelial cells and pericytes are important cell types that play key roles in the maintenance of vascular homeostasis. Endothelial cells form the innermost layer of the vascular wall, and they are responsible for controlling the passage of substances, such as ions and small molecules, into and out of the vascular lumen. Pericytes are found in the basement membrane of the vascular wall and are involved in the regulation of vascular formation, maturation, and function.<sup>3</sup> In addition, pericytes play an important role in vessel stability, repair and regulating angiogenesis.<sup>4,5</sup>

Angiogenesis is the process of forming new blood vessels from pre-existing ones. It plays an important role in many physiological and pathological processes, such as wound healing, tumor growth and metastasis.<sup>6,7</sup> The interaction between endothelial cells and pericytes is essential for proper vessel formation and stabilization.(Ribatti, Nico, and Crivellato 2011) For example, when endothelial sprouts form during angiogenesis, pericytes migrate towards them and attach themselves to the growing vessel wall. Without pericytes, endothelial sprouts are unstable and prone to collapse, which can lead to impaired blood flow and tissue damage.8 Although in vivo model systems for angiogenesis have been used for decades,9 there is a growing need for accurate in vitro model systems to study this process. In vitro models are generally more easily controlled, less expensive and more ethically responsible than the use of in vivo models.<sup>10</sup> The gold standard in vitro assays, like spheroid-based outgrowth and 2D vessel models, offer precise platforms for studying angiogenesis. Spheroid assays mimic early angiogenesis by analyzing tip cell formation, while 2D models focus on endothelial cell migration and tube formation.<sup>11,12</sup>

### 128 | Robust and high-throughput quantification of 3D vascular beds

Studying these complex biological processes, particularly angiogenesis, necessitates imaging methods that can accurately capture the three-dimensional structure of the vascular bed. Conventional two-dimensional (2D) imaging techniques, like Computed Tomography (CT) or Magnetic Resonance Imaging (MRI), often fall short due to limited spatial resolution and difficulties in adapting these techniques to in vitro models.<sup>13–15</sup> These challenges, compounded by the complexity of multiple cell layers and various cell types, have prompted a shift towards three-dimensional (3D) imaging techniques.

The application of 3D imaging promises significant advantages, notably superior spatial resolution, that allow for a more detailed and comprehensive understanding of the vascular bed. Unlike 2D imaging, 3D imaging enables the visualization of structures in their natural context, enhancing the representation of cell-to-cell interactions, morphologies, and positions. These attributes make 3D imaging indispensable when investigating complex processes like angiogenesis and the precise roles played by endothelial cells and pericytes.

In this study, we investigated a method that capitalizes on the advantages of 3D imaging and quantification for studying in vitro vascular beds in high-throughput fashion. Building upon our previously optimized angiogenesis assay using a microfluidic device, <sup>16,17</sup> our approach incorporates the application of a fluorescent confocal method and subsequent analysis of the 3D images. This approach was compared with a more traditional Z-projection imaging quantification method, to identify the potential advantages of 3D quantification.

With the developed methods, the enrichment of our model system was investigated by introducing pericytes, alongside the endothelial cells, to better understand their roles and interactions in angiogenesis. By enhancing the spatial resolution of our imaging and expanding our cellular scope, we anticipate gaining a more comprehensive understanding of the complexities involved in blood vessel formation. Ultimately, this knowledge could expedite the development of targeted therapies for diseases characterized by abnormal angiogenesis.

### Materials and methods

#### **Cell culture**

Primary Human Umbilical Vein Endothelial Cells (HUVECs, Lonza C2915AS) were cultured in T-75 Flasks (Corning, #734–2705) in MV2 (PromoCell, #C-22121) supplemented with 1% penicillin/streptomycin (Sigma, #P4333) and used at maximum passage 5 for experiments. Cells were cryopreserved by dissociation from the flasks with Trypsin/EDTA solution 0.25 mg/mL (Lonza CC-5012), counted and cryopreserved in a solution of 50% Fetal Calf Serum (FCS, Gibco, cat# A13450), 40% MV2 medium and 10% Dimethyl Sulfoxide (DMSO, Sigma, cat# D8418). For experiments, HUVECs were seeded in the microfluidic plate immediately after thawing a cryopreserved vial. Human Primary Brain Vascular Pericytes (Sciencell, cat# 1200) were expanded in Poly-L-Lysine (AMSbio Cultrex, cat# 3438-100-01) coated T-75 flasks in Pericyte medium (Sciencell, cat# 1201) and used at maximum passage 4 for experiments. Cells were cryopreserved by dissociation from the flasks with Trypsin/EDTA solution 0.25 mg/mL (Lonza CC-5012) and counted before using them for experiments.

#### **Microfluidic Device Culture**

Microfluidic culture was performed using the OrganoPlate Graft (MIMETAS). The microfluidics are patterned under a 384 wells industry standard titer plate divided in 64 microfluidic chips (Figure 1A). Each chip consists of two perfusion channels and a center gel channel (the graft chamber). The graft chamber is connected directly to the well above it, allowing for the addition of a small tissue or growth factors. 2.3  $\mu$ L of hydrogel composed of 4 mg/mL Collagen I (AMSbio Cultrex 3D Collagen I Rat Tail, 5 mg/ml, #3447–020-01), 100 mM HEPES (Life Technologies, #15,630–122), and 3.7 mg/ml NaHCO3 (Sigma, #S5761) was dispensed in the gel inlet and incubated 15 min at 37 °C. 1.5  $\mu$ L of endothelial cell suspension (or coculture suspension) was seeded in a density of 1×10 $^7$  of cells/mL in the inlets of the perfusion channels (Figure 1B, well A1 and A3). In the co-culture conditions,

cells were loaded in a 1:19 ratio (pericyte:HUVEC). For the pericyte monoculture condition the seeding density was  $4.5 \times 10^6$  cells/mL. After cell loading, the device was transferred to an incubator (37 °C and 5% CO<sub>2</sub>) to allow for cell attachment over 2.5 hours. After cell attachment, 50  $\mu$ L of medium was added to the perfusion outlets and on top of the graft chamber, HBSS was removed from the gel inlets and the plates were placed on an interval rocker platform to ensure constant perfusion (OrganoFlow; MIMETAS, Leiden, The Netherlands). Medium was changed in all wells every 2-3 days.

When confluent endothelial vessels formed in the perfusion channels, sprouting was triggered by using an angiogenic cocktail consisting of 50 ng/mL vascular endothelial growth factor (VEGF, PeproTech, cat# 100-20), 500 nM Sphingosine 1-phosphate (S1P, Sigma-Aldrich, cat # 73914), 20 ng/mL Phorbol 12-myristate 13-acetate (PMA, Sigma-Aldrich, cat# P1585) and 20 ng/mL basic fibroblast growth factor (bFGF, PeproTech, cat# 100-18B). This cocktail was added to the medium on top of the graft chamber (Figure 1A, well B2) and the cells were allowed to sprout towards the center of the gel chamber up to 96 hours.

#### **Fixation**

HUVEC (+ pericytes) vessels and sprouts were fixated using 3.7% formaldehyde (Sigma, 252,549) in HBSS (Sigma H6648) for 15 min, washed twice with HBSS for 5 min and stored with 50ul HBSS per well at room temperature until immunofluorescent staining.

### **Perfusion assay**

Fluorescein isothiocyanate (FITC)-dextran or Tetramethylrhodamine (TRITC)-dextran 150-155 kDa (Sigma-Aldrich, cat46946 or T1287) was used to visualize the perfusion of the vessels. 0.5 mg/mL FICT- or TRITC- dextran in medium was added in a volume of 20 and 40  $\mu$ L in the left perfusion inlet and outlet. 20  $\mu$ L of media was placed on top of the graft chamber, gel inlet, right perfusion inlet and outlet. Time-lapse images were taken every two minutes (up till 20 minutes) with the

ImageXpress Micro Confocal High-Content Imaging System (Molecular devices). Visualization of the images was done in ImageJ (Fiji).

#### **Immunostaining**

Staining, Cultures were washed with washing solution containing 4% Fetal Calf Serum (FCS) (Gibco, cat# A13450) in PBS (Gibco, cat# 70,013,065) for 5 min and permeabilized with 0.3% Triton X-100 (Sigma, T8787) in PBS for 10 min. After permeabilization, the cells were washed with washing solution for 5 min before the blocking buffer, containing 2% FCS, 2% BSA (Sigma, cat# A2153), and 0.1% Tween20 (Sigma, cat# P9616) in PBS, was added for 50 min. After blocking, the cells were immediately incubated for 2 h with a primary antibody in blocking solution, washed two times for 3 min with washing solution and incubated with a secondary antibody in blocking solution, including a nuclear stain, for 30 min. Primary antibodies used were: Rabbit anti-human VE-Cadherin 1:1000 (Abcam, Ab33168), Mouse anti-human αSMA 1:100 (Sigma, A2547), Rabbit antihuman PDGFR-beta 1:180 (Abcam ab32570), Mouse anti-human CD31 (1:50; Agilent M082301-2). Secondary antibodies used were: Goat-anti-Mouse IgG-Alexa 647 (1:250, Life Technologies) Goat-anti-Mouse IgG-Alexa 488 (1:250, Life Technologies), Goat-anti-Rabbit IgG-Alexa 488 (1:250, Life Technologies), Goatanti-

Rabbit IgG-Alexa 647 (1:250, Life Technologies). For direct stains, Lectin 1:100 (Sigma L9006) and Actin, 2 drops per mL, (Life Technologies R37110) were used. For nuclear staining Hoechst 33342 (Thermo Fisher Scientific H3570) 1:2000 was used.

### **Sprouting quantification**

### **Nuclei quantification**

Images of the Hoechst signal were acquired with the ImageXpress Micro Confocal High-Content Imaging System (Molecular Devices) and a maximum-projection was saved. Images were loaded in Fiji (ImageJ) and the number of nuclei from the images was extracted by thresholding the image and the 'analyze particles' function. Visualization of the data points was performed in GraphPad (Prism).

### 3-dimensional vascular bed quantification

Images were acquired with the ImageXpress Micro Confocal High-Content Imaging System (Molecular Devices). 55-70 images were acquired per chip from the middle region of the graft chamber. The quantification process is depicted in Figure 3B. Quantification was performed with the MetaXpress software (Molecular Devices). Gaussian blurs were performed to subtract background. Subsequently, objects were identified using the build-in neurite outgrowth module. With a filter mask, disconnected fragments were filtered out. The objects that were detected in each slide were connected via the connect by the maximum replacement feature. This feature connects the found objects based on the distance between them. Subsequent analysis was done in JMP (SAS institute) to generate summery values of the quantified sprouting segments. Nuclei counting was performed in ImageJ (FIJI) with the analyze particles tool. Visualization of the data points and statistical analysis was performed in GraphPad (Prism V9).

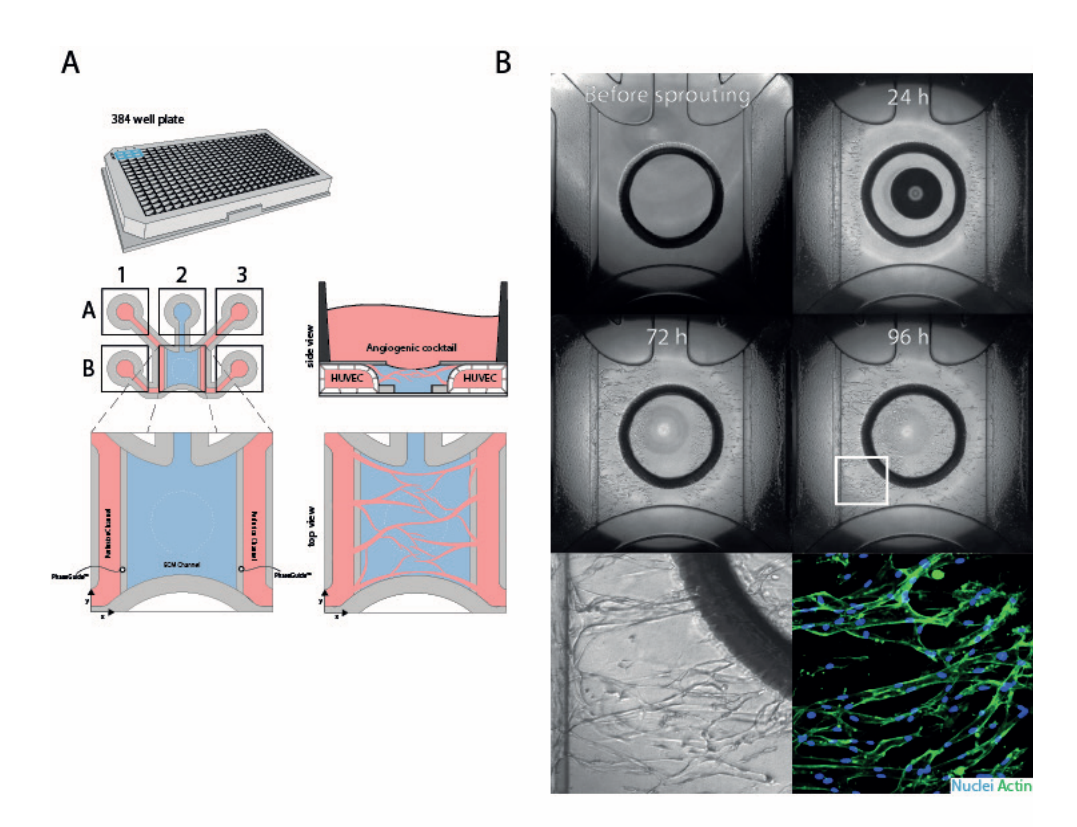
### Results

#### Vascular bed formation in a 3D microenvironment

The microfluidic platform used in this study (OrganoPlate Graft) is based on a 384 wells industry standard titer plate divided in 64 microfluidic chips (Figure 1A). Human Umbilical Vein Endothelial Cells (HUVECs) were loaded on both sides of a collagen hydrogel and formed a tubular structure over time. Subsequently, angiogenesis was initiated towards the middle of the chip by addition of an angiogenic cocktail, where sprouts from both sides meet each other. Over 96 hours, a vascular bed formed in the middle 'graft chamber' of the chip (Figure 1A, well B2). To prove the perfusability of the formed vascular bed, a fluorescent dextran molecule was perfused through the left lateral HUVEC tubule. A fluorescent signal in the graft chamber was observed directly after addition of the dye (Figure 1C, middle panel), indicating that the formed sprouts were perfusable. After 20 minutes, the dye retained in the vessels, indicating that the formed vessels have a high barrier integrity (Figure 1C, right panel). In some cases, the dye reached the right lateral HUVEC tubule, proving a connection between the sprouts that formed from both HUVEC lateral vessels.

### Development of the HUVEC/Pericyte co-culture

To investigate the effect of pericytes on endothelial cells in our microfluidic system, HUVECs and primary pericytes were co-seeded in the lateral channels and applied the angiogenic cocktail to the graft well. Vascular bed formation was observed, and the culture was characterized to investigate the position of the pericytes. HUVEC monoculture was positive for the adherence junction markers CD31 (also known as PECAM-1) and VE-cadherin and negative for the pericyte markers Platelet-derived growth factor receptor beta (PDGFR- $\beta$ ) and Smooth Muscle Actin alpha ( $\alpha$ -SMA) (Figure 2A). In the pericyte monoculture condition, the cells seem to have migrated towards the angiogenic cocktail, without the formation of sprouts. The monoculture was positive for both PDGFR- $\beta$  and  $\alpha$ -SMA (Figure



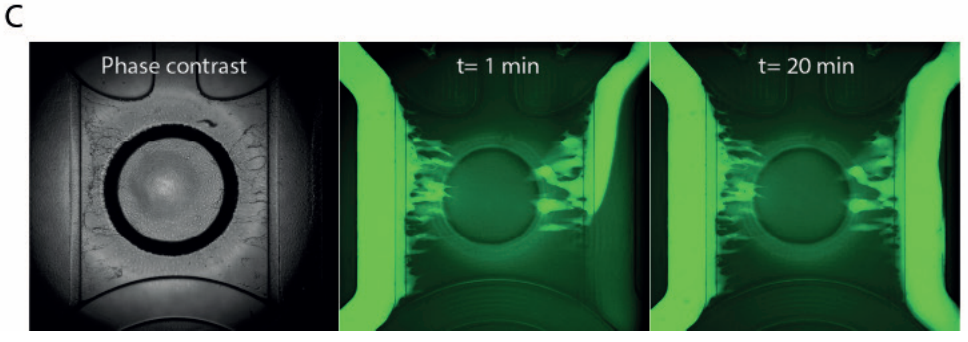


**Figure 1 Endothelial microvessel culture and angiogenic sprouting. (A)** The OrganoPlate Graft, based on a 384 well plate interface with 64 microfluidic chips integrated in the bottom, was used to assess angiogenesis. Endothelial vessels were formed on both sides of the chip, and sprouting was initiated with the addition of an angiogenic cocktail, which forms a gradient towards the endothelial vessel. **(B)** Phase contrast images of HUVECs sprouting towards an angiogenic cocktail over the course of 96 hours. Bottom left: zoom of the 96 h timepoint (zoom from white square of 96 h timepoint). Bottom right: immunofluorescent image of the same site as the bottom left. **(C)** A fluorescent dye was perfused through the left-lateral perfusion lane, and fluorescent were captured over time to visualize the perfusability of the vascular bed.

2B). Interestingly, we noticed that the pericytes located near the center of the chip stained predominantly more positive for  $\alpha$ -SMA, and the pericytes located on the lateral side of the chip stained predominantly positive for PDGFR- $\beta$ . When HUVECs and pericytes were co-cultured, angiogenic sprouts were observed after application of the angiogenic gradient (Figure 2C). Interestingly,  $\alpha$ -SMA positive pericytes were found alongside the angiogenic sprouts.

Immunostaining revealed a complex network of sprouts, interacting and branching, but also growing over and under each other (Figure 1B, bottom right panel and Figure 3B). To accurately quantify the characteristics of this complex network, it is not sufficient to only image two-dimensional image data (as shown in Figure 1B and C), but to acquire and visualize the whole network in three dimensions.

### High-throughput 3-dimensional vascular bed quantification

To study the vascular bed properties more precisely, we aimed to set up a method of quantifying the angiogenic sprouts in three dimensions. For optimization of the quantification method, a dataset was generated of vascular beds that sprouted for different durations ranging from 0 hours till 96 hours (Figure 3A). A rapid population of the graft chamber was observed with elongating angiogenic sprouts in till 72 hours after application of the cocktail, where in the period from 72 hours till 96 hours the sprouts seemed to start widening. A rapid and significant increase in the number of nuclei was found in the sprouting area from day 1 till day 4 quantified from a 2 dimensional maximum projection (Figure 3C, quantified from a maximum projection).

Subsequently, a workflow was developed to automatically combine and post process the z-images of the vascular bed (Figure 3B), to extract metrics such as sprout number and volume. The 3-dimensional quantification showed a similar trend, where the number of objects detected (Figure 3D) and the total volume in the angiogenic sprouts (Figure 3E) increased over time. Interestingly, the number

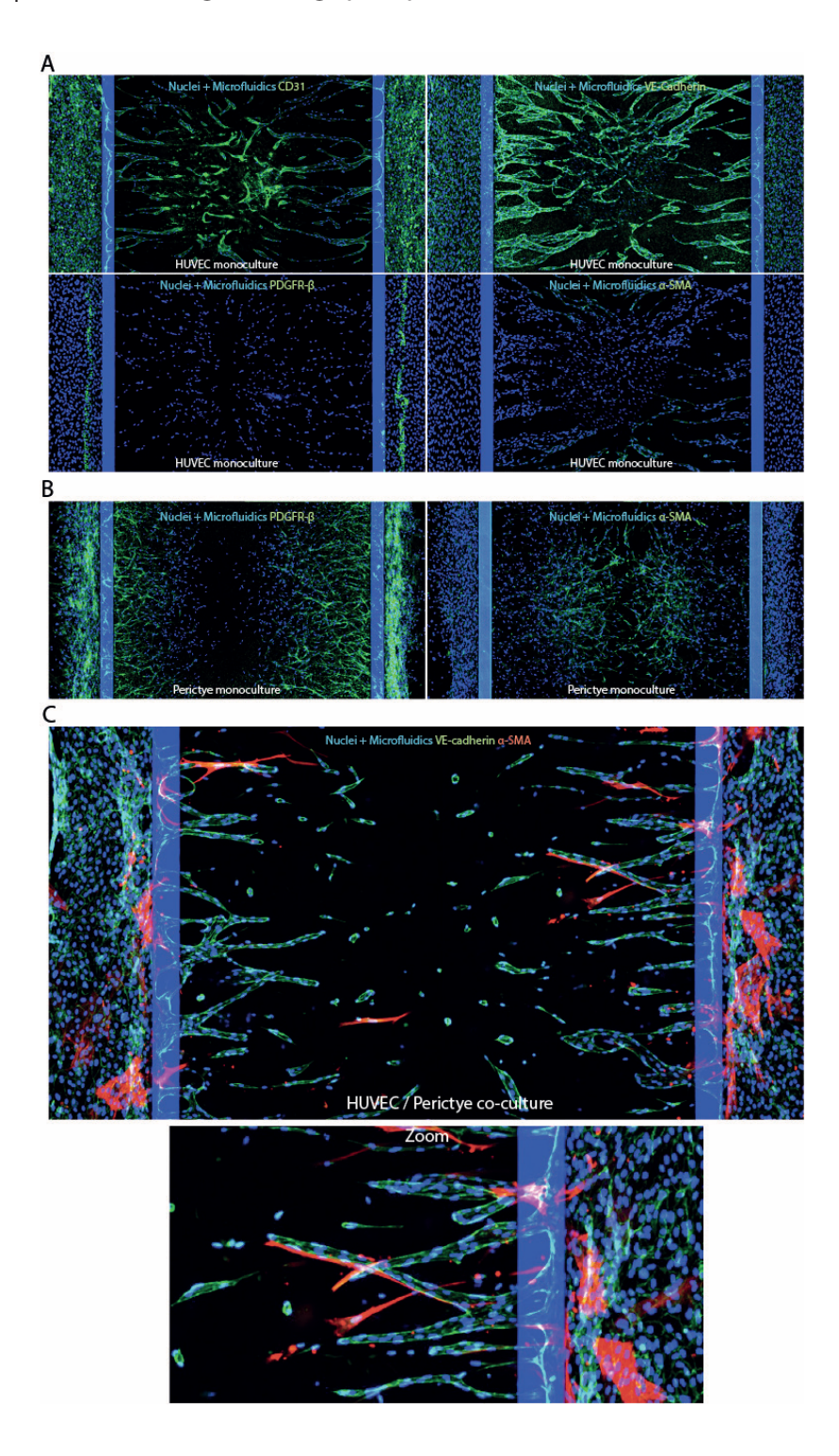


Figure 2 Immunofluorescent characterization of HUVEC monoculture and HUVEC/Pericyte co-culture in the OrganoPlate Graft after 4 days of sprouting. (A) Immunostaining of the HUVEC monoculture for various markers. The PhaseGuide are autofluorescent (blue lines), separating the center gel chamber from the adjacent perfusion lanes in the image. (B) Immunostaining of the pericyte monoculture. (C) Immunostaining of the HUVEC/Pericyte co-culture.

of objects detected from the 3 dimensional image did not increase from day 3 compared to day 4, where the total volume still increased.

#### Influence of withdrawal of growth factors on the pericyte-HUVEC co-culture

As a proof-of-concept, the newly developed imaging quantification method was assessed on the feasibility of angiogenesis inhibition studies. The inhibition of angiogenesis is an important focus in cancer therapy, and having a robust quantification method of angiogenesis inhibition would benefit drug development.<sup>18</sup> To this end, our optimized HUVEC monoculture and HUVEC/pericyte co-culture was cultured, parts of our angiogenic sprouting cocktail were withdrawn to assess the effect on vascular bed formation (Figure 4A). No obvious difference was observed between the HUVEC monoculture and the HUVEC + pericyte co-culture condition. With the withdrawal of the complete cocktail, sprouts did not form in both monoculture and co-culture. Withdrawal of Sphingosine 1-phosphate (S1P) led to a visible regressed vascular bed formation in both monoculture and co-culture. Withdrawal of VEGF leads to a minor regression in vascular bed formation in both cultures.

After visual observation, our findings were confirmed with both our 2-D and 3-D quantification method (Figure 4B-D). Both quantification methods did not show a significant difference between the HUVEC monoculture and the co-culture conditions. A reduction in metrics was observed in the S1P and total sprouting mix withdrawal condition. In the 2D images (Figure 4B), 55% less nuclei were detected when S1P was withdrawn from the sprouting cocktail, where 75% less objects were detected in the 3D quantification (Figure 4C) in the HUVEC monoculture condition. When pericytes were added in the culture, these reductions changed to 65% and 68% respectively. Withdrawal of VEGF from the sprouting mix a 10%

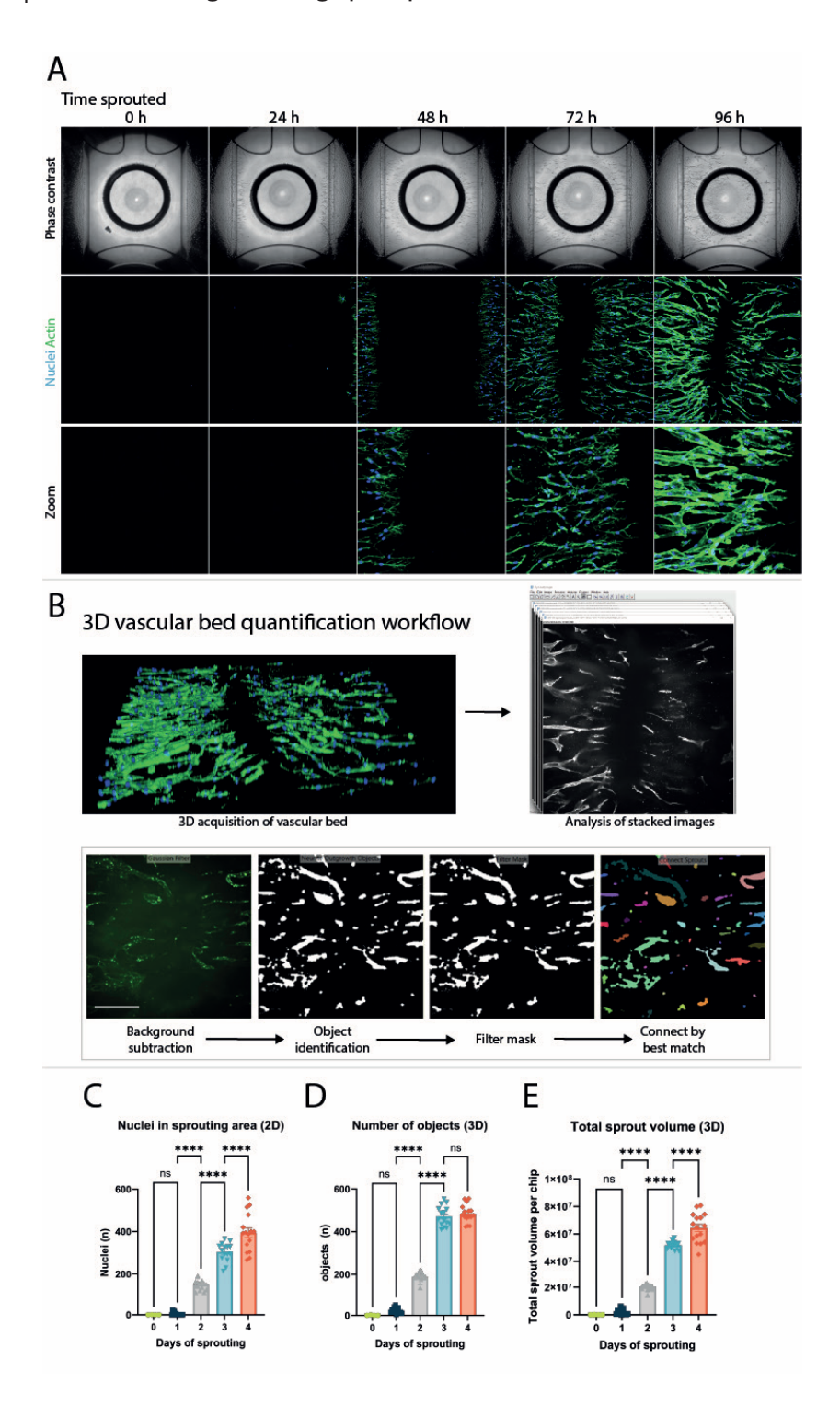


**Figure 3 High-throughput 3-dimensional vascular bed quantification in HUVEC monoculture (A)** Phase contrast (top) and immunofluorescent (middle and bottom) images of an angiogenesis induced vascular bed at different time points. **(B)** Workflow for the quantification of vascular beds in 3D. **(C-E)** Quantification of the vascular beds for number of nuclei in 2D **(C)**, number of detected objects in 3D **(D)** and total volume of the sprouts 3D **(E)**. Significance is calculated with an ordinary one-way ANOVA (Šídák's multiple comparisons test, ns = not significant, \* p < 0.05, \*\* p < 0.01, \*\*\* p < 0.001, \*\*\*\* p < 0.0001, n=4 for day 0 condition and n = 14-16 chips for day 1-4 conditions)

reduction of total sprout volume was observed (Figure 4D) in the monoculture HUVEC and a 36% reduction in the co-culture HUVEC/Pericyte. This difference was also not significant. Interestingly, we found that the standard deviation of the measurements for the 'number of objects' metrics was lower than the other metrics, an average coefficient of variation (CV) was calculated of 24% for the total objects metric (3D imaging), whereas CV of 29% and 31% were calculated for the sprout volume (3D imaging) and nuclei (2D imaging) metrics, respectively.

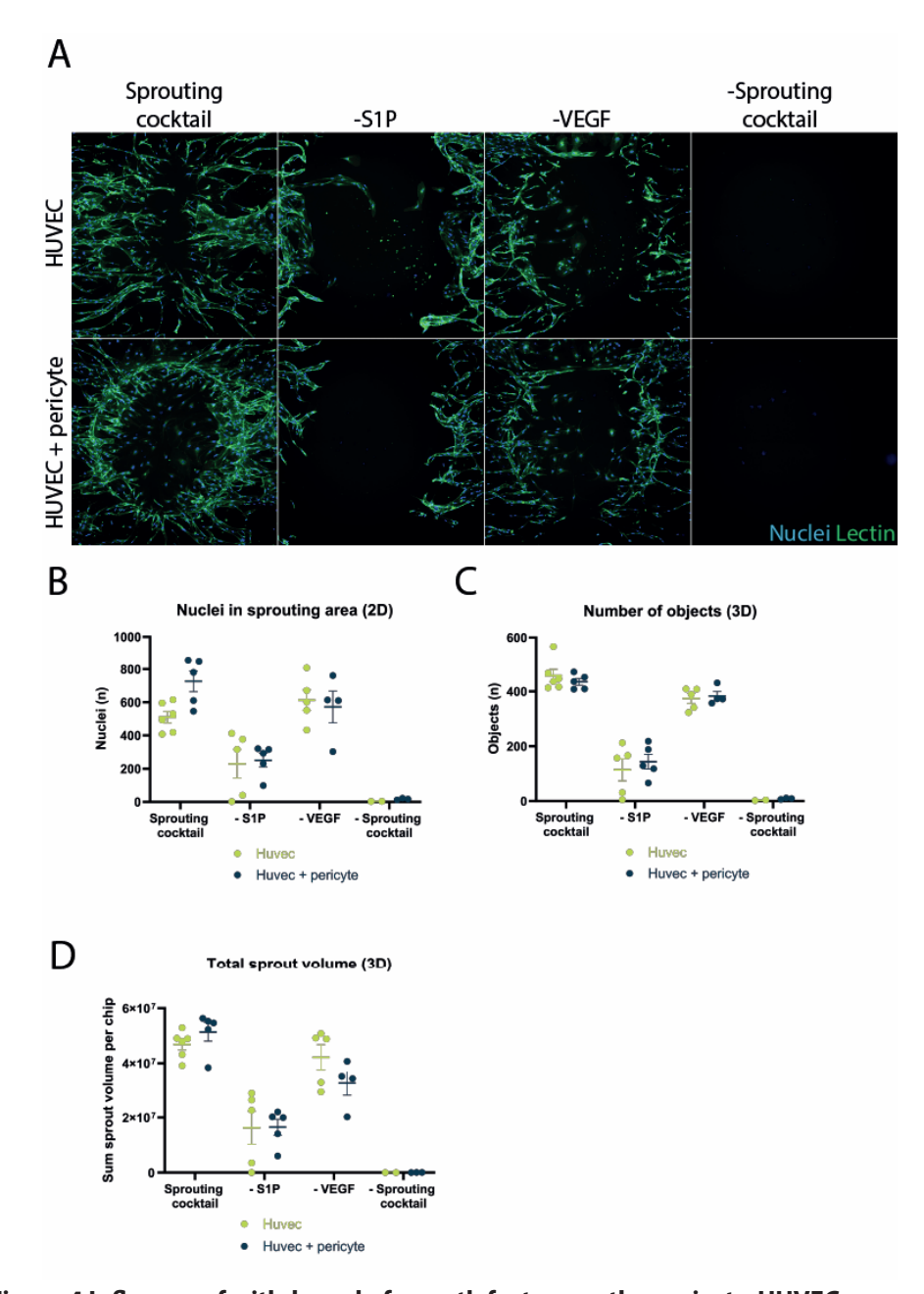


Figure 4 Influence of withdrawal of growth factors on the pericyte-HUVEC coculture (A) Immunofluorescent images of sprouted vascular beds with the sprouting cocktail added or (partly) withdrawn. (B-D) Quantification of the vascular beds for number of nuclei (2D) (B), number of detected objects (3D) (C) and total volume of the sprouts (3D) (D), n=3-6

### Discussion

To capture the full properties of a complex three-dimensional structure such as a vascular bed, conventional 2D imaging and analysis, although more straightforward to automate, may not capture the full properties of the three dimensional structure. Our study strives to overcome these limitations by leveraging an innovative methodology, capable of automating the quantification of up to 64 vascular beds in a single session.

While similar methodologies exist for 2D in vitro cultures<sup>19,20</sup> or in vivo,<sup>21</sup> our approach of quantification of in vitro 3D angiogenic sprouts is unprecedented. Readouts were optimized to measure the number of objects and the total volume of sprouts in 3D, and compared this to a more general 2D quantification method (the total amount of nuclei present in the sample).

Interestingly, our comparison with conventional 2D quantification - based on the total amount of nuclei present in the sample - did not reveal significant differences, either in terms of vascular bed development or response to the withdrawal of growth factors from the sprouting mix. This result suggests that the information obtained from 2D and 3D quantification methods are complementary, providing a more comprehensive view of angiogenesis. Our study, however, highlighted an advantage of the 3D quantification approach: precision. Although this needs to be confirmed in repeat experiments, having a more precise measurement means more consistent results across multiple studies can be obtained, increasing the reliability of our findings. This could allow us to further estimate the maturity of the vascular bed, which is important for the development of new drugs that affect angiogenesis, for example in cancer treatment.<sup>22,23</sup>

The inclusion of pericytes in our system was initially expected to yield significant differences in vascular bed formation in the growth factor withdrawal experiment compared to the monoculture HUVEC condition. Contrary to our expectations, no notable differences were observed, which could be attributed to a relatively short

culture duration to observe anastomosis of the sprouted vessels. Anastomosis plays a crucial role in vascular stabilization, with poorly or non-perfusable vessels being eliminated (pruning), while perfusable vessels get stabilized.<sup>24</sup>

Looking ahead, our model could be further improved by extending our timelines to more thoroughly investigate the impact of pericytes on vascular stabilization post-anastomosis. Moreover, we intend to explore the potential role of pericytes in vasculogenesis, a process integral to vascular system development during embryonic stages and adult tissue repair and regeneration (Velazquez 2007). An additional optimization that could be undertaken involves the optimization of our 3D readout. In our study, we limited our examination to two descriptors of the vascular bed, recognizing that our readouts could be enhanced by incorporating additional descriptors like branching points into our model. Evaluating branching points is a critical aspect in the study of tumor angiogenesis, making their inclusion imperative for our model, especially if the aim is to broaden its applicability for the investigation of anti-cancer drugs.<sup>25</sup>

In conclusion, our research provides a robust and innovative approach for quantifying a vascular bed in the OrganoPlate Graft. Alterations were tracked over time in sprout numbers under various conditions, thus facilitating high-throughput compound screening. The readout was compared to conventional two-dimensional quantification, and where similar observations in both readouts were made, the three-dimensional readout was found to be more precise. This readout establishes a solid base for future research aimed at optimizing in vitro angiogenesis study. By being able to quantify up to 64 vascular beds in 1 session, this opens the door to high-throughput compound screening.

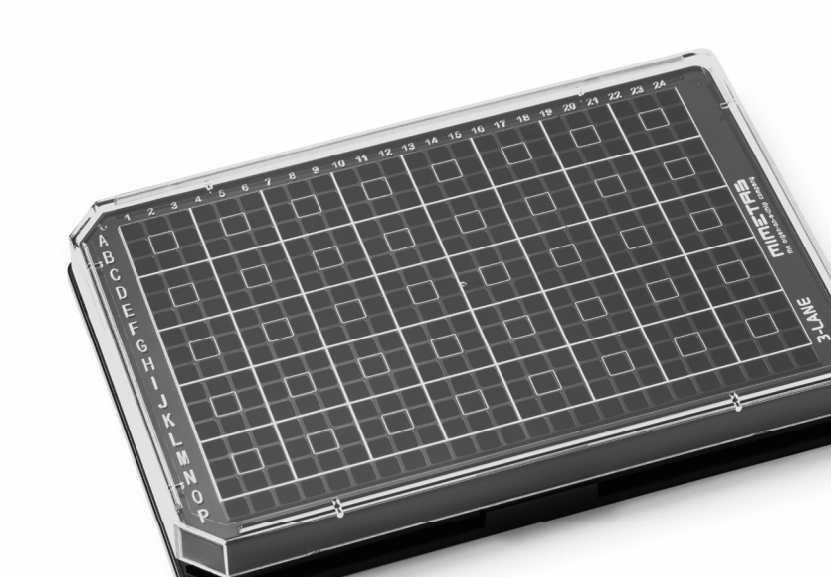
### References

- 1. Ouarné, M., Pena, A. & Franco, C. A. From remodeling to quiescence: The transformation of the vascular network. Cells and Development 168, (2021).
- 2. Rodriguez-iturbe, B., Pons, H. & Johnson, R. J. RÓLE OF THE IMMUNE SYSTEM IN HYPERTENSION. Physiol Rev 97, 1127–1164 (2022).
- 3. Betsholtz, C. Review Pericytes: Developmental, Physiological, and Pathological

- Perspectives, Problems, and Promises. (2011) doi:10.1016/j.devcel.2011.07.001.
- 4. Armulik, A., Abramsson, A. & Betsholtz, C. Endothelial/pericyte interactions. Circ Res 97, 512–523 (2005).
- 5. Gerhardt, H. & Betsholtz, C. Endothelial-pericyte interactions in angiogenesis. Cell Tissue Res 314, 15–23 (2003).
- 6. Viallard, C. & Larrive, B. Tumor angiogenesis and vascular normalization: alternative therapeutic targets. 409–426 (2017) doi:10.1007/s10456-017-9562-9.
- 7. Velnar, T. & Gradisnik, L. Tissue Augmentation in Wound Healing: the Role of Endothelial and Epithelial Cells. 72, 444–448 (2018).
- 8. Payne, L. B. et al. The pericyte microenvironment during vascular development. Microcirculation vol. 26 Preprint at https://doi.org/10.1111/micc.12554 (2019).
- 9. Norrby, K. In vivo models of angiogenesis. JCMM 10, 588–612 (2006).
- 10. Cimpéan, A. M. & Raica, M. Historical Overview of In Vivo and In Vitro Angiogenesis Assays.
- 11. Ponce, M. L. Tube formation: an in vitro matrigel angiogenesis assay. Methods Mol Biol 467, 183–188 (2009).
- 12. Heiss, M. et al. Endothelial cell spheroids as a versatile tool to study angiogenesis in vitro. The FASEB Journal 29, 3076–3084 (2015).
- 13. Rennie, M. Y., Whiteley, K. J., Kulandavelu, S., Adamson, S. L. & Sled, J. G. 3D Visualisation and Quantification by Microcomputed Tomography of Late Gestational Changes in the Arterial and Venous Feto-Placental Vasculature of the Mouse. Placenta 28, 833–840 (2007).
- 14. Dockery, P. & Fraher, J. The quantification of vascular beds: A stereological approach. Exp Mol Pathol 82, 110–120 (2007).
- 15. Lederlin, M. et al. Coronary imaging techniques with emphasis on CT and MRI. Pediatr Radiol 41, 1516–1525 (2011).
- 16. van Duinen, V. et al. Robust and scalable angiogenesis assay of perfused 3D human ipsc-derived endothelium for anti-angiogenic drug screening. Int J Mol Sci 21, 1–9 (2020).
- 17. Bonanini, F. et al. In vitro grafting of hepatic spheroids and organoids on a microfluidic vascular bed. Angiogenesis 25, 455–470 (2022).
- 18. El-Kenawi, A. E. & El-Remessy, A. B. Angiogenesis inhibitors in cancer therapy: Mechanistic perspective on classification and treatment rationales. Br J Pharmacol 170, 712–729 (2013).
- 19. Evensen, L., Micklem, D. R., Link, W. & Lorens, J. B. A novel imaging-based high-throughput screening approach to anti-angiogenic drug discovery. Cytometry Part A 77, 41–51 (2010).
- 20. Niemistö, A., Dunmire, V., Yli-Harja, O., Zhang, W. & Shmulevich, I. Robust quantification of in vitro angiogenesis through image analysis. IEEE Trans Med Imaging 24, 549–553 (2005).
- 21. Liu, M., Xie, S. & Zhou, J. Use of Animal Models for the Imaging and Quantification of Angiogenesis. (2018).
- 22. Vafopoulou, P. & Kourti, M. Anti-angiogenic drugs in cancer therapeutics: A review of the latest preclinical and clinical studies of anti-angiogenic agents with anticancer potential. Journal of Cancer Metastasis and Treatment vol. 8 Preprint at https://doi.org/10.20517/2394-4722.2022.08 (2022).
- 23. Qi, S., Deng, S., Lian, Z. & Yu, K. Novel Drugs with High Efficacy against Tumor Angiogenesis. International Journal of Molecular Sciences vol. 23 Preprint at https://doi.org/10.3390/ijms23136934 (2022).
- 24. Campinho, P., Vilfan, A. & Vermot, J. Blood Flow Forces in Shaping the Vascular System: A Focus on Endothelial Cell Behavior. Frontiers in Physiology vol. 11 Preprint at https://doi.org/10.3389/fphys.2020.00552 (2020).
- 25. Seano, G. et al. Modeling human tumor angiogenesis in a three-dimensional culture system. (2013) doi:10.1182/blood-2012-08.

# Chapter 6

**Conclusions and perspectives** 



# Conclusions and perspectives

The aim of the research described in this thesis was to develop physiological relevant models that utilize the capabilities of Organ-on-a-Chip technology, such as the incorporation of vasculature and fluid flow. Fluid flow is pivotal in various physiological processes, including the transport of molecules and cells, cell signaling, and tissue development. The hypothesis of this thesis was that Incorporating flow in Organ-on-a-Chip systems is crucial for accurately mimicking the physiological conditions of in vivo organs. The aim was to demonstrate that the introduction of flow into microfluidic devices provides a more realistic simulation of the human body's environment. This is particularly important in the context of drug development, where an accurate prediction of drug responses can significantly streamline the drug development pipeline and therefore lead more efficiently to new therapies, improve the safety of these therapies and reduces costs. This is underscored by recent research highlighting the significance of flow dynamics in microfluidic devices for mimicking in vivo conditions. These studies demonstrate the potential for accelerating the drug development pipeline. <sup>1,2</sup>

#### Organ-on-a-Chip in drug development

Organ-on-a-Chip is a promising technology to be integrated into the drug development pipeline. The microscale devices are designed to mimic the microenvironment of an organ, including its physical structure, cellular composition and signaling pathways. This thesis discusses the potential of the OrganoPlate as a candidate to enhance the drug development pipeline by serving as an organ modeling tool, with a focus on the incorporation of vasculature and fluid flow into this systems. The emphasis in all the models developed was a balance between high throughput and complex biology, as scalable models are crucial for successful integration of the models into the drug development pipeline. However, the models still need to have adequate physiological relevance to be applicable in drug development.

In **chapter 2**, the aim was to develop a Panreatic Ductal AdenoCarcinoma (PDAC) model in the OrganoPlate 3-lane 40 where chemoresistance with the standard of care (SoC) drug gemcitabine is modeled. Gemcitabine therapy in PDAC patients is not very effective.3 However, when the PDAC cell line S2-028 in 2D and treated with gemcitabine was cultured, rapid cell death with a low EC50 value was observed. When similar drug exposure in the OrganoPlate model with laminar perfusion flow was performed, increase of the EC50 of three-fold was observed, meaning the cells were more resistant in the three dimensional environment of the Organo Plate. Furthermore, when the flow pattern was redirected to interstitial flow, another three-fold increase in the EC50 (nine-fold compared to the 2D experiment) was observed. As PDAC is known for its poor drug penetration and high chemoresistance, one would expect an in vitro model to have similar traits. However, in the 2D experiment this expectation was not met, as indicated with the low EC50 value for gemcitabine, suggesting low chemoresistance. In contrast, in the 3D interstitial flow experiment this value was significantly higher, indicating an increase in chemoresistance. This higher resistance better reflects the in vivo scenario, providing a more accurate representation of the challenges associated with therapy development in PDAC. These findings emphasize the importance of recapitulating physiological conditions, such as 3D environments and flow dynamics, into in vitro models to more accurately capture the complexity of drug responses in vivo, not only in PDAC but in other cancers and diseases as well.

Next to drug development, toxicological assessment of compounds is also an important application in Organ-on-a-Chip. In **chapter 3**, the aim was to optimize a microvessel-on-a-chip model for studying monocyte-to-endothelium adhesion under flow. Monocyte adhesion on endothelium occurs when the surrounding tissue is inflamed. Leukocyte adhesion is one of the early stages and hallmarks of atherosclerosis. Primary coronary artery endothelial cells were used to form a microvessel, and an increase of adhesion molecules (ICAM) and oxidative stress (GSH) were observed after application of an inflammatory trigger, while this did not impact the viability of the culture. This inflammatory trigger also significantly

increased monocyte adhesion to the endothelial vessel after 4 and 16 hours. As a proof-of-concept, the application of this model as a toxicology model for cigarette smoke conditioned medium was investigated. An increase in all tested markers with both tested cigarette types was observed, and this was in line with the TNF- $\alpha$  concentrations measured in the samples. Toxicological assessments on the early stage of atherosclerosis development are essential for understanding the impact of various compounds on cardiovascular health. The presented microvessel-on-a-chip model presents a powerful tool for such studies. By revealing increased inflammatory markers and monocyte adhesion in response to cigarette smoke, this model not only confirmed the harmful effects of smoking, but also underscores the utility of organ-a-chip systems in toxicology studies. This assay could not only be applied to study the effects of smoking, but can also be used to study cardiovascular disease in general, and diseases where the inflammation plays a major role, such as rheumatoid arthritis and inflammatory bowel disease.

In **chapter 4** the aim as to optimize a model to assess the effect of human patient serum on the formation and stability of angiogenic sprouts. This was done in the context of systemic sclerosis (SSc), where the endothelium is often dysregulated. Dysregulation of angiogenic sprouts, formed in the Organoplate 3-lane, with cytokines, and subsequently rescue this effect with inhibitors of those cytokines was developed. This was optimized with the use of human serum, as a substitute for the commonly used fetal bovine serum. This approach enabled the investigation of disease scenarios, by using patient derived serum to evaluate the effects on the formation and stability of angiogenic sprouts. In a proof-ofconcept study, serum derived from SSc patients had an effect on sprout formation and stability when added during the sprout formation process. This capability to utilize patient-derived serum in Organ-on-a-Chip models underscores a significant advancement in personalized medicine. By capturing the unique cytokine profiles and molecular signatures present in individual patient sera, this model provided a powerful tool for dissecting the pathophysiological mechanisms of diseases like SSc. Furthermore, it offered a promising platform for testing and

6

developing targeted therapies that are specifically tailored to the molecular and cellular characteristics of each patient, potentially leading to more effective and personalized treatment strategies. Beyond SSc, this approach could be applied to other diseases, such as diabetic retinopathy, where cytokine dysregulation is critical to understanding the disease progression and treatment strategy.

To facilitate targeted drug screening or personalized medicine studies on a highthroughput scale, an automated quantification method of the metric of interest is an necessity. In **chapter 5**, the aim was to develop a novel method to perform a detailed three-dimensional analysis in high-throughput. A vascular angiogenesis model on the OrganoPlate Graft to develop a quantification method to analyze the angiogenic sprout formation in 3D was utilized. Through this method, the progression of vascular beds over time and extracted key metrics, including the count of individual objects and the cumulative sprout volume were successfully measured. This approach could also be applied to a co-culture of endothelial cells and pericytes. The newly developed 3D quantification was compared with a more conventional 2D analysis, and although the quantification methods are comparable in outcome, the 3D analysis method gave more precise results. Having an assay with reduced variability is particularly advantageous for integration into a drug screening setup, as it enables the identification of positive responses to newly tested compounds more quickly. In addition, the 3D dataset comprises a multitude of (spatial and intensity) information on the immunostaining of interest compared to a 2D dataset. Further improvement of the quantification method, such as the inclusion of additional metrics, such as branching points and the z-height distribution of the angiogenic sprouts, may yield crucial information for developing new therapies. This automated quantification approach has potential for applications beyond angiogenesis research, including fields such as tumor microenvironment modeling or neurovascular studies, where spatial organization and precise measurements are critical to understand the complex biological processes and to study therapeutic interventions.

#### 150 | Conclusions and perspectives

In conclusion, the integration of Organ-on-a-Chip technology into the drug development pipeline offers significant promise to address the high failure rate observed currently in the preclinical stages of the drug development pipeline. A key aspect of this technology is its ability to incorporate fluid flow and vasculature, which are crucial for creating physiologically relevant models. The examples discussed in this thesis illustrate the potential of the OrganoPlate technology to address bridging the gap between traditional in vitro models, animal and clinical studies, offering physiologically relevant insights into drug efficacy and toxicological assessments. Organ-on-a-Chip technology has the potential to transform the drug discovery process by providing more physiologically relevant models. By reducing the reliance on animal testing and improving the translational relevance of preclinical studies, this technology could accelerate the identification of promising drug candidates. Additionally, the thesis showcases the adaptability and growing interest in Organ-on-a-Chip technology among other commercial entities, as evidenced by the successful collaborations in chapters 3 and 4. The emphasis on vasculature and fluid flow in these models underscores their importance in creating more accurate and reliable platforms for drug development.

In this thesis, the hypothesis was that incorporating flow in Organ-on-a-Chip systems is crucial for accurately mimicking the physiological conditions of in vivo organs. The findings in chapters 2, 3, 4 and 5 support this hypothesis by demonstrating that the presence of flow assists in recreating models with complex biology and a relevant microenvironment of specific organs. In chapter 2, the inclusion of laminar and interstitial flow revealed significant differences in drug resistance compared to a 2D culture without flow. In chapter 3, flow through a microvessel was needed to recapitulate the monocyte adhesion process. In chapter 4, the incorporation of vasculature allowed the study of angiogenic sprouts, which highlighted the role of flow in these sprouts maintaining the endothelial health and structure, and allowed to study the effect of patient sera on the stability of these sprouts. Finally, in chapter 5, a vascular angiogenesis

model is presented. Capturing the complexity of the angiogenic sprouts in three dimensions allows for a more precise assay for assessing the effects of compound exposure on the angiogenic sprouts. These findings collectively affirm the hypothesis by showing that flow and vasculature in Organ-on-a-Chip models enhances the physiological relevance. This enhanced physiological relevance is critical for improving the predictability of drug responses and toxicological outcomes, reducing the likelihood of drug candidates failing in clinical trials due to unforeseen issues in more traditional in vitro models and animal studies.

To further enhance the utility of Organ-on-a-Chip models in drug development, several areas could be investigated:

Translatability to In Vivo: While Organ-on-a-Chip models provide a closer representation of in vivo physiology compared to traditional cell cultures, it remains a main challenge to ensure the translatability of findings to human patients. To validate the predictive value of these models, studies need to be conducted that bridge the gap between Organ-on-a-Chip data and clinical outcomes. This could involve the use of validated animal models, with a longterm goal of eventually replacing animal studies, or integrating Organ-on-a-Chip the incorporation of parallel Organ-on-a-Chip studies next to clinical studies to correlate the chip-based predictions with human responses from the clinical trial. Whether Organ-on-a-Chip systems ultimately replace animal models or serve as an addition to the preclinical pipeline will depend on the specific model and the disease or biological process being targeted.

**Incorporating Patient-Derived Materials:** The ability to assess patient-derived materials, as discussed in chapter 4, offers exciting prospects for personalized medicine and disease modeling. The OrganoPlate's microfluidic design enables the establishment of flow controlled co-culture systems, making it well suited to replicate the complex microenvironments of human tissues. In addition, the low amount of material needed in the OrganoPlate platform, makes it an attractive option for incorporating patient derived materials as the availability of such

materials is severely limited. However, as the patient materials in chapter 4 were incorporated as a proof-of-concept, further research is needed to standardize and validate these approaches, ensuring that the effects observed in Organ-on-a-Chip models accurately reflect patient responses. The scalability and flexibility of the OrganoPlate platform position it as a valuable tool for incorporating patient materials in both preclinical models and the use for personalized therapeutic strategies.

**Data Analysis and Integration:** As Organ-on-a-Chip models generate complex, multi-dimensional data, robust data analysis methods are essential. As it is rather straightforward to extract data from the Organ-on-a-Chip models on multiple levels, such as analytes from medium, RNA for gene expression analysis and protein expression by immunofluorescent staining, the challenge lies with integrating this data to extract more comprehensive information. In this thesis, computational analyses were somewhat limited, primarily explored in Chapter 5. However, the recent advancements in computing power, algorithms, and artificial intelligence (AI) technologies<sup>4,5</sup> offer promising opportunities to integrate molecular data, such as multi-omics approaches, and correlate these findings with phenotypic observations for a comprehensive insight in the outcomes of the studies.

Automation for High-Throughput Screening: The automation of experimental setups, as briefly discussed in chapter 5, is essential to increase the throughput of drug screening. The footprint of the OrganoPlate and the practical handling make this platform suitable for automation, which was demonstrated recently.<sup>6</sup> High throughput is critical in evaluating a large number of compounds efficiently. Streamlining the process can accelerate drug development and reduce costs, ultimately increasing the chances of identifying successful candidates. To be able to perform high-throughput screening on an assay, such as the assays established in this thesis, some steps need to be taken. First, robust positive and negative controls need to be established for the assay. Second, the assay needs to have proven reproducibility over multiple iterations. Third, quality control must be

implemented, to ensure consistent results over multiple experiments. Fourth, the automated systems must be integrated to manage the addition and removal of media, reagents and compounds across multiple chips simultaneously. Fifth, standardized protocols for imaging and data acquisition need to be developed. Finally, a robust data analysis pipeline is essential to be able to process the large volume of data generated, and allow for the identification of hits and trends in the data. By addressing these steps, the models described in this thesis could be optimized for high throughput applications.

Incorporating these improvements into Organ-on-a-Chip technology holds the potential to revolutionize the drug development pipeline by reducing the attrition rate of drug candidates, minimizing costly late-stage failures, and enabling more precise and personalized therapies. While challenges remain, the continued development of these models in a collaborative effort between academia, industry, and regulatory agencies can help reshape the landscape of drug discovery and ultimately benefit patients worldwide.

### References

- Regmi, S., Poudel, C., Adhikari, R. & Luo, K. Q. Applications of Microfluidics and Organ-on-a-Chip in Cancer Research. Biosensors (Basel) 12, (2022).
- Wilkinson, J. M. A review of complex in vitro cell culture stressing the importance of fluid flow and illustrated by organ on a chip liver models. Frontiers in toxicology 5, (2023).
- Koltai, T. et al. Resistance to Gemcitabine in Pancreatic Ductal Adenocarcinoma: A Physiopathologic and Pharmacologic Review. Cancers (Basel) 14, (2022).
- Wang, D. et al. Human-Al Collaboration in Data Science. Proc ACM Hum Comput Interact 3, 24 (2019).
- M. Alshater, M. Exploring the Role of Artificial Intelligence in Enhancing Academic Performance: A Case Study of ChatGPT. SSRN Electronic Journal (2022) doi:10.2139/ SSRN.4312358.
- Soragni, C. et al. Phenotypic screening in Organ-on-a-Chip systems: a 1537 kinase inhibitor library screen on a 3D angiogenesis assay. Angiogenesis 1, 1–13 (2023).

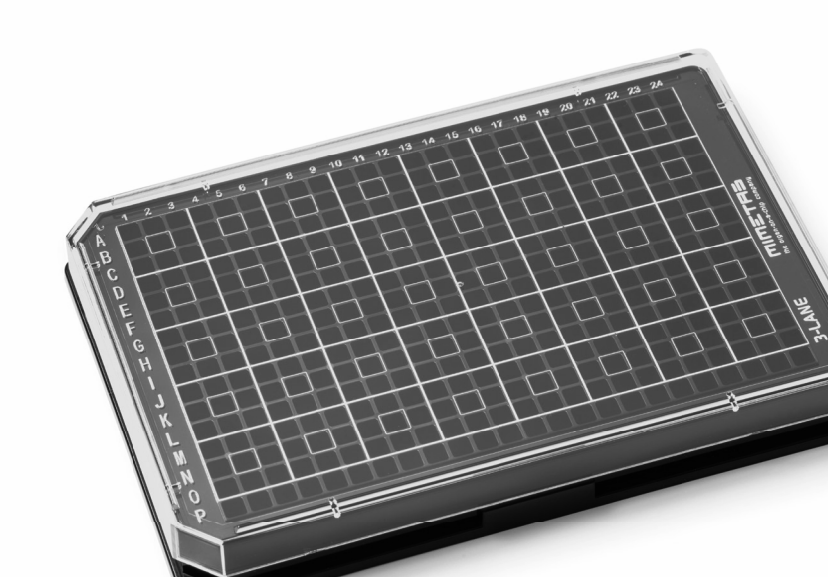
# Addendum

Nederlandse samenvatting

Curriculum Vitae

List of publications

Dankwoord



### **Nederlandse Samenvatting**

De ontwikkeling van nieuwe geneesmiddelen is een langdurig, kostbaar en complex proces, dat doorgaans meer dan tien jaar in beslag neemt en wordt gekenmerkt door een hoge uitval van kandidaatstoffen. Het traject begint met de ontdekking en validatie van ziekte-gerelateerde doelwitten, waarbij onderzoekers op zoek gaan naar moleculen, vaak eiwitten of genen, die een rol spelen in het ontstaan of verloop van een ziekte. Vervolgens worden duizenden tot miljoenen stoffen gescreend op hun vermogen om deze doelwitten te beïnvloeden. Slechts een klein deel van deze verbindingen blijkt in vroege in vitro experimenten en diermodellen daadwerkelijk effectief en veilig genoeg om als kandidaatgeneesmiddel verder te worden ontwikkeld.

Na deze ontdekkingsfase volgt het preklinisch onderzoek, waarin de veiligheid, werkzaamheid en farmacokinetiek van de kandidaatstoffen uitgebreid worden getest, meestal in diermodellen. Een van de grootste uitdagingen in deze fase is dat resultaten uit dierproeven vaak niet goed vertalen naar de menselijke situatie, waardoor veelbelovende stoffen alsnog kunnen falen in latere stadia. Wanneer een kandidaat voldoende potentie toont, wordt toestemming gevraagd om klinische studies bij mensen te starten. Deze klinische ontwikkeling verloopt in meerdere fasen, waarin achtereenvolgens de veiligheid, dosering, werkzaamheid en bijwerkingen van het middel bij steeds grotere groepen patiënten worden onderzocht. Ook hier zijn de uitdagingen groot: het werven van geschikte proefpersonen, het selecteren van relevante eindpunten en het voldoen aan strenge regelgeving vergen veel tijd en middelen.

Na succesvolle afronding van de klinische studies volgt een uitgebreide beoordelingsprocedure door regelgevende instanties zoals de FDA of EMA, die alle verzamelde gegevens beoordelen alvorens het middel op de markt mag komen. Zelfs na markttoelating blijft voortdurende bewaking noodzakelijk om



zeldzame of langetermijngevolgen te identificeren, wat het belang van een voorspellende preklinische en klinische fase onderstreept.

De hoge uitval in het ontwikkelingsproces en de beperkte voorspelbaarheid van bestaande preklinische modellen vormen een belangrijke belemmering voor efficiënte geneesmiddelenontwikkeling. Hier komt Organ-on-a-Chip (OoC) technologie in beeld als een veelbelovende innovatie. Deze technologie maakt het mogelijk om de complexe fysiologische en biochemische omgeving van menselijke organen op microschaal na te bootsen, door gebruik te maken van relevante celtypen, extracellulaire matrix componenten en microfluïdische kanalen die gecontroleerde stroming van voedingsstoffen en metabolieten mogelijk maken. Door deze nauwkeurige nabootsing kunnen OoC-systemen bijdragen aan het verbeteren van de voorspelbaarheid van geneesmiddelresponsen, het verminderen van het gebruik van proefdieren en het versnellen van de identificatie van veelbelovende kandidaatstoffen. OoC-systemen zijn er in verschillende vormen: van complexe, lage-doorvoer systemen die zeer gedetailleerde analyses mogelijk maken, tot schaalbare, hoge-doorvoer systemen die geschikt zijn voor grootschalige screenings en automatisering. Beide benaderingen hebben hun eigen voordelen en beperkingen, maar delen het potentieel om het geneesmiddelenontwikkelingsproces fundamenteel te verbeteren.

Het onderzoek in dit proefschrift richt zich op het ontwikkelen van fysiologisch relevante modellen met behulp van Organ-on-a-Chip technologie, met speciale aandacht voor de integratie van vasculatuur en stroming. Door stroming te incorporeren kunnen belangrijke fysiologische processen, zoals het transport van moleculen, cel signalering en weefselontwikkeling, beter worden nagebootst. De centrale hypothese is dat het toevoegen van stroming aan Organ-on-a-Chip systemen essentieel is voor het accuraat simuleren van de omstandigheden in het menselijk lichaam, wat uiteindelijk leidt tot betrouwbaardere voorspellingen van geneesmiddelresponsen en een efficiënter ontwikkelingsproces.

А

#### 158 | Appendix

In **hoofdstuk 2** wordt een driedimensionaal Pancreatic Ductal Adenocarcinoma (PDAC) model ontwikkeld dat geschikt is om de medicijnresistentie van bestaande en nieuwe therapieën te beoordelen. Hierbij ligt de nadruk op de incorporatie van interstitiële stroming, een kenmerkend aspect van PDAC. De resultaten tonen aan dat er een significante toename in chemoresistentie is in het 3D-model met stroming vergeleken met traditionele 2D-culturen zonder stroming. Deze bevindingen benadrukken het belang van het nabootsen van fysiologische stromingscondities om de complexiteit van medicijnresponsen in vivo beter te kunnen vatten.

**Hoofdstuk 3** richt zich op de ontwikkeling van een vasculatuur-on-a-Chip model voor de toxicologische beoordeling van stoffen in een vroeg stadium van atherosclerose. Er is een microvaatmodel met coronaire arteriële bloedvatcellen opgezet, waarbij de aanwezigheid van adhesiemoleculen en oxidatieve stress werd geëvalueerd. Tevens is een functionele assay ontwikkeld om de adhesie van monocyten aan het bloedvat live te beoordelen. Als proof-of-concept is het schadelijke effect van rookconditie-medium van sigaretten onderzocht, waarbij een toename van ontstekingsmarkers en monocytenadhesie werd waargenomen, wat de bruikbaarheid van het model voor toxicologische studies onderstreept.

In **hoofdstuk 4** wordt een microvaten-on-a-chip model ontwikkeld om defecte angiogenese bij systemische sclerose (SSc) te bestuderen. Met behulp van menselijke serummonsters van SSc-patiënten is aangetoond dat het serum de vorming en stabiliteit van angiogene bloedvatuitlopers beïnvloedt. Dit model maakt het mogelijk om ziekteprocessen in een patiëntspecifieke context te onderzoeken en biedt een platform voor de ontwikkeling van gepersonaliseerde therapieën, wat een belangrijke stap is richting precisiegeneeskunde.

**Hoofdstuk 5** beschrijft de ontwikkeling van een robuuste en geautomatiseerde methode voor de kwantificering van driedimensionale vasculaire netwerken in hoge doorvoer. Met behulp van confocale beeldvorming en geavanceerde beeldverwerkingstechnieken worden kenmerken van vasculaire netwerken, zoals het aantal objecten en het cumulatieve volume van angiogene uitlopers, nauwkeurig gemeten. Deze methode biedt een verbeterde precisie ten opzichte van conventionele 2D-analyses en is essentieel voor het integreren van Organ-ona-Chip modellen in grootschalige screenings voor geneesmiddelenontwikkeling.

In **hoofdstuk 6** wordt een perspectief op de toekomst gegeven. De algemene conclusies van dit proefschrift bevestigen dat het incorporeren van stroming en vasculatuur in Organ-on-a-Chip systemen de fysiologische relevantie van deze modellen verhoogt. Dit is cruciaal voor het verbeteren van de voorspelbaarheid van geneesmiddelresponsen en toxicologische uitkomsten, wat kan bijdragen aan het verminderen van falingen in klinische fases en het versnellen van de ontwikkeling van nieuwe therapieën. De bevindingen illustreren het potentieel van de Organ-on-a-Chip technologie om de kloof te overbruggen tussen traditionele in vitro modellen, dierstudies en klinische onderzoeken. Toekomstig onderzoek zou zich kunnen richten op het verbeteren van de transleerbaarheid naar in vivo situaties, het standaardiseren van patiëntmateriaal in modellen, het integreren van geavanceerde data-analyse en het automatiseren van screenings. Deze ontwikkelingen kunnen de Organ-on-a-Chip technologie verder positioneren als een krachtige tool in de geneesmiddelenontwikkeling en gepersonaliseerde geneeskunde.

### Curriculum Vitae

**Bart Kramer** was born on July 20th, 1991, in Woerden, The Netherlands. In 2009, he completed his pre-university education (VWO) at the Minkema College in Woerden. He went on to pursue a Bachelor's degree in Biomedical Sciences at Utrecht University, graduating in 2012 with a thesis titled "MicroRNA intervention in Calcific Aortic Valve Disease."

Following his Bachelor's he enrolled in the Master's program Regenerative Medicine and Technology at Utrecht University. During this program, he conducted a research internship at the University of Cambridge, studying liver organoids in disease under the supervision of Prof. Dr. M. Huch. After earning his Master's degree in 2015, he undertook a secondment at BioTalentum (Hungary), where he worked on the chondrogenic differentiation of induced pluripotent stem cells.

In 2016, Bart joined Mimetas BV as a junior scientist to study and develop tissue models on the OrganoPlate platform. He was promoted to scientist in 2017 and has held the role of scientific project lead since 2020. In parallel, he began his PhD at the Leiden Academic Centre for Drug Research in 2019 as an external candidate, under the supervision of Prof. Dr. T. Hankemeier, Dr. H.L. Lanz and Dr. L.J. van den Broek. This work has culminated in the current thesis.



## List of publications

Kramer, B., de Haan, L., Vermeer, M., Olivier, T., Hankemeier, T., Vulto, P., Joore, J., & Lanz, H. L.

Interstitial flow recapitulates gemcitabine chemoresistance in a 3D microfluidic pancreatic ductal adenocarcinoma model by induction of multidrug resistance proteins. *International Journal of Molecular Sciences*, 20(18), 4647, (2019)

Poussin, C., **Kramer, B.**, Lanz, H. L., van den Heuvel, A., Laurent, A., Olivier, T., Vermeer, M., Peric, D., Baumer, K., Dulize, R., Guedj, E., Ivanov, N. V., Peitsch, M. C., Hoeng, J., & Joore, J. 3D human microvessel-on-a-chip model for studying monocyte-to-endothelium adhesion under flow-application in systems toxicology.

*ALTEX-Alternatives to Animal Experimentation*, 37(1), 47–63. (2020)

**Kramer, B.**, Corallo, C., van den Heuvel, A., Crawford, J., Olivier, T., Elstak, E., Giordano, N., Vulto, P., Lanz, H. L., Janssen, R. A. J., & Tessari, M. A.

High-throughput 3D microvessel-on-a-chip model to study defective angiogenesis in systemic sclerosis.

Scientific Reports, 12(1), 16930 (2022)

Lanz, H. L., Saleh, A., **Kramer, B.**, Cairns, J., Ng, C. P., Yu, J., Trietsch, S. J., Hankemeier, T., Joore, J., Vulto, P., Weinshilboum, R., & Wang, L.

Therapy response testing of breast cancer in a 3D high-throughput perfused microfluidic platform.

BMC Cancer, 17(1), 709 (2017)

Bonanini, F., Kurek, D., Previdi, S., Nicolas, A., Hendriks, D., de Ruiter, S., Meyer, M., Clapés Cabrer, M., Dinkelberg, R., Bonilla García, S., **Kramer, B.**, Olivier, T., Hu, H., López-Iglesias, C., Schavemaker, F., Walinga, E., Dutta, D., Queiroz, K., Domansky, K., ... Vulto, P. (2022). In vitro grafting of hepatic spheroids and organoids on a microfluidic vascular bed. *Angiogenesis*, 25(4), 455–470 (2022)

Mori, A., Vermeer, M., van den Broek, L. J., Heijmans, J., Nicolas, A., Bouwhuis, J., Burton, T., Matsumura, K., Ohashi, K., Ito, S., & **Kramer, B.** 

High-throughput Bronchus-on-a-Chip system for modeling the human bronchus. *Scientific Reports,* 14(1), 26248 (2024)

Trietsch, SJ, Nicolas, A.Y.M., van den Broek, L.J. **Kramer, B.** & Vulto, P.V. Microfluidic cell culture device (U.S. Patent Application No. US20230250377A1). U.S. Patent and Trademark Office. (2023)

А

#### **Dankwoord**

Met deze thesis komt er een einde aan een intensief en leerzaam traject. Zoiets doe je niet alleen, dus dit is het moment om stil te staan bij de mensen die op verschillende manieren hebben bijgedragen.

Allereerst dank aan mijn promotor, **Thomas Hankemeier**. Dank voor de begeleiding, de vrijheid om mijn eigen richting te bepalen en voor de ruimte om te leren.

Ook wil ik mijn co-promotoren, **Lenie van den Broek en Henriette Lanz**, bedanken. Henriette, jouw betrokkenheid en nuchtere blik waardeer ik enorm. Bedankt dat je me bij Mimetas hebt betrokken en mij de ruimte hebt gegeven om mezelf te ontwikkelen. Lenie, jij was altijd beschikbaar voor feedback, biologische vragen of gewoon een praatje, en hield het proces scherp. Zonder jullie was deze thesis niet tot stand gekomen.

De oud-stagiairs die hebben meegebouwd aan het project: **Marjolein, Luuk, Willem, Hicham, Annina en Marianne**, dank voor jullie werk, inzet en de samenwerking.

Bij Mimetas was het vooral de kantoorsfeer die het werk een stuk aangenamer maakte. In BP2 waren het de vaste buddies: **Nienke, Linda, Xandor, Thomas, Angelique, Chiwan, Wijnand en Vincent**, jullie zorgden voor afleiding op de juiste momenten. Dank voor het delen van frustraties, koffie, droge humor en de betere memes.



In BP5 zette die sfeer zich voort. **Marije, Xandor, Linda, Niels, Chiwan en Trisa**: dank voor de gesprekken, praktische hulp en het dagelijks geklets dat het werk net iets lichter maakt.

Daarnaast dank aan alle collega's bij Mimetas voor de samenwerking, support en betrokkenheid gedurende het hele traject.

Mijn paranimfen, **Iris en Nienke**: fijn dat jullie naast me staan tijdens de verdediging. Dank voor jullie steun in de aanloop daarnaartoe.

Ook wil ik **Rody, Sjaak, Ellen en Mariska** bedanken. De avonden vol bordspellen en gezelligheid waren een fijne tegenhanger van het werk aan deze thesis. Dank voor het meedenken, afleiden en vooral voor het plezier samen.

Daarnaast wil ik **Iris, Simon, Joris, Karin en Veerle** bedanken. Fijn dat jullie er waren, met steun, gezelligheid en een luisterend oor wanneer dat nodig was.

Dan mijn ouders, **Luuk en Anneloes.** Jullie steun is altijd vanzelfsprekend geweest, en dat is precies waarom ik die zo waardeer.

Tot slot: **Isabella en Ruben**. Isabella, bedankt voor je geduld, je nuchterheid, en voor het opvangen van de chaos die er soms bij kwam kijken. Vooral wil ik je ook bedanken voor het motiveren op de momenten dat het even tegen zat. En Ruben: je hebt nog geen idee, maar jouw aanwezigheid maakt alles de moeite waard.